THE EFFECT OF BEAM SEAS ON A STATIONARY SHIP IN SHALLOW WATER

by

Peter James Taylor
B.Sc. (Hons.), University of Adelaide

Thesis submitted for the degree of Doctor of Philosophy in the Applied Mathematics Department, University of Adelaide, December, 1971.

CONTENTS

SUMMARY

The ultimate result of this thesis is a procedure by which estimates can be made of some of the forces on a stationary ship in shallow water due to the impact of waves. This procedure consists of numerical solution of two distinct boundary value problems (designated as the inner and outer problems) which are linked in the overall scheme by a matching process.

Part 1 consists of a study of a class of problems similar to the outer problem, which is a ribbon diffraction problem strictly analogous to similar problems in acoustics or optics. Chapters 1 and 2 discuss an efficient numerical procedure which solves this type of problem when there is a Dirichlet or Neumann boundary condition on the ribbon. This procedure is extended in Chapter 3 to allow for a mixed boundary value problem directly applicable to the ship hydrodynamics problem to be solved.

Part 2 contains two different approaches to solving the inner problem. Chapter 4 describes an accurate numerical procedure for solving this problem in a general context, whereas Chapter 5 describes some methods which enable convenient asymptotic estimates of the solution to be made in certain cases where the clearance under the ship is small.

Finally, Part 3 discusses the general ship hydrodynamics problem, shows how the methods of Part 1 and 2 are linked by a matching process, and makes some sample calculations of force coefficients for a particular ship.

SIGNED STATEMENT

I hereby declare that this thesis contains no material which has been accepted for the award of any other degree or diploma in any University, and, to the best of my knowledge and belief, it contains no material previously published by any other person, except where due reference is made in the text of the thesis.

P. J. Taylor

PREFACE

I wish to express my thanks to my supervisor, Dr. E.O. Tuck, for his encouragement and numerous suggestions, as well as for valuable discussions on many aspects of the work. I also wish to thank Dr. R. F. Beck for many useful discussions, particularly on the application of this work to Naval Architectural problems. Finally, I wish to thank Barbara McDonald for her excellent typing and patience during the alterations which occurred during the composition of the thesis.

The research leading to the results contained in this thesis was carried out between July, 1968 and December, 1971. During the last three years of this research the author was the holder of a Commonwealth Postgraduate Award. This research has also at various times been supported by funds made available by the Naval Ship Research and Development Center, Washington, D.C., and by the Australian Research Grants Committee.

GENERAL INTRODUCTION

A problem which has become of increasing commercial importance in recent years is the design of off-shore harbour facilities. One of the reasons for this is the development of giant supertankers and ore carriers, which are too large to operate from many harbours. The other reason, which is of particular significance to Australia, is the discovery of minerals in remote areas, which has led to the development of off-shore mooring facilities simply because of the lack of a suitable harbour in the vicinity.

One of the factors influencing the design of such a facility is the magnitude of the very large forces which will act on a moored ship under the impact of waves. The aim of this thesis is to go part of the way to a theoretical estimate of the exciting forces corresponding to the six degrees of freedom of an arbitrary ship under the influence of waves of all frequencies, incident from any angle.

In setting up the mathematical model we make a number of assumptions which are customary in the literature on ship hydrodynamics. We ignore viscosity and compressibility, and assume that we can linearize the free surface boundary condition. We also assume that the ship is a slender body, i.e. the beam and draft of the ship are small compared with its length. We also assume here that the ship is stationary, and that the water is shallow.

Tuck[19] has shown that the exciting forces associated with the six modes of motion of the ship are related to a jump in velocity potential across the ship, this jump being a function of the station co-ordinate along the length of the ship. Furthermore (in his equation (82)), Tuck gives a formula for the sway exciting force. Beck and Tuck[2] have also calculated the exciting force corresponding to other modes of motion. The jump in potential is also needed for other modes.

This thesis describes numerical and analytical methods by which this potential jump can be computed, as well as giving an example of the actual calculation of the sway exciting force for a particular ship, using Tuck's[19] equation (82).

The problem is solved by formulating a boundary value problem in an "outer" region, i.e. a region which extends far abeam of the ship. Under the slender body assumption, since the ship becomes vanishingly thin, we can consider this problem to be one of diffraction of plane waves about a finite ribbon. In fact this outer problem is strictly analogous to corresponding acoustic or optical diffraction problems. It is also necessary to solve an "inner" boundary value problem near the ship to provide the correct boundary condition on the ribbon.

Part 1 of this thesis deals with a range of ribbon diffraction problems, all of which are solved by a similar numerical method, viz. by obtaining an integral formulation of the problem via Green's

Theorem, and solving the resulting integral equation numerically. Such integral methods, if they can be used, have the natural advantage that unknown quantities in the problemlie exclusively on the boundary. This can be compared with the more frequently applied finite difference numerical methods for solving such elliptic boundary value problems, which involve setting up a fine grid throughout a large region of space, often leading to large round-off errors, as well as to considerable expenditure of computing time.

Chapter 1 describes a numerical solution for the ribbon diffraction problem in which there is a Dirichlet boundary condition (i.e. specified potential) on the ribbon. Chapter 2 treats the complementary problem, with a Neumann boundary condition (i.e. specified normal velocity). These two problems are commonly discussed in the acoustic literature, e.g. Hönl, Maue, and Westphal [9], and Morse and Rubenstein [13]. In fact our integral formulation agrees with that of Hönl, Maue and Westphal.

In Chapter 3 we treat a problem of more direct relevance to the ship hydrodynamics problem, in which the boundary condition is neither of Neumannnor Dirichlet type, but a mixture of the two, in fact a linear combination of potential and velocity is prescribed. The coefficient in this linear relationship (supposed known in this chapter) is the effective porosity of the ribbon, in an acoustic analogy, and may vary along the ribbon.

Part 2 deals with the inner problem which has already been mentioned. The inner region is one close to the ship, in which it follows that we can treat the problem as two-dimensional in each cross-flow plane, and represent the free surface as a rigid boundary. Solution of this problem leads directly to the evaluation of the porosity.

Flagg and Newman [6] have solved this inner problem analytically for the special case where the ship cross-sections are rectangular. Chapter 4 describes a numerical solution to the problem for a general cross-section. Once again we use Green's Theorem to obtain an integral equation, in which the unknown is now a source-density function around the cross-section contour.

Chapter 5 uses the method of matched asymptotic expansions to obtain small clearance asymptotic solutions of this inner problem for a particular family of cross-sections, which are similar to cross-sections of many commercial ships.

Finally, in Part 3, the ship hydrodynamics problem is formally set up, and it is seen how the numerical methods described in Parts 1 and 2 combine to give an evaluation of the potential jump along an arbitrary ship under the impact of plane waves of any frequency, incident from any angle. Sample calculations using Tuck's [19] equation (82) are also made of the sway exciting force for the Series 60, block 0.80 ship.

PART 1 - THE NUMERICAL SOLUTION OF SOME FINITE RIBBON DIFFRACTION PROBLEMS

CHAPTER 1

DIRICHLET BOUNDARY CONDITION - ON THE RIBBON

1.1 INTRODUCTION

This chapter describes the numerical solution of a boundary value problem which arises in the theory of diffraction.

The problem is solved numerically over a wide range of values of the frequency of the incident wave, and the numerical results are tested by comparing results for high and low values of the frequency with asymptotic solutions at these frequencies.

As a further test, farfield intensity patterns are drawn for certain frequencies, and these are compared with those of Morse and Rubènstein [13], who solved the problem analytically by separation of variables in elliptic cylindrical co-ordinates, obtaining a solution as a series of Mathieu functions.

1.2 THE BOUNDARY VALUE PROBLEM

We consider in the X-Y plane a surface S which takes the form of a ribbon of length 2, and infinitesimal thickness, which lies on the X-axis, and has its centre at the origin.

Consider a normally incident plane wave of the form

$$\Phi_1 = - e^{iky - i\sigma t} = \phi_1(x,y)\, e^{-i\sigma t} ,$$

where $\phi_1(x,y) = -e^{iky}$. Then there will be a scattered wave of the same frequency of the form $\Phi_2 = \phi_2(x,y)\, e^{-i\sigma t}$, the total field at any point being $\Phi = \Phi_1 + \Phi_2 = \phi(x,y)\, e^{-i\sigma t}$. Since Φ_1 and Φ_2 must satisfy the wave equation, we know that ϕ_1, ϕ_2 and $\phi = \phi_1 + \phi_2$ must satisfy the Helmholtz equation, viz.

$$(\nabla^2 + k^2)\phi = 0 \qquad (1.2.1)$$

outside the surface S.

We shall assume that the Dirichlet boundary condition

$$\phi = 0 \qquad (1.2.2)$$

holds on the surface S;

since $\phi_1 = -1$ on S, this means that the scattered amplitude takes the value

$$\phi_2 = 1 \qquad (1.2.3)$$

on the surface S.

The primary aim in considering this problem is because of its relation to various diffraction problems in the theory of ship motions in shallow water, but similar problems can be formulated for acoustic and electro-magnetic waves.

One can also formulate similar problems in which k may be complex. Tuck[17] has discussed one such problem, which relates to viscous-fluid oscillations. In that case k^2 is pure imaginary, i.e. k is a complex number of argument $\frac{\pi}{4}$. The program to solve the present problem was devised to allow complex values of k, but

the results and discussion in the remainder of this chapter are concerned only with real positive k.

1.3 DERIVATION OF THE INTEGRAL EQUATION

Because of the symmetry properties of the boundary value problem for the scattered amplitude ϕ_2 (thus ϕ_2 has the same value on both sides of the ribbon), we can make an integral formulation of the boundary value problem using the distribution of sources method (see Copley[5]).

We assume that a solution for the potential function in the X-Y plane takes the form

$$\phi_2(x,y) = \int_{-1}^{1} P(\xi) H_o^{(1)}(kR)\,d\xi \qquad (1.3.1)$$

where

$$R = \sqrt{(x - \xi)^2 + y^2}$$

and $H_o^{(1)}(z)$ is a Hankel function, equal to $J_o(z) + iY_o(z)$. Since $H_o^{(1)}(z)$ itself satisfies the Helmholtz equation (1.2.1), this solution for ϕ_2 must necessarily satisfy (1.2.1). $P(\xi)$ is the source density function, and is as yet unknown.

To satisfy the boundary condition (1.2.3), we force (1.3.1) to hold on the boundary y = 0, giving the integral equation

$$\int_{-1}^{1} P(\xi) H_o^{(1)}(k\,|\xi - x|)\,d\xi = 1\,. \qquad (1.3.2)$$

We now have an integral equation which we can solve explicitly for $P(\xi)$.

Differentiating (1.3.1) with respect to y (the direction normal to the boundary of the ribbon), we find that

$$\frac{\partial \phi_2(x,y)}{\partial y} = \int_{-1}^{1} P(\xi) \frac{ky}{R} H_o^{(1)'}(kR)d\xi \ . \qquad (1.3.3)$$

If we let $y \downarrow 0$ in (1.3.3), the contribution to $\frac{\partial \phi_2}{\partial y}$ will clearly be zero unless $\xi = x$, i.e. $R = 0$, i.e.

$$\frac{\partial \phi_2}{\partial y}(x,0+) = \lim_{y \downarrow 0} kyP(x) \int_{-1}^{1} \frac{1}{R}\left[\frac{2i}{\pi kR} + O(\log R)\right]d\xi$$

$$= \begin{cases} 0 & \text{if } |x| > 1 \\ 2iP(x) & \text{if } |x| < 1 \end{cases} . \qquad (1.3.4)$$

Thus $P(x)$ is a scalar multiple of the normal derivative $\frac{\partial \phi_2}{\partial y}$ on the upper boundary of the ribbon. In fact on the lower boundary $\frac{\partial \phi_2}{\partial y}$ takes the opposite sign, but has the same magnitude.

1.4 DESCRIPTION OF THE NUMERICAL PROCESS

A comprehensive description of the technique used may be found in [18]. In that paper, Tuck solved an integral equation similar to (1.3.2), but with a different kernel function. However, his kernel had similar properties to $H_o^{(1)}$ in that it contained a logarithmic singularity at $\xi = x$, and also oscillated rapidly while decaying to zero for k tending to infinity.

From the theory of singular integral equations, we notice that the solution will have a square root singularity at $\xi = \pm 1$, and we counter this by using an unequal interval quadrature formula with grid points defined by $\xi_j = -\cos\frac{\pi j}{N}$, $j = 0, \ldots, N$. In the method we assume that $P(\xi)$ will not vary rapidly, and therefore approximate $P(\xi) = P_j$ = constant on each interval $\xi_j < \xi < \xi_{j+1}$; but we do not approximate the kernel. Thus we have

$$\sum_{j=0}^{N} P_j \int_{\xi_j}^{\xi_{j+1}} H_o^{(1)}(k\,|\xi - x|)d\xi = 1 . \qquad (1.4.1)$$

We now force this equation to hold at the mid-point

$$x = \xi_k' = \tfrac{1}{2}\xi_k + \tfrac{1}{2}\xi_{k+1}$$

of the k^{th} segment, giving a matrix equation of the form

$$\sum_{j=0}^{N-1} P_j A_{kj} = 1 \qquad k = 0,1, \ldots, N-1 , \qquad (1.4.2)$$

where

$$A_{kj} = \int_{\xi_j}^{\xi_{j+1}} H_o^{(1)}(k\,|\xi - \xi'_k|)d\xi$$

$$= \frac{F(k\,(\xi_{j+1} - \xi'_k)) - F(k\,(\xi_j - \xi_k'))}{k} , \qquad (1.4.3)$$

where

$$F(z) = \int_o^z H_o^{(1)}(t)dt . \qquad (1.4.4)$$

There are several advantages of this method which are worth noting.

(1) The matrix $[A_{jk}]$ can be set up with just N^2 calls to a subroutine for the function F.

(2) The method has been designed to give uniform accuracy as k increases.

(3) The problem of having a singularity in the kernel has been eliminated, as it has been integrated through in the analytic evaluation of the diagonal elements A_{kk}.

A description of the computed output follows later in this chapter.

1.5 THE LOW FREQUENCY ASYMPTOTE

In the next two sections, analytic solutions of the integral equation will be obtained for the low and high frequency asymptotes (i.e. $k \to 0$ and $k \to \infty$).

To consider the low frequency asymptote we substitute the small argument expansion of the kernel, viz.

$$H_o^{(1)}(z) \sim \frac{2i}{\pi} \log \frac{z}{2} + \frac{2i\gamma}{\pi} + 1 \qquad \text{as } z \to 0 \qquad (1.5.1)$$

into the integral equation, giving

$$\int_{-1}^{1} P(\xi) \left[\frac{2i}{\pi} \log \left(\frac{k}{2} |\xi - x|\right) + \frac{2i\gamma}{\pi} + 1\right] d\xi = 1. \qquad (1.5.2)$$

Differentiating (1.5.2) with respect to x gives

$$\int_{-1}^{1} \frac{P(\xi)}{\xi - x}\, d\xi = 0 \ , \qquad (1.5.3)$$

which is known to have a solution

$$P(\xi) = \frac{c}{\sqrt{1 - \xi^2}} \qquad (1.5.4)$$

for any constant c. But this is only a solution of (1.5.2) if

$$c = \frac{1}{\int_{-1}^{1} \frac{d\xi}{\sqrt{1 - \xi^2}} \left(\frac{2i}{\pi} \log \left\{ \frac{k}{2} |\xi - x| \right\} + \frac{2i\gamma}{\pi} + 1 \right)} \ ,$$

i.e.

$$c = P(0) = \frac{1}{\pi\left(\frac{2i}{\pi} \log \frac{k}{2} + \frac{2i\gamma}{\pi} + 1\right) - 2i\pi \log 2} \ . \qquad (1.5.5)$$

Equations (1.5.4) and (1.5.5) form the low frequency asymptotic solution.

1.6 THE HIGH FREQUENCY ASYMPTOTE

The method used in obtaining the analytic solution for the high frequency asymptote is based on the results of Carrier[4]. His method predicts as the solution

$$\frac{P(\xi)}{k} = c + \chi[k(1 + \xi)] + \chi[k(1 - \xi)] \ ,$$

where

$$c = \frac{1}{\int_{-\infty}^{\infty} H_0^{(1)}(|x - t|)\, dt} \ ,$$

$$\chi(t) = \phi(t) - c \ ,$$

and $\phi(t)$ is the solution of

$$\int_0^\infty \phi(t) H_0^{(1)}(|x - t|)dt = 1 \ . \qquad (1.6.1)$$

From standard references on Bessel functions, e.g.[1], one can verify that $c = \frac{1}{2}$, but the evaluation of $\phi(t)$ (and hence $\chi(t)$) is not so trivial. In fact $\phi(t)$ is Sommerfeld's solution for the diffraction of a plane wave about an infinitesimally thin half-plane (see[3]), i.e.

$$\phi(t) = \tfrac{1}{2}\left[(-i\pi t)^{-\frac{1}{2}} \exp(it) + \frac{2\left[C\left(\sqrt{\frac{2t}{\pi}}\right) + iS\left(\sqrt{\frac{2t}{\pi}}\right)\right]}{1 + i}\right],$$

where $C(z)$ and $S(z)$ are Fresnel integrals defined as in[1] by

$$C(z) = \int_0^z \cos\frac{\pi}{2}\xi^2 \, d\xi$$

$$S(z) = \int_0^z \sin\frac{\pi}{2}\xi^2 \, d\xi \ .$$

Thus for large k,

$$\begin{aligned}\frac{P(\xi)}{k} \sim -\tfrac{1}{2} + \tfrac{1}{2}\Bigg[&\left(-i\pi k(1 + \xi)\right)^{-\frac{1}{2}} \exp(ik(1 + \xi)) \\ &+ \frac{2\left[C\left(\sqrt{\frac{2k(1 + \xi)}{\pi}}\right) + iS\left(\sqrt{\frac{2k(1 + \xi)}{\pi}}\right)\right]}{1 + i} \\ &+ \left(-i\pi k(1 - \xi)\right)^{-\frac{1}{2}} \exp(ik(1 - \xi)) \\ &+ \frac{2\left[C\left(\sqrt{\frac{2k(1 - \xi)}{\pi}}\right) + iS\left(\sqrt{\frac{2k(1 - \xi)}{\pi}}\right)\right]}{1 + i}\Bigg]. \qquad (1.6.2)\end{aligned}$$

1.7 DESCRIPTION OF COMPUTED OUTPUT

The real and imaginary parts of the unknown function $P(\xi)$ as computed for various values of k are shown in figures 1 - 10.

Figures 1 and 2 show the real and imaginary parts respectively of $P(\xi)$ for small values of k ranging from k = 0.01 to k = 1.0, together with the low asymptote solution evaluated at k = 0.01.

In figures 3 - 10 the real and imaginary parts of $\frac{P(\xi)}{k}$ calculated for k = 5.0, 10.0, 100.0, and 1000.0 are plotted separately, together with their high asymptotic analytic equivalents.

It is seen that at low values of k both the real and imaginary parts of $P(\xi)$ are concave curves. As k increases, the curves gradually flatten out, until at about k = 5 where they begin to bend back, giving an oscillation. From here, more oscillations develop as k increases, although the central loop becomes more dominant, and the curves do not begin to break off towards their square root singularities until they get closer to $\xi = \pm 1$.

When k reaches values of the order of 100.0 to 1000.0 the number of oscillations becomes too large for the function $P(\xi)$ to be plotted smoothly with only 49 grid points, which was the largest number used in the program.

It is interesting to compare the numerical values with the analytic values at the high and low values of k. At k = 0.01 the analytic solution is a concave curve very similar to the numerical solution, especially for values of ξ near $\xi = 0$. For instance the

analytic solution at $\xi = 0$ is 0.02471 + 0.8518 i whereas the corresponding numerical solution is 0.0247 + 0.8511 i with N = 21, and 0.02471 + 0.8516 i with N = 49.

Due to the oscillatory nature of the solution for high k it is hardly surprising that some degree of numerical instability is evident here, for the assumption that $P(\xi) = P_j$ = constant on each subinterval is no longer really valid, even when 49 intervals are used. In fact when k = 1000.0, the real part of $\frac{P(0)}{k}$ was computed inaccurately as 0.4971 for N = 21 and 0.4905 for N = 49, compared with the value of 0.5000 predicted by the analytic solution (1.6.2) for the high asymptote.

In view of the fact that there is already very close agreement between the numerical and the high frequency asymptotic solutions when k is as small as 5.0 (the asymptotic value here of $\frac{P(0)}{k}$ is 0.5161 + 0.0170 i compared with the numerical solution for N = 49 of 0.5162 + 0.0172 i), it is suggested that the asymptotic solution for the high frequency is more reliable than the numerical solution when k is (say) $\geq$ 5.0.

1.8 FARFIELD INTENSITY DIAGRAMS

As a further check on the numerical solution, we recompute the farfield intensity diagrams which were obtained by Morse and Rubenstein [13]. These authors used the exact analytic solution to the boundary value problem, expressed as a series of Mathieu functions.

Two preliminary results are needed. The first is the asymptotic expansion of the Hankel function for large argument, viz.

$$H_o^{(1)}(kR) \sim \sqrt{\frac{2}{\pi kR}}\, e^{ikR - i\frac{\pi}{4}}, \quad R \to \infty . \qquad (1.8.1)$$

Also, we need the relation

$$\begin{aligned} R^2 &= (x - \xi)^2 + y^2 \\ &= R_o^2 - 2x\xi + \xi^2 \quad \text{where} \quad R_o^2 = x^2 + y^2 \\ &= R_o^2 \left(1 - \frac{2\xi \cos\theta}{R_o} + O(R_o^{-2})\right), \quad R \to \infty , \end{aligned}$$

i.e.

$$R \sim R_o\left(1 - \frac{\xi \cos\theta}{R_o}\right) = R_o - \xi \cos\theta$$

$$\text{as } R \to \infty \qquad (1.8.2)$$

$$(\text{where } x = R_o \cos\theta).$$

Substituting (1.8.1) and (1.8.2) into the equation

$$\phi_2(x,y) = \int_{-1}^{1} P(\xi) H_o^{(1)}(kR)\, d\xi \qquad (1.8.3)$$

we have, letting $R \to \infty$

$$\begin{aligned} \phi_2(x,y) &\sim \sqrt{\frac{2}{\pi kR_o}}\, e^{-i\frac{\pi}{4}}\, e^{ikR_o} \int_{-1}^{1} e^{-ik\xi\cos\theta}\, P(\xi)\, d\xi \\ &= \frac{G(\theta) e^{ikR_o}}{\sqrt{R_o}} . \qquad (1.8.4) \end{aligned}$$

where

$$G(\theta) = \sqrt{\frac{2}{\pi k}}\ e^{-i\frac{\pi}{4}} \int_{-1}^{1} e^{-ik\xi\cos\theta}\, P(\xi)d\xi \ . \qquad (1.8.5)$$

By plotting $I = |G(\theta)|^2$ against θ we then have the farfield intensity scattering diagrams. The plots for k = 1,2 and 4 are shown in figure 11, and these are seen to agree in shape with those of Morse and Rubenstein.

1.9 CONCLUSIONS

The big advantage in using this technique is that it gives accurate solutions in the range of k where the wavelength of the oncoming waves is of the same order as the length of the ribbon, i.e. in the range of k between the regions where the low and high asymptotic theories are valid.

It has been shown that the method can also be used when k is small, but that it is really more reliable to use the high frequency asymptotic solution when k > 5.

It will be seen in the following chapters that this method can be adapted to solving similar diffraction problems with different boundary conditions. It will be further seen that these problems can represent the diffraction of water waves around ships' hulls, especially in shallow water. In this case the wavelengths will often be of the order of the length of the ship, which corresponds to k = O(1).

CHAPTER 2

NEUMANN BOUNDARY CONDITION ON THE RIBBON

2.1 INTRODUCTION

In this chapter, the method described in Chapter 1 is used to solve the complementary problem, i.e. one with the same geometry, but a Neumann boundary condition on the ribbon.

From the point of view of ship hydrodynamics, the Neumann problem is more relevant than the Dirichlet, being in fact directly applicable to cases when a ship is touching the sea floor. In the acoustic context the Dirichlet problem would have corresponded to a "soft" ribbon (e.g. see Morse and Ingard[12]), whereas the Neumann problem corresponds to a "hard" ribbon. In the electromagnetic context, one may consider the Dirichlet problem to correspond to the case of diffraction of an E-polarised wave about a perfectly conducting ribbon, with the Neumann problem the same, except that the incident wave is H-polarised.

Low and high frequency asymptotic solutions are also obtained in this chapter, and compared with corresponding numerical solutions.

2.2 THE BOUNDARY VALUE PROBLEM

We assume the same geometry and incident wave as in Chapter 1. If as before ϕ_1 and ϕ_2 represent the velocity potentials of the incident and diffracted waves once sinusoidal time dependence has been removed, and $\phi = \phi_1 + \phi_2$, then as before we have that ϕ_1, ϕ_2 and ϕ all satisfy

$$(\nabla^2 + k^2)\phi = 0$$

outside the surface S . (2.2.1)

If we assume that the Neumann boundary condition

$$\frac{\partial \phi}{\partial y} = 0$$

holds on the surface S , (2.2.2)

then since $\frac{\partial \phi_1}{\partial y} = -ik$ on S, the scattered amplitude satisfies

$$\frac{\partial \phi_2}{\partial y} = ik$$

on the surface S. (2.2.3)

Equations (2.2.1) for ϕ_2 and (2.2.3) do not have a unique solution unless we say something further about the behaviour of ϕ_2 near the ends. A discussion on this aspect of the problem follows, and the value of $\phi_2(\pm 1, 0)$ is shown to be zero.

2.3 DERIVATION OF THE INTEGRAL EQUATION

To derive the integral representation of the above problem, we use Green's Theorem for the Helmholtz equation (2.2.1), viz.

$$\phi_2(x,y) = \int_C \left[\phi_2(\xi,\eta)\,\frac{\partial G}{\partial n}(x,y;\xi,\eta) - \frac{\partial \phi_2}{\partial \eta}(\xi,\eta)G(x,y;\xi,\eta)\right] d\ell \qquad (2.3.1)$$

where

$$G(x,y;\xi,\eta) = -\frac{i}{4} H_o^{(1)}(kR) \qquad (2.3.2)$$

and

$$R = \sqrt{(x-\xi)^2 + (y-\eta)^2}\ . \qquad (2.3.3)$$

C is any closed curve surrounding fluid in the (ξ,η) plane, chosen as in fig. 12, $\frac{\partial}{\partial n}$ represents differentiation normal to the curve C, and $d\ell$ is an element of arc along C.

The contributions along C_2 and C_5 cancel each other, and that along C_1 (at infinity) vanishes because ϕ_2 and G both represent dispersing outgoing waves.

Thus the only contribution to the integral comes from C_3 and C_4, i.e. the upper and lower faces of the ribbon, and

$$\phi_2(x,y) = \frac{i}{4}\int_{-1}^{1}\left[\phi_2(\xi,0+)\,\frac{\partial}{\partial \eta} H_o^{(1)}(kR) - \frac{\partial \phi_2}{\partial \eta}(\xi,0+)H_o^{(1)}(kR)\right] d\xi$$

$$-\frac{i}{4}\int_{-1}^{1}\left[\phi_2(\xi,0-)\,\frac{\partial}{\partial \eta} H_o^{(1)}(kR) - \frac{\partial \phi_2}{\partial \eta}(\xi,0-)H_o^{(1)}(kR)\right] d\xi \qquad (2.3.4)$$

and using (2.2.2) and (2.2.3),

$$\phi_2(x,y) = \frac{i}{2}\int_{-1}^{1} P(\xi)\,\frac{\partial}{\partial \eta} H_o^{(1)}(kR)\,d\xi \qquad (2.3.5)$$

where

$$P(\xi) = \tfrac{1}{2}(\phi_2(\xi,0+) - \phi_2(\xi,0-))\ . \qquad (2.3.6)$$

Now it follows immediately from (2.3.5) that $\phi_2(x,y)$ is anti-symmetric in y, i.e.

$$\phi_2(x,y) = - \phi_2(x,y).$$

Thus, combining this and (2.3.6), $P(\xi) = \phi_2(\xi,0+)$, and hence the integral equation (2.3.5) becomes

$$\phi_2(x,y) = \frac{i}{2} \int_{-1}^{1} \phi_2(\xi,0+) \frac{\partial}{\partial \eta} H_o^{(1)}(kR) d\xi \ . \qquad (2.3.7)$$

This integral equation in its present form is unsuitable for numerical integration. However, using the fact that under the integral sign

$$\frac{\partial}{\partial \eta} = - \frac{\partial}{\partial y} \ , \qquad (2.3.8)$$

equation (2.3.7) becomes,

$$\phi_2(x,y) = - \frac{i}{2} \frac{\partial}{\partial y} \int_{-1}^{1} \phi_2(\xi,0+) H_o^{(1)}(kR) d\xi \ . \qquad (2.3.9)$$

Thus

$$\phi_2(x,y) = \frac{\partial \psi_2}{\partial y} (x,y) \qquad (2.3.10)$$

where

$$\psi_2(x,y) = - \frac{i}{2} \int_{-1}^{1} \phi_2(\xi,0+) H_o^{(1)}(kR) d\xi \ . \qquad (2.3.11)$$

Since $\psi_2(x,y)$ satisfies Helmholtz's equation,

$$\begin{aligned} \frac{\partial^2 \psi_2}{\partial x^2} (x,y) + k^2 \psi_2(x,y) &= - \frac{\partial^2 \psi_2}{\partial y^2} (x,y) \\ &= - \frac{\partial \phi_2}{\partial y} (x,y) \\ &= - ik \quad \text{when} \quad |x| < 1, \quad y = 0+ \end{aligned} \qquad (2.3.12)$$

and so

$$\psi_2(x,0+) = -\frac{i}{k} + A_1 \cos kx + B_1 \sin kx \quad , \qquad (2.3.13)$$

where A_1 and B_1 are arbitrary constants.

Thus, on the upper surface of the ribbon, equation (2.3.11) becomes

$$-\frac{i}{k} + A_1 \cos kx + B_1 \sin kx = -\frac{i}{2}\int_{-1}^{1} \phi_2(\xi,0+)H_o^{(1)}(k|\xi - x|)d\xi \ . \qquad (2.3.14)$$

If the constants A_1 and B_1 were known, this equation could be solved for $\phi_2(\xi,0+)$ using the same method as in Chapter 1. If we assume fore-and-aft symmetry we can set $B_1 = 0$. Because of the anti-symmetry property of $\phi_2(x,y)$, we have that $\phi_2(x,0+) = 0$ when $|x| > 1$, and so, assuming continuity of $\phi_2(x,y)$ at the end of the ribbon, it is necessary that $\phi_2(\pm 1,0+) = 0$. Thus a constant A_1 must be found such that this relation holds.

2.4 THE CALCULATION OF THE CONSTANT A_1

If we set $B_1 = 0$, equation (2.3.14) can be rewritten as

$$-\frac{i}{2}\int_{-1}^{1} \phi_2(\xi,0+)H_o^{(1)}(k|\xi - x|)d\xi = -\frac{i}{k}(1 + A \cos kx)$$

where

$$A = -\frac{k}{i}A_1 = ikA_1 \quad , \qquad (2.4.1)$$

i.e.

$$\int_{-1}^{1} Q(\xi)H_o^{(1)}(k|\xi - x|)d\xi = 1 + A\cos kx \qquad (2.4.2)$$

where

$$Q(\xi) = \frac{k}{2}\,\phi_2(\xi,0+) \ .$$

In practice we solve (2.4.2) separately with 1 on the R.H.S. giving a solution $Q_1(\xi)$ and with coskx on the R.H.S. giving a solution $Q_2(\xi)$. The solution of (2.4.2) is then $Q(\xi) = Q_1(\xi) + AQ_2(\xi)$, and we must have that $Q(\pm 1) = 0$; hence A must be such that

$$A = -\lim_{\xi\uparrow 1}\frac{Q_2(\xi)}{Q_1(\xi)} = -\lim_{\xi\downarrow -1}\frac{Q_2(\xi)}{Q_1(\xi)} \ . \qquad (2.4.3)$$

A simple way of calculating A is therefore to set

$$A = -\frac{Q_2(\xi_o')}{Q_1(\xi_o')} = -\frac{Q_2(\xi_{N-1}')}{Q_1(\xi_{N-1}')} \ , \qquad (2.4.4)$$

where ξ_o' and $\xi_{N-1}' = -\xi_o'$ are respectively the mid-points of the first and last intervals into which the strip $|\xi| < 1$ is divided during the numerical analysis (see Section 1.4).

This method has some drawbacks from the numerical point of view. In Chapter 1 it was established that the numerical solutions of integral equations such as (2.4.2) were accurate near $\xi = 0$. In fact, however, this is a region in which the highest accuracy is obtained, as this is a region in which the source strength is generally most nearly a "constant". At $\xi = \pm 1$, the solutions of such integral equations generally tend in an oscillatory manner to square root singularities, and the numerical accuracy of the computed values is less than near the centre of the strip. We now derive a more accurate formula for A, which will depend more on the values of the solution

at all arguments, and thus be less critically dependent on the dubious values near the ends.

Differentiating (2.4.2) with respect to x gives

$$\int_{-1}^{1} Q(\xi) \frac{\partial}{\partial x} H_o^{(1)}(k|\xi - x|)d\xi = - kA \sin kx \qquad (2.4.5)$$

and hence

$$\int_{-1}^{1} Q(\xi)\left(- \frac{\partial}{\partial \xi}\right) H_o^{(1)}(k|\xi - x|)d\xi = - kA \sin kx \, . \qquad (2.4.6)$$

Integrating by parts, and assuming that $Q(\pm 1) = 0$, i.e. $\phi_2(\pm 1, 0+) = 0$, gives

$$\int_{-1}^{1} \frac{\partial Q}{\partial \xi} (\xi) H_o^{(1)}(k|\xi - x|)d\xi = - kA \sin kx \, , \qquad (2.4.7)$$

i.e. we can solve for $\frac{\partial Q}{\partial x} = \frac{k}{2} \frac{\partial \phi_2}{\partial x} (x, 0+)$ on the ribbon (except for a constant factor), and finally calculate ϕ_2 by using

$$\phi_2(x, 0+) = \int_{-1}^{x} \frac{\partial \phi_2}{\partial \xi} (\xi, 0+)d\xi \, . \qquad (2.4.8)$$

(Note that this immediately implies that $\phi_2(-1, 0+) = 0$, and also that $\phi_2(+1, 0+) = 0$, because $\frac{\partial \phi_2}{\partial x} (x, 0+)$ will be odd.)

Now if $Q_1(x)$ and $Q_2(x)$ are the solutions of (2.4.2) with 1 and coskx respectively on the R.H.S., we can write

$$Q(x) = Q_1(x) + AQ_2(x)$$

$$= \int_{-1}^{x} \frac{\partial Q}{\partial \xi} (\xi)d\xi \, . \qquad (2.4.9)$$

Thus, if $Q_3(x)$ is the solution of (2.4.2), with sinkx on the R.H.S., then

$$\frac{\partial Q}{\partial x} = - kAQ_3 \quad . \tag{2.4.10}$$

Combining (2.4.9) and (2.4.10),

$$Q_1(x) + AQ_2(x) = - kA \int_{-1}^{x} Q_3(\xi)d\xi \quad , \tag{2.4.11}$$

and thus

$$A = - \frac{Q_1(x)}{Q_2(x) + k \int_{-1}^{x} Q_3(\xi)d\xi} \quad . \tag{2.4.12}$$

This is the formula we set out to obtain. Note that in particular

$$A = - \frac{Q_1(0)}{Q_2(0) + k \int_{-1}^{0} Q_3(\xi)d\xi} \, , \tag{2.4.13}$$

the major contribution to which comes from solutions to integral equations of type (2.4.2) evaluated at or near $\xi = 0$.

In summary, the present method requires us to solve an integral equation such as (2.4.2) three times, i.e.

$$\int_{-1}^{1} Q_j(\xi) H_o^{(1)}(k|\xi - x|)d\xi = F_j(x), \quad j = 1,2,3,$$

where

$$F_1(x) = 1$$
$$F_2(x) = \text{coskx} \tag{2.4.14}$$

and

$$F_3(x) = \text{sinkx} \quad .$$

This takes very little extra time compared with a solution with only one right-hand side, since the same inverted kernel matrix can be used. Once the three solutions Q_1, Q_2, Q_3 are determined, the quotient (2.4.12) is computed. This expression should be independent of x, and the extent to which it is not is a measure of numerical inaccuracy. Setting A equal to some averaged measure of this quotient (or, as in (2.4.13), equal to its value at the centre, $\xi = 0$), the solution follows from (2.4.9).

2.5 THE LOW AND HIGH FREQUENCY ASYMPTOTES

In this section we derive an analytic solution for the integral equation (2.4.2) for the low frequency asymptote ($k \to 0$) and deduce a corresponding analytic expression for the constant A. We also give an analytic solution for the high frequency asymptote ($k \to \infty$).

To obtain the low frequency asymptotic solution, we substitute into (2.4.2) the small argument expansion of the kernel, viz.

$$H_o^{(1)}(z) \sim \frac{2i}{\pi} \log \frac{z}{2} + \frac{2i\gamma}{\pi} + 1 \quad \text{as} \quad z \sim 0 \ , \qquad (2.5.1)$$

giving

$$\int_{-1}^{1} Q(\xi) \left[\frac{2i}{\pi} \log \left(\frac{k}{2} |\xi - x| \right) + \frac{2i\gamma}{\pi} + 1 \right] d\xi = 1 + A \cos kx . \qquad (2.5.2)$$

Differentiating with respect to x gives

$$\frac{2i}{\pi} \int_{-1}^{1} \frac{Q(\xi)}{\xi - x} \, d\xi = - kA \sin kx \ ,$$

i.e.

$$\frac{1}{\pi}\int_{-1}^{1}\frac{Q(\xi)}{\xi - x}\,d\xi = -\frac{ikA}{2}\sin kx$$

$$\sim \frac{ik^2Ax}{2} \text{ for } k \sim 0,\ |x| < 1\ . \qquad (2.5.3)$$

This integral equation can be solved readily (e.g. see Tricomi[16], page 180), giving

$$Q(\xi) = \tfrac{1}{2}ik^2A\sqrt{1 - \xi^2}\ , \qquad (2.5.4)$$

where ~~A has been chosen so as to ensure that $Q(\pm 1) = 0$.~~ that particular solution has been chosen which satisfies $Q(\pm 1) = 0$.

PJT

But (2.5.4) is only a solution of the original equation (2.5.2) if

$$\int_{-1}^{1}\tfrac{1}{2}ik^2A\sqrt{1 - \xi}\left[\frac{2i}{\pi}\log\left(\frac{k}{2}|\xi - x|\right) + \frac{2i\gamma}{\pi} + 1\right]d\xi$$

$$= 1 + A\cos kx\ , \qquad (2.5.5)$$

i.e.

$$A = \frac{2Q(0)}{ik} = \frac{1}{-1 + \int_{-1}^{1}\tfrac{1}{2}ik^2\sqrt{1 - \xi^2}\left[\frac{2i}{\pi}\log\left(\frac{k}{2}|\xi|\right) + \frac{2i\gamma}{\pi} + 1\right]d\xi}\ , \qquad (2.5.6)$$

i.e., using the relations

$$\int_{-1}^{1}\sqrt{1 - \xi^2}\,d\xi = \frac{\pi}{2}\ ,$$

$$\int_{-1}^{1}\sqrt{1 - \xi^2}\,\ln|\xi|\,d\xi = -\frac{\pi}{4} - \frac{\pi}{2}\ln 2\ ,$$

$$A = \frac{1}{-1 + k^2(\log 2 + \tfrac{1}{4} - \frac{\gamma}{2} + \frac{i\pi}{4}) - \tfrac{1}{2}k^2 \log k}, \qquad (2.5.7)$$

i.e.

$$A = -1 + C_1 k^2 \log k + C_2 k^2 + O(k^4)$$

where $$C_1 = \tfrac{1}{2} \qquad (2.5.8)$$

$$C_2 = -\log 2 - \tfrac{1}{4} + \frac{\gamma}{2} - \frac{i\pi}{4} .$$

Equation (2.5.8) is a low frequency asymptotic solution for the constant A, and together with (2.5.4), this forms a low frequency asymptotic solution for $Q(\xi)$.

The high frequency asymptotic solution for $Q(\xi)$ will merely be stated. It can be obtained from Sommerfeld's solution of the semi-infinite ribbon diffraction problem for electromagnetic waves (see Born and Wolf[3]) in a manner similar to that described in Chapter 1 for the corresponding Dirichlet boundary value problem.

The solution of (2.4.2) as $k \sim \infty$ is

$$\frac{Q(\xi)}{k} \sim \tfrac{1}{2} - \frac{1}{1+i}\left[C\left(\sqrt{\frac{2k(1+\xi)}{\pi}}\right) + iS\left(\sqrt{\frac{2k(1+\xi)}{\pi}}\right)\right]$$

$$- \frac{1}{1+i}\left[C\left(\sqrt{\frac{2k(1-\xi)}{\pi}}\right) + iS\left(\sqrt{\frac{2k(1-\xi)}{\pi}}\right)\right], \qquad (2.5.9)$$

where C, S denote Fresnel integrals as in Section (1.6).

2.6 DESCRIPTION OF COMPUTED OUTPUT

The constant A was calculated for values of k from 0.001 to 1000.0 using equation (2.4.12) for various values of x.

It was found that for very low values of k, the values of A calculated were most nearly constant for all x. This constancy gradually decreased until there were significant variations for the values k = 100.0 and k = 1000.0.

In the limit as $k \to 0$ it was observed that $A \to -1$, this result agreeing with that predicted from the asymptotic value in (2.5.8). This means that as $k \to 0$, the R.H.S. of equation (2.4.2) $\to 0$, and so the solution $\phi_2(x,0+) \to 0$ for $|x| < 1$.

For values of $k < 0.1$, (2.4.12) gave results for A constant to 4 significant figures for all x. The numerical and asymptotic values for A agreed almost exactly; for example, at k = 0.1 these values were $-1.0182 - 0.0080\,i$ and $-1.0181 - 0.0079\,i$ respectively.

Through the middle-order frequencies ($0.1 < k < 10.0$) the consistency of the calculations dropped until at k = 10.0 only two significant figures could be relied upon. However, the values of A remained constant in a region around x = 0.

It is thus apparent that the numerical procedure leads to a solution which, at low values of k, agrees with the analytic solution for the low frequency asymptote. However it is obvious that the numerical procedure is going to be unreliable at high frequencies, and that at these frequencies the solution should be evaluated by

(2.5.9). The only question thus remaining is then: which is the most convenient value of k at which to change over from a numerical solution to the high frequency asymptotic solution, and then what is the discrepancy between the two solutions at this changeover point.

We recall that in Chapter 1, the high frequency asymptotic solution for the Dirichlet problem was shown to be accurate to 4 significant figures at k = 5.0, and in fact it was suggested that this should be used instead of the numerical solution for $k \geq 5.0$.

In figures 13 and 14, the numerical and analytic solutions to the Neumann problem at k = 5.0 are shown. It is noted that the two solutions do not agree as closely as the corresponding solutions for the unknown function in the Dirichlet problem. This appears to be due to inability to make a sufficiently accurate calculation of the term

$$\int_{-1}^{x} Q_3(\xi)d\xi$$

in equation (2.4.12), as several different quadrature formulae for evaluating this term resulted in different numerical solutions to the Neumann problem, which varied by amounts of the same order as the difference between the two solutions in figs. 13 and 14.

However, the solutions of figs. 13 and 14 show reasonable agreement throughout the range of the solution, and in fact all the characteristics of the asymptotic solution, such as maxima, minima,

and points of inflexion, are also strongly evident in the numerical solution.

Finally, it should be remarked that we cannot be at all sure that the asymptotic solution is sufficiently accurate at a frequency as low as $k = 5.0$ to provide a check on the numerical solution. Some evidence suggesting that one should perhaps go to a higher frequency is apparent from the fact that the asymptotic solution itself does not quite vanish at the end $\xi = 1$ in figure 14. Thus we may observe that the asymptotic solution and the numerical calculation differ by a small amount from each other and probably by a similar amount from the exact solution at $k = 5.0$.

2.7 CONCLUSIONS

It has been shown that the numerical procedure used to solve the Dirichlet diffraction problem, as in Chapter 1, can be extended so that the complementary problem with a Neumann boundary condition can also be solved.

Accuracy of the method is very good in the low frequency asymptote region, and gradually decreases until it is accurate to about 2 significant figures for $\xi = 0$ at $k = 5.0$. The high frequency asymptotic solution may then be more reliable for $k > 5.0$, and naturally this becomes more accurate as k increases.

As will become more apparent later, this problem can be directly applied to cases when waves are being diffracted about ships which are touching the sea floor.

CHAPTER 3

A MIXED BOUNDARY CONDITION ON THE RIBBON

3.1 INTRODUCTION

In this final chapter of Part 1, we show how the method of solving the previous two diffraction problems can be extended to solve a third and more difficult diffraction problem, i.e. one with a mixed boundary condition on the ribbon.

The previous two problems were classical problems which had already been dealt with in literature on acoustic diffraction, e.g. by Morse and Rubenstein [13] and Hönl, Maue and Westphal [9]. In the literature appear many physical applications, e.g. to electro magnetic and acoustic waves, which are equivalent to the problems solved in Chapters 1 and 2. In all of these cases, however, the ribbon may be regarded as a rigid, impenetrable object, through which no fluid or energy may pass. In the case of ship hydrodynamics, as will become more apparent in Part 2, there is no physical problem equivalent to the Dirichlet problem, but the Neumann problem is equivalent to cases where waves are being diffracted about ships which are actually touching the sea floor, i.e. no fluid or energy is allowed to pass through or under the ship.

The introduction of a mixed boundary condition will open the possibility of allowing fluid and energy to pass through the ribbon. Thus this will be equivalent to a problem of diffraction of, e.g.

acoustic waves about a permeable strip, or of electromagnetic waves about a strip of variable impedance. In the theory of ship motions in shallow water, the relevant problem is that of diffraction of waves about a ship which is not touching the bottom, i.e. fluid and energy is able to pass underneath the ship in a manner dependent on the geometry of the ship.

The ship motions problem will be dealt with in Part 3. In this chapter the mixed boundary value problem will merely be formulated and solved by a method which is an extension of that used in Chapters 1 and 2. As no general procedure appears to be available in the literature for solving this type of problem, testing of the numerical method cannot be as satisfactory as before. However the general integral equation is shown to reduce to a more simple integral equation in the low frequency asymptote region, with a known analytic solution, and it will be seen that an excellent test of the numerical method can be obtained in this region.

3.2 THE BOUNDARY VALUE PROBLEM

In this chapter we shall use the same geometry as in the previous two chapters, i.e. the X-Y plane, with a ribbon S, of length 2 and negligible thickness, lying in the region $|x| < 1$, $y = 0$.

We do not state at this stage what the incident wave looks like, except to say that it has frequency k, and is plane, with wave-fronts parallel to the X-axis. As in the previous two chapters we assume

that due to the presence of the ribbon there will be a diffracted potential $\phi_2(x,y)$ which satisfies

$$\left(\frac{\partial^2}{\partial x^2} + \frac{\partial^2}{\partial y^2} + k^2\right) \phi_2(x,y) = 0 \ . \qquad (3.2.1)$$

In this chapter we wish to solve the same problem as in the previous two chapters, but this time with the mixed boundary condition

$$\frac{\partial \phi_2}{\partial y}(x,0\pm) = 1 \pm \frac{\phi_2(x,0\pm)}{C(x)}$$

$$\text{for} \quad |x| \leq 1 \ . \qquad (3.2.2)$$

As will be seen in a later chapter, $C(x)$ can be regarded as a "blockage" or "inverse porosity" coefficient of the ribbon at the point x. In other words a decrease in $C(x)$ represents an increase in the amount of flow possible through the ribbon at point x. In the ship motions problem, $C(x)$ is directly computable from the geometry of the ship. However discussion of this aspect of the problem follows later, and for the purposes of this chapter we will assume $C(x)$ to be given.

We will also apply the condition

$$\frac{\partial \phi_2}{\partial y}(x,0+) = \frac{\partial \phi_2}{\partial y}(x,0-), \quad |x| < 1 \ ; \qquad (3.2.3)$$

i.e. we assume that there is no jump in the normal derivative of the potential across the ribbon.

3.3 INTEGRAL FORMULATION OF THE PROBLEM

By use of Green's Theorem for the Helmholtz equation (3.2.1) we have for the scattered potential $\phi_2(x,y)$,

$$\phi_2(x,y) = \int_C \left[\phi_2(\xi,\eta)\,\frac{\partial}{\partial n}\,G(x,y;\xi,\eta) - \frac{\partial\phi_2}{\partial n}\,(\xi,\eta)G(x,y;\xi,\eta)\right]d\ell\ , \tag{3.3.1}$$

where

$$G(x,y;\xi,\eta) = -\tfrac{1}{4}\,i\,H_o^{(1)}(kR)\ , \tag{3.3.2}$$

with

$$R = \sqrt{(x-\xi)^2 + (y-\eta)^2}\ . \tag{3.3.3}$$

The curve C is any closed curve surrounding fluid in the (ξ,η) plane, and will be chosen as in Figure 12, while $d\ell$ is an element of arc along C.

In fact the only contribution to the above integral comes from the top and bottom faces C_3 and C_4 of the ribbon. This is because the integrals along C_2 and C_5 cancel each other and that along C_1 (at infinity) is zero because both ϕ_2 and G represent dispersing outgoing waves. Thus

$$\phi_2(x,y) = \frac{i}{4}\int_{-1}^{1}\left[\phi_2(\xi,0+)\,\frac{\partial}{\partial\eta}\,H_o^{(1)}(kR) - \frac{\partial\phi_2}{\partial\eta}\,(\xi,0+)H_o^{(1)}(kR)\right]d\xi$$

$$-\frac{i}{4}\int_{-1}^{1}\left[\phi_2(\xi,0-)\,\frac{\partial}{\partial\eta}\,H_o^{(1)}(kR) - \frac{\partial\phi_2}{\partial\eta}\,(\xi,0-)H_o^{(1)}(kR)\right]d\xi\ , \tag{3.3.4}$$

$\left(R = \sqrt{(x - \xi)^2 + (y - \eta)^2}\right)$, or, using the jump condition (3.2.3),

$$\phi_2(x,y) = \frac{i}{2} \int_{-1}^{1} P(\xi) \frac{\partial}{\partial \eta} H_o^{(1)}(kR) d\xi \ , \qquad (3.3.5)$$

where

$$P(\xi) = \tfrac{1}{2}\left[\phi_2(\xi,0+) - \phi_2(\xi,0-)\right] \ . \qquad (3.3.6)$$

From (3.3.5) it follows immediately that $\phi_2(x,y)$ is antisymmetric with respect to y, i.e. $\phi_2(x, -y) = -\phi_2(x,y)$. In particular we have $\phi_2(x,0+) = -\phi_2(x,0-)$, and hence from (3.3.6)

$$P(\xi) = \phi_2(\xi,0+) \ . \qquad (3.3.7)$$

A further result of the antisymmetry of $\phi_2(x,y)$ is that $\phi(x,0\pm) = 0$ for $|x| > 1$, and hence due to continuity

$$\phi_2(\pm 1,0) = 0 \ . \qquad (3.3.8)$$

Since, under the integral sign in (3.3.5), $\frac{\partial}{\partial \eta} = -\frac{\partial}{\partial y}$, we can rewrite (3.3.5) as

$$\psi(x,y) = -\frac{i}{2} \int_{-1}^{1} \phi_2(\xi,0+) H_o^{(1)}(kR) d\xi \ , \qquad (3.3.9)$$

where

$$\phi_2(x,y) = \frac{\partial \psi}{\partial y} \ (x,y) \ . \qquad (3.3.10)$$

Clearly, ψ must satisfy the Helmholtz equation as well as ϕ_2, and hence

$$\frac{\partial^2\psi}{\partial x^2}(x,0+) + k^2\psi(x,0+) = -\frac{\partial^2\psi}{\partial y^2}(x,0+)$$

$$= -\frac{\partial\phi_2}{\partial y}(x,0+)$$

$$= -1 - \frac{\phi_2(x,0+)}{C(x)} \qquad (3.3.11)$$

(using the boundary condition (3.2.2)). Equation (3.3.11) has solution

$$\psi(x,0+) = -\frac{1}{k^2} - \frac{1}{k}\int_0^x \frac{\phi_2(\xi,0+)}{C(\xi)} \sin k(\xi - x)d\xi$$

$$+ A\cos kx + B\sin kx \; . \qquad (3.3.12)$$

Thus, evaluating the integral equation (3.3.9) on $y = 0+$ gives

$$-\frac{i}{2}\int_{-1}^{1}\phi_2(\xi,0+)H_0^{(1)}(k|\xi - x|)d\xi + \frac{1}{k}\int_0^x \frac{\phi_2(\xi,0+)}{C(\xi)} \sin k(x - \xi)d\xi$$

$$= -\frac{1}{k^2} + A\cos kx + B\sin kx \; . \qquad (3.3.13)$$

This is the integral equation we must solve, where A and B must be found subject to (3.3.8). A method for solution follows in the next section.

3.4 THE NUMERICAL METHOD

It is readily seen that (3.3.13) is of the form

$$\int_{-1}^{1}\phi_2(\xi,0+)K(x,\xi;k)d\xi = H(x) \; , \qquad (3.4.1)$$

where $K(x,\xi;k)$ has a logarithmic singularity at $\xi = x$. Equation (3.4.1) thus has essentially the same properties as (1.3.2) and

(2.4.2) and can be solved by a further extension of the methods which have been given for their solution.

The main difficulties involved in solving (3.4.1) are in the evaluation of the R.H.S. H(x), and in the evaluation of the kernel matrix elements.

Due to the fact that the kernel is no longer a difference kernel, as it was in the Neumann diffraction problem, we can no longer find such an accurate method as was found then for the evaluation of the constant A. Also, since we do not want to assume fore-and-aft symmetry in the case of the ship motions problem we are not free in this problem to set B = 0.

The restriction on A and B is that they must be chosen so as to ensure that $\phi_2(\pm 1,0) = 0$. To do this we solve (3.4.1) separately with right hand sides $-\frac{1}{k^2}$, coskx and sinkx, giving solutions $R_1(x)$, $R_2(x)$ and $R_3(x)$ respectively. The condition that $\phi(\pm 1,0) = 0$ is thus equivalent to saying that

$$\left.\begin{aligned} R_1(1) + A\,R_2(1) + B\,R_3(1) &= 0 \\ R_1(-1) + A\,R_2(-1) + B\,R_3(-1) &= 0 \end{aligned}\right\} . \qquad (3.4.2)$$

Using the same notation for the grid under the integral we can say that $R_i(-1) \doteq R_i(\xi'_0)$ and $R_i(1) \doteq R_i(\xi'_{N-1})$, enabling estimates of A and B to be made by solution of the simultaneous linear equations (3.4.2) above.

Our experience in solving the Neumann problem tells us that the above method is not as satisfactory as one would like, as it depends on solutions of integral equations of type (3.4.1) near singularities. It would have been better if the method for calculating A and B depended on evaluations of such solutions taken nearer the centre of the range of integration, where we know the solutions are more nearly constant on each subinterval. However, our experience with the Neumann problem does tell us that we can expect reasonable results, at least up to medium-range frequencies.

3.5 EVALUATION OF THE KERNEL MATRIX ELEMENTS

The evaluation of the kernel matrix elements A_{kj} (using the notation of Chapters 1 and 2) becomes a more difficult task than in the Dirichlet and Neumann cases, due to the introduction of a new term to the kernel, which is of Volterra type. We can write the kernel as

$$K(x,\xi;k) = -\frac{i}{2} H_o^{(1)}(k|\xi - x|) + \frac{\varepsilon(\xi,x)}{k} \frac{\sin k(x - \xi)}{C(\xi)}$$

where $\varepsilon(\xi,x) = 1$ if $0 < x$ and $\xi \varepsilon(0,x)$

$= -1$ if $x < 0$ and $\xi \varepsilon(x,0)$

$= 0$ otherwise . (3.5.1)

To evaluate the elements A_{kj} we consider (3.3.13) and assume that $\phi_2(\xi,0+) = \text{constant} = R_j$ and that $C(\xi) = \text{constant} = C_j$ on each interval (ξ_j,ξ_{j+1}) (following the notation of Section 1.4). Equation (3.3.13) thus becomes

$$\sum_{j=0}^{N-1} R_j E_{kj} + \sum_{j=0}^{N-1} \frac{R_j}{C_j} D_{kj} = H_k, \quad k = 0,1, \ldots, N-1 , \tag{3.5.2}$$

where

$$E_{kj} = -\frac{i}{2} \int_{\xi_j}^{\xi_{j+1}} H_o^{(1)}(k|\xi - \xi_k'|)d\xi , \tag{3.5.3}$$

and

$$D_{kj} = \int_{\xi_j}^{\xi_{j+1}} \frac{\varepsilon(\xi,\xi_k')}{k} \sin k(\xi_k' - \xi)d\xi . \tag{3.5.4}$$

We then have a system of linear equations of type (1.4.2), with A_{kj} defined as

$$A_{kj} = E_{kj} + \frac{D_{kj}}{C_j} . \tag{3.5.5}$$

The evaluation of the elements E_{kj} presents no problems, as it is similar to the evaluation of the kernel matrix elements A_{kj} of Section 1.4. In fact,

$$E_{kj} = \frac{F(k(\xi_{j+1} - \xi_k')) - F(k(\xi_j - \xi_k'))}{k} , \tag{3.5.6}$$

where

$$F(z) = -\frac{i}{2} \int_o^z H_o^{(1)}(t)dt . \tag{3.5.7}$$

Because of the presence of the function $\varepsilon(\xi,\xi_k')$, some care is required if the most accurate analytic evaluation of the elements D_{kj} is to be made. We have to consider several distinct possibilities:

Case A: When $\varepsilon(\xi,\xi_k')$ changes in value in the interval (ξ_j,ξ_{j+1}).

(i) $\xi_k' < 0,\ \xi_k' \varepsilon (\xi_j, \xi_{j+1})$

Here,

$$D_{kj} = -\int_{\xi_k'}^{\xi_{j+1}} \frac{1}{k} \sin k\,(\xi_k' - \xi)\,d\xi$$

$$= -\frac{1}{k} G(k(\xi_k' - \xi_{j+1})) + \frac{1}{k} G(0)\ , \qquad (3.5.8)$$

where

$$G(z) = \frac{\cos z}{k}\ . \qquad (3.5.9)$$

(ii) $\xi_k' > 0,\ \xi_k' \varepsilon (\xi_j, \xi_{j+1})$

$$D_{kj} = \int_{\xi_j}^{\xi_k'} \frac{1}{k} \sin k\,(\xi_k' - \xi)\,d\xi$$

$$= \frac{1}{k} G(0) - \frac{1}{k} G(k(\xi_k' - \xi_j))\ . \qquad (3.5.10)$$

(iii) $\xi_k' < 0,\ 0 \varepsilon (\xi_j, \xi_{j+1})$

$$D_{kj} = -\int_{\xi_j}^{0} \frac{1}{k} \sin k\,(\xi_k' - \xi)\,d\xi$$

$$= -\frac{1}{k} G(k\xi_k') + \frac{1}{k} G(k(\xi_k' - \xi_j))\ . \qquad (3.5.11)$$

(iv) $\xi_k' > 0,\ 0 \varepsilon (\xi_j, \xi_{j+1})$

$$D_{kj} = \int_{0}^{\xi_{j+1}} \frac{1}{k} \sin k\,(\xi_k' - \xi)\,d\xi$$

$$= \frac{1}{k} G(k(\xi_k' - \xi_{j+1})) - \frac{1}{k} G(k\xi_k')\ . \qquad (3.5.12)$$

Case B: When $\varepsilon(\xi,\xi_k') = 0$ throughout the interval (ξ_j, ξ_{j+1}). This corresponds to the possibilities

(i) $\xi_k' = 0$.

(ii) $\xi_k' < 0$ and either (a) $\xi_{j+1} < \xi_k'$ or (b) $\xi_j > 0$.

(iii) $\xi_k' > 0$ and either (a) $\xi_{j+1} < 0$ or (b) $\xi_j > \xi_k'$.

In Case B it is clearly true that

$$D_{kj} = 0 . \tag{3.5.13}$$

Case C: When $\varepsilon(\xi,\xi_k') = 1$ throughout the interval (ξ_j, ξ_{j+1}). This corresponds to the possibility

$$0 < \xi_j < \xi_{j+1} < \xi_k' .$$

In this case,

$$D_{kj} = \int_{\xi_j}^{\xi_{j+1}} \frac{1}{k} \operatorname{sink} (\xi_k' - \xi)d\xi$$

$$= \frac{1}{k} G(k(\xi_k' - \xi_{j+1})) - \frac{1}{k} G(k(\xi_k' - \xi_j)). \tag{3.5.14}$$

Case D: When $\varepsilon(\xi,\xi_k') = -1$ throughout the interval (ξ_j, ξ_{j+1}). This corresponds to the possibility

$$\xi_k' < \xi_j < \xi_{j+1} < 0 .$$

In this case,

$$D_{kj} = \int_{\xi_j}^{\xi_{j+1}} \left(-\frac{1}{k}\right) \operatorname{sink} (\xi_k' - \xi)d\xi$$

$$= -\frac{1}{k} G(k(\xi_k' - \xi_{j+1})) + \frac{1}{k} G(k(\xi_k' - \xi_j)) . \tag{3.5.15}$$

Precise analytic evaluations of D_{kj} can now be made. It will thus be possible to make analytic evaluations of the kernel matrix elements A_{kj} with the aid of (3.5.5).

Figure 15 shows the structure of the matrix D_{kj}.

3.6 LOW AND HIGH FREQUENCY ASYMPTOTIC SOLUTIONS

In this section we use a different integral formulation of the boundary value problem in order to derive a solution at the low frequency asymptote ($k \to 0$). We then indicate briefly the expected behaviour of the solution at the high frequency asymptote ($k \to \infty$), where no general high asymptotic solution has yet been obtained for arbitrary $C(x)$.

For a low frequency asymptotic solution, we note from (3.2.2) that $\frac{\partial \phi_2}{\partial y}$ has the same value on each side of the ribbon. Thus, using the distribution of sources method, as in Section 1.3, we can derive the equation

$$\frac{\partial \phi_2}{\partial y}(x,y) = \frac{i}{2} \int_{-1}^{1} \frac{\partial^2 \phi_2}{\partial y^2}(\xi,0+)\, H_o^{(1)}(kR)\, d\xi \ , \qquad (3.6.1)$$

where $R = \sqrt{(x-\xi)^2 + y^2}$. Thus, forcing this equation to hold on the boundary, and applying (3.2.2), we obtain

$$1 + \frac{\phi_2(x,0+)}{C(x)} = \frac{-i}{2} \int_{-1}^{1} \left[\frac{\partial^2 \phi_2}{\partial \xi^2}(\xi,0+) + k^2 \phi_2(\xi,0+) \right] H_o^{(1)}(k|\xi - x|)\, d\xi . \qquad (3.6.2)$$

To determine the low frequency asymptotic behaviour of ϕ_2, we consider the small argument expansion of $H_o^{(1)}(z)$, viz.

$$H_o^{(1)}(z) \sim \frac{2i}{\pi} \log z + \frac{2i\gamma}{\pi} + 1 \quad \text{as } z \sim 0 , \qquad (3.6.3)$$

and let $k \to 0$ in equation (3.6.2), giving on integration by parts,

$$-\frac{i}{2} \int_{-1}^{1} \frac{\partial \psi_2}{\partial \xi}(\xi,0+) \frac{2i}{\pi} \frac{(\operatorname{sgn}(x-\xi))}{|x-\xi|} d\xi = 1 + \frac{\phi_2(x,0+)}{C(x)} , \qquad (3.6.4)$$

i.e.

$$-\frac{1}{\pi} \int_{-1}^{1} \frac{\partial \phi_2}{\partial \xi}(\xi,0+) \frac{1}{x-\xi} d\xi = 1 + \frac{\phi_2(x,0+)}{C(x)} , \qquad (3.6.5)$$

which is the airfoil equation (Muskhelishvili [14], p.373, equation (121.1)).

This equation can in general be solved using the method described in Muskhelishvili [14]. In the simple case $C(x) = C_o\sqrt{1-x^2}$ (the "elliptic wing") it is readily verified (e.g. by the method of trigonometric substitution, Tricomi [16], p.180), that the solution of (3.6.5) is

$$\phi_2(x,0+) = \frac{-C_o}{C_o + 1} \sqrt{1-x^2} . \qquad (3.6.6)$$

For the high frequency asymptotic case we can observe that the term in (3.3.13) containing the function $C(\xi)$ will tend to zero for high values of k. Thus at high values of k we can expect the solution to approximate that of the Neumann problem discussed in Chapter 2. In addition, if one considers $C(x) = C_o\sqrt{1-x^2}$ one should expect

the solution to begin to approximate the solution to the Neumann problem most rapidly when C_o is large.

3.7 COMPUTED RESULTS AND CONCLUSIONS

Numerical solutions of (3.3.13) have been obtained using the method just described, using the function $C(x) = C_o\sqrt{1 - x^2}$ over a wide range of C_o and k.

Although the low and high frequency asymptotic solutions discussed in the previous section are only complete to one term, the numerical solutions for $\phi_2(x,0+)$ agreed so closely with them for $k \sim 0$ (in particular) and $k \sim \infty$ throughout the whole interval $x\varepsilon[-1, 1]$ to suggest that the method described yields quite accurate results (especially for $k < 5.0$).

For $k = 0.01$ it is found that $\phi(x,0+)$ agrees with $\frac{-C_o}{C_o + 1}\sqrt{1 - x^2}$ throughout the interval $x\varepsilon[-1, 1]$ and for a wide range of values of C_o to three significant figures. For example when $C_o = 0.5$ the value of the low frequency asymptotic solution evaluated at $x = 0$ is $\phi_2(0,0+) = -0.3333 + 0.00000\ i$ whereas the numerical solution yields $-0.3332 + 0.00000\ i$. For $C_o = 1.0$ these values are $-0.5000 + 0.0000\ i$ and $-0.4999 + 0.0000\ i$ respectively, and for $C_o = \infty$, $-1.0000 + 0.0000\ i$ and $-0.9994 + 0.0000\ i$ respectively. While it must be realised that the low frequency asymptotic solutions are for $k = 0$ exactly and the numerical solutions are for $k = 0.01$ it must still be appreciated that the agreement between the solutions is very close.

At arbitrary values of k, for high C_o equation (3.3.13) should yield solutions of the Neumann problem, and this is verified. In addition the solution of (3.3.13) for high k should eventually (for high enough k) approximate solutions of the Neumann problem, irrespective of the value of C_o, and this is also verified numerically.

However, such verification is not necessarily a valid test of the numerical method for high k, since it does not test the accuracy of the kernel matrix elements of type D_{kj}. What is needed to test this is a high frequency asymptotic solution of (3.3.13) for arbitrary functions C(x).

PART 2 - SOME PROBLEMS CONCERNING THE FLOW ABOUT A BODY IMMERSED IN A CHANNEL

CHAPTER 4

THE NUMERICAL SOLUTION FOR THE OBSTRUCTION DUE TO AN ARBITRARY BODY

4.1 DESCRIPTION OF THE PROBLEM

Consider a 2-D x-y Cartesian scheme, and a channel surrounded by the walls $y = 0$ and $y = -h$. Assume that there is a continuous body immersed in the channel of form $y = S(x)$, where $S(-x) = S(x)$, as in figure 16, such that the flow in the channel can only pass underneath the body.

Without the presence of the body, the complex potential for the flow in the channel could have been expressed in the form $\Omega = V(x + C_1)$ say, where C_1 is constant throughout the channel. When the body is immersed, the flow is locally affected, but in the limits $x \sim \pm \infty$ the flow retains its channel characteristics. In these cases we can thus say that $\Omega \sim V(x + C_+)$ as $x \sim \infty$ and $\Omega \sim V(x + C_-)$ as $x \sim -\infty$. However, due to the presence of the immersed body we can no longer say that $C_+ = C_-$. Moreover, we can say that $C = \frac{1}{2}(C_+ - C_-)$, say, is a measure of the obstruction, or blockage due to the immersed body, and assert that the value of C is uniquely dependent on the geometry of the body.

In this chapter we will formulate this problem, and describe an accurate numerical solution thereof; it will be left until later to show the particular significance this problem has to the theory of ship hydrodynamics.

The boundary value problem for the velocity potential ϕ of the water passing under the body is defined by

(i) $\nabla^2\phi(x,y) = 0$ for all x, y in the region R bounded by the walls of the channel and the immersed body.

(ii) $\frac{\partial\phi}{\partial y} = 0$ on y = 0 and y = - h (rigid wall boundary condition).

(iii) $\frac{\partial\phi}{\partial n} = 0$ for all x, y such that y = S(x).

(iv) $\phi \sim V(x + C_+)$ as $x \sim \infty$,

$\phi \sim V(x + C_-)$ as $x \sim -\infty$,

where V is arbitrary.

For the purpose of calculating $C = \frac{1}{2}(C_+ - C_-)$ we let the arbitrary multiplier V = 1 and consider a new problem for $\phi' = \phi - x$. Since the shape of the surface is symmetric in x it can then be assumed that $C_+ = - C_- = C$. The new boundary value problem is almost the same as the old, since Laplace's equation will still hold for ϕ' and we still have $\frac{\partial\phi'}{\partial y} = 0$ on y = 0 and y = - h.

However the condition (iv) now becomes

(iv) $\phi' = \pm C$ as $x \sim \pm \infty$,

and (iii) must be adjusted to give

(iii) $\frac{\partial \phi'}{\partial n} = \alpha(x) = - \frac{\partial x}{\partial n}$,

where $\alpha(x)$ is known when we are given the shape of the body. A method for its calculation will be given later.

Solving the above problem for ϕ' will lead to the value of C in terms of the behaviour of the solution for ϕ' when $x \to \infty$. From now on we drop the dash on ϕ'.

4.2 INTEGRAL FORMULATION OF THE PROBLEM

To obtain an integral formulation for the boundary value problem we assume a distribution of sources over the body of the form $Q(\xi,\eta)$, where ξ and η are the co-ordinates on the boundary, which we designate as S.

The potential $\phi(x,y)$ in the region R will then be given by

$$\phi(x,y) = \int_S dS\ Q(\xi,\eta)G(x,y;\xi,\eta) \ , \qquad (4.2.1)$$

where $G(x,y;\xi,\eta)$ is a Green's function for a source at $x,y = \xi,\eta$ in a region R bounded in the x - y Cartesian co-ordinate scheme by $y = 0$ and $y = - h$. Such a function is

$$G(x,y;\xi,\eta) = \mathrm{Re}\left[\frac{1}{2\pi} \log \left\{\cos \frac{\pi\eta}{h} - \cosh \frac{\pi}{h} ((x - \xi) + iy)\right\}\right] . \qquad (4.2.2)$$

Applying boundary condition (iii) to equation (4.2.1) gives

$$\frac{\partial \phi}{\partial n} (\xi',\eta') = \lim_{x,y \to \xi',\eta'} \frac{\partial}{\partial n} \int_S dS\ Q(\xi,\eta)G(x,y;\xi,\eta) = \alpha(\xi',\eta') \ , \qquad (4.2.3)$$

where the contour of integration is deformed along a small circle around the point ξ', η' on the boundary S with radius ε.

Equation (4.2.3) must now be solved for $Q(\xi,\eta)$. When this is known it can then be substituted back into the integral of (4.2.1), making it possible to evaluate ϕ at any point (x,y).

4.3 NUMERICAL SOLUTION

The method used to solve (4.2.3) is to divide the boundary S into N segments ΔS_j, $j = 1, \ldots, N$. These segments are defined by the input data for the shape of the body. The subintervals need not be uniform, but must be small enough so that we can assume that $Q(\xi,\eta)$ is constant on each segment, say $Q = Q_j$ on segment ΔS_j.

If we evaluate midpoints, we can approximate the integral equation (4.2.3) as

$$\sum_{j=1}^{N} B_{ij}\, Q_j = b_i \,, \quad i = 1, \ldots, N \,, \tag{4.3.1}$$

where

$$b_i = \frac{\partial \phi}{\partial n}(x_i, y_i)$$

$$B_{ij} = \lim_{x,y \to x_i,y_i} \frac{\partial}{\partial n} \int_{\Delta S_j} \left[G(x,y;\xi,\eta)\, dS \right]$$

$$\Delta S_j = ((\xi_j,\eta_j), (\xi_{j+1},\eta_{j+1}))$$

$$x_i, y_i = \tfrac{1}{2}(\xi_i + \xi_{i+1}, \eta_i + \eta_{i+1}) \,. \tag{4.3.2}$$

Using the method of Frank[7], and the fact that

$$G(x,y;\xi,\eta) = \frac{Re}{2\pi} \log \left(\cos \frac{\pi\eta}{h} - \cosh \frac{\pi}{h} ((x - \xi) + iy)\right)$$

$$= \frac{Re}{2\pi} \log \left(\cosh \frac{\pi}{2h} ((z - \bar{\zeta}) - (z - \zeta)\right)$$

$$- \cosh \frac{\pi}{2h} ((z - \bar{\zeta}) + (z - \zeta))\Big)$$

$$= \frac{1}{2\pi} \log 2 + Re\left[H(z - \bar{\zeta}) + H(z - \zeta)\right] , \quad (4.3.3)$$

where

$$z = x + iy$$

$$\zeta = \xi + i\eta$$

$$H(Z) = \frac{1}{2\pi} \log \sinh \frac{\pi Z}{2h} , \quad (4.3.4)$$

we can readily show that

$$B_{ij} = - Im\Big[e^{i(\alpha_i - \alpha_j)} \{H(z_i - \zeta_{j+1}) - H(z_i - \zeta_j)\}$$

$$+ e^{i(\alpha_i + \alpha_j)} \{H(z_i - \bar{\zeta}_{j+1}) - H(z_i - \bar{\zeta}_j)\}\Big] , \quad (4.3.5)$$

where α_i is the angle made by the i^{th} segment with the positive x axis, and is given by

$$\alpha_i = \tan^{-1} \frac{\eta_{i+1} - \eta_i}{\xi_{i+1} - \xi_i} . \quad (4.3.6)$$

It is found in fact that the matrix B_{ij} is diagonally dominant, this being desirable in order that the system (4.3.1) be solvable. For example, if i = j in (4.3.5) it can be verified that B_{ij} takes a value close to 0.5, and all the non-diagonal elements are very small in comparison.

It can be shown by geometric arguments, that the right-hand side elements b_i, i = 1, ..., N, can be calculated using

$$b_i = \frac{\partial \phi}{\partial n}(x_i, y_i) = - \frac{(\eta_{i+1} - \eta_i)}{\sqrt{(\eta_{i+1} - \eta_i)^2 + (\xi_{i+1} - \xi_i)^2}} . \quad (4.3.7)$$

Solution of the system (4.3.1) can now be performed easily, yielding a solution for Q_j, j=1, ..., N, i.e. the distribution of sources $Q(\xi,\eta)$ on the surface of the hull.

4.4 CALCULATION OF THE CONSTANT C

Having solved the system of equations (4.3.1), we have available numerical values of the source density function $Q(\xi,\eta)$, evaluated at various points on the surface S. Thus we can substitute these values in (4.2.1) to obtain numerical values for the potential ϕ, evaluated at any desired point (x,y). Since we know $\phi \to \pm C$ as $x \to \pm \infty$ we are in a position to make a numerical estimation of C for the prescribed hull geometry.

Thus

$$C = \lim_{x \to \infty} \int_S dS \; Q(\xi,\eta) G(x,y;\xi,\eta) . \quad (4.4.1)$$

Since

$$G(x,y;\xi,\eta) = \frac{Re}{2\pi} \log \left(\cos \frac{\pi\eta}{h} - \cosh \frac{\pi}{h} ((x - \xi) + iy) \right) , \quad (4.4.2)$$

we obtain the result that

$$\lim_{x \to \infty} G(x,y;\xi,\eta) = \frac{1}{2h} (x - \xi) , \quad (4.4.3)$$

and so

$$C = \frac{1}{2h} \int_S dS\ (x - \xi)Q(\xi,\eta)$$

$$= -\frac{1}{2h} \int_S dS\ \xi Q(\xi,\eta) \qquad (4.4.4)$$

since Q is antisymmetric in ξ.

4.5 ANALYTIC CALCULATIONS OF C FOR CERTAIN CROSS-SECTIONS

The calculation of C analytically is in itself a non-trivial theory. Two results will be given in this section, and used to appraise the accuracy of the numerical program described here.

One of the most interesting exact analytical formulae known for C corresponds to the oval-shaped body whose surface is a streamline in an example given in Lamb [11], p.71. Lamb considers the potential- and stream- functions due to a row of equidistant dipoles in a uniform stream. Between each of the dipoles there is a straight streamline which in our case corresponds to y = - h, and a parallel line through the dipole can be taken as y = 0.

Lamb shows that the complex potential in the channel bounded by y = 0 and y = - h is given by

$$\Omega = z + C_1 \coth \frac{\pi z}{h}\ , \qquad (4.5.1)$$

where z = x + iy, and C_1 is real, or,

$$\phi = x + \frac{C_1 \sinh\left(\frac{2\pi x}{h}\right)}{\cosh\left(\frac{2\pi x}{h}\right) - \cos\left(\frac{2\pi y}{h}\right)} , \qquad (4.5.2)$$

and

$$\psi = y - \frac{C_1 \sin\left(\frac{2\pi y}{h}\right)}{\cosh\left(\frac{2\pi x}{h}\right) - \cos\left(\frac{2\pi y}{a}\right)} . \qquad (4.5.3)$$

Lamb shows that the streamline $\psi = 0$ consists in part of the line $y = 0$ and in part of an oval curve whose semi-diameters parallel to x and y are given by the equations

$$\sinh^2 \frac{\pi x}{h} = \frac{\pi C_1}{h} , \quad y \tan \frac{\pi y}{h} = C_1 . \qquad (4.5.4)$$

It is readily shown from (4.5.2) that

$$\phi \sim x + C_1 \qquad (4.5.5)$$

as $x \sim \infty$, and thus each value of C_1 generates an oval body defined by $\psi = 0$, which if used as an input in our numerical program should yield a value $C = C_1$ if the numerical program is accurate.

Values of C obtained numerically for $C_1 = 0.01$, 0.1, 1.0 and 10.0, were 0.0100, 0.1016, 1.0175 and 10.5717 respectively, and these errors ranged up to 6%. However it is suggested that these errors are not mainly due to the method, which is designed so as to give a uniform accuracy for all cross-sections, but due to the inaccuracy of the input data, which tended to be less reliable for high values of C_1.

The second set of analytic calculations of C which will be given here is due to Flagg and Newman[6], who have calculated the

added mass due to flow past a rectangular shape using an equation of Gurevich [8]. It is readily shown that the added mass for a rectangular body with vertical walls 2a units apart and a clearance b is related to C by

$$C = h\left(\frac{\lambda_x}{2\rho_b^2}\right) + a - \frac{ab}{h} . \qquad (4.5.6)$$

To test the numerical method using these results, C was calculated numerically for $a = \frac{1}{2}$, $d = h - b = \frac{1}{2}$, and various values of h. These are plotted in Fig. 17 where the solid line represents C due to Flagg and Newman and crosses mark the numerical estimates. It is seen that the accuracy remains within 1% for all calculated cases. Sample calculations are, for $h = \frac{50}{95}$, C = 10.4722 numerically compared with the Flagg and Newman value of C = 10.3834, whereas for $h = \frac{5}{4}$ these values are 0.5326 and 0.5315 respectively. Furthermore, it must be pointed out that these discrepancies remain within 1% for all intermediate values of h, and that this is the full range of h for which Flagg and Newman results are available.

These results speak highly for the accuracy of the numerical program. A 5% error would have been acceptable from the point of view of physical application, so a uniform error of no more than 1% can be considered of very high practical value.

The value of N used to obtain the above numerical results was 48. Calculations to determine how C varied with N were carried out for the above rectangular cross-section with h = 0.625, where Flagg

and Newman predict the value C = 2.4920. For N = 12, the above method predicted C = 2.7413, this calculation taking 0.764 seconds on the CDC 6400 computer. For N = 24, 36 and 48 the values calculated for C were 2.5387 (2.189 secs.), 2.5200 (4.593 secs.), and 2.5038 (7.964 secs.) respectively. Thus, in this rectangular case at least 36 steps are needed in order to obtain accuracy within 1%.

However, it must be pointed out that analysis of this type is arbitrary in some sense, e.g. it is difficult to judge whether to take equal subintervals, or to concentrate the grid points near the corners in some way. In the above examples, the grid points were concentrated near the corners. This was in order to overcome the fact that the assumption $Q = Q_j$ = constant on each subinterval tends to break down near the sharp corners. In fact the source density function Q has a singularity at a sharp corner. For these reasons we can expect to obtain even higher accuracy in calculating C for a cross-section of the type found in ship hulls, as these are generally free of sharp corners and even regions of high curvature.

CHAPTER 5

ASYMPTOTIC FORMULAE FOR C FOR SMALL CLEARANCE

5.1 INTRODUCTION

In this chapter are derived asymptotic formulae for C for a family of related cross-sections, all valid when the clearance is small. All of these cross-sections have something in common in that they are considered to have substantially flat bottoms giving a small clearance b, and substantially vertical walls 2a units apart. These are considered to be of significant practical use, as many cross-sections of ships' hulls are found to have these properties. Although the previous section has shown that the values of C can be calculated numerically for these cross-sections with accuracies of better than 1%, it will be seen in this chapter that values of C can be calculated with similar accuracy without having to use the numerical procedure of the previous chapter which involves in some cases inversion of large matrices. Instead all that will be required will be to substitute certain parameters associated with the cross-section into a simple formula.

The method used to obtain these formulae is the method of matched asymptotic expansions (Van Dyke[21]). While no-one can argue that the method of matched asymptotic expansions is founded on a rigorous basis, it will be seen that the method still produces in the case of the rectangular cross-section, a formula

identical to that of Flagg and Newman and in other cases where no rigorous analytic result is known, formulae which yield values close to those predicted numerically.

5.2 AN ARBITRARY CROSS-SECTION

In this section, we derive, using the method of matched asymptotic expansions, a general asymptotic formula for C, valid for cross-sections with substantially vertical walls 2a units apart, and a substantially flat bottom leaving a shallow clearance b. Such a cross-section is illustrated in fig. 18, and it will be seen that the cross-section is arbitrary mainly in the sense that it can take varying shapes near the corners.

In proceeding to find our formula, we ignore the region to the left of the y-axis, this being allowable due to the symmetry of the problem about this axis. We then consider the remaining area to consist basically of two parts, an inner region (fig. 19) and an outer region (fig. 20).

The inner region is essentially one in which fluid passes from a channel of width b into a quarter-plane. In this region we ignore the effect of the upper wall of the channel and do not need to assume that b is small. We find the solution for the flow in this region by conformal transformation into an upper ζ-plane, with a source at the origin $\zeta = 0$ corresponding to $z = -\infty$. It can be assumed that the most general form for the complex potential in the ζ-plane is then

$$\Omega = \frac{Vb}{\pi} \log \zeta + \sum_{n=0}^{\infty} A_n \zeta^n \ , \qquad (5.2.1)$$

where V and A_n, n = 1,2, ... are real and to be determined. It should be noted at this stage that the outer behaviour of this potential in the z-plane should be that of a source transmitting into a quarter-plane, whereas the inner behaviour ($z \to -\infty$) should resemble channel flow.

The outer region is in fact a semi-infinite channel with a point-source at one of the corners. Near this corner, we will expect the solution for the flow to resemble a point source transmitting into a quarter-plane (matching the solution for the outer part of the inner region), whereas as $z \to \infty$, we expect the flow to resemble that in a channel. It is convenient in this case to once again find the general flow solution by conformal transformation of the region into an upper ζ-plane, and to assume that the most general solution for the flow in this region is

$$\Omega = \frac{Uh}{\pi} \log \zeta + \sum_{n=0}^{\infty} B_n \zeta^{-n} \ , \qquad (5.2.2)$$

where U and B_n, n = 0,1,2, ... are real and to be determined.

It can be readily shown that the outer region and an upper ζ-plane are related by the transformation

$$\zeta = -\tfrac{1}{2} + \tfrac{1}{2} \cosh \frac{\pi}{h} (z - a) \ , \qquad (5.2.3)$$

which, as $\zeta \sim 0$ behaves like

$$\zeta = \left(\frac{\pi}{2h}\right)^2 (z - a)^2 \left[1 + \frac{\pi^2}{12h^2} (z - a)^2 + \frac{\pi^4}{360h^4} (z - a)^4 + O(z - a)^6\right] , \qquad (5.2.4)$$

and, as $|\zeta| \to \infty$, like

$$\zeta = \tfrac{1}{4} e^{\frac{\pi}{h}(z-a)} \left[1 + O(e^{-x})\right] . \qquad (5.2.5)$$

No general transformation such as (5.2.3) can be given for the inner region because of the arbitrary nature of the boundary. However, due to the channel-like nature of this region for $z \sim -\infty$, it is safe to assume that as $\zeta \sim 0$ the transformation always behaves like

$$\zeta \sim e^{\frac{\pi}{b}(z-a)} \left[1 + O(e^{x})\right] , \qquad (5.2.6)$$

where

$$x = \frac{z - a}{b} . \qquad (5.2.7)$$

For $|\zeta| \sim \infty$ in the inner region we will assume that

$$\zeta = \frac{d_o}{b^2} (z - a)^2 \left[1 + b^2 d_2 (z - a)^{-2} + b^4 d_4 (z - a)^{-4} + O(z - a)^{-6}\right] , \qquad (5.2.8)$$

where the coefficients d_o, d_2 and d_4 are arbitrary, depending on the cross-section.

Substituting (5.2.5) into (5.2.2) shows that in the outer part of the outer region, the complex potential satisfies

$$\Omega = \frac{Uh}{\pi} \log \left(\tfrac{1}{4} e^{\frac{\pi}{h}(z-a)}\right) + O(e^{-x}) + B_o + O(e^{-x})$$

$$= Uz + \left(B_o - Ua - \frac{2Uh}{\pi} \log 2\right) + O(e^{-x}) \sim U(z + C)$$

where

$$C = \frac{B_o}{U} - a - \frac{2h}{\pi} \log 2 \ . \qquad (5.2.9)$$

We wish to determine this as a series in $\varepsilon = \frac{b}{h}$.

Substituting (5.2.6) into (5.2.1) gives the inner behaviour of the complex potential in the inner region as being

$$\Omega = \frac{Vb}{\pi} \cdot \frac{\pi}{b} (z - a) + A_o + O(e^x)$$

$$\sim Vz + (A_o - Va) \ . \qquad (5.2.10)$$

By symmetry at the centre of the channel we would require that

$$\Omega \sim Va + 0 \ , \qquad (5.2.11)$$

i.e. the constant term must vanish. Hence

$$A_o = Va \ . \qquad (5.2.12)$$

From (5.2.4) we can readily show that in the inner part of the outer region,

$$\log \zeta = \log \frac{\pi^2}{4h^2} + 2 \log (z - a) + \frac{\pi^2}{12h^2} (z - a)^2$$

$$- \frac{\pi^4}{1440h^4} (z - a)^4 + O(z - a)^6 \ , \qquad (5.2.13)$$

$$\zeta^{-1} = \frac{4h^2}{\pi^2} (z - a)^{-2} - \frac{1}{3} + \frac{\pi^2}{60h^2} (z - a)^2$$

$$+ \frac{\pi^4}{240h^4} (z - a)^4 + O(z - a)^6 \ , \qquad (5.2.14)$$

and

$$\zeta^{-2} = \frac{16h^4}{\pi^4}(z-a)^{-4} - \frac{8h^2}{3\pi^2}(z-a)^{-2} + \frac{176}{45} - \frac{239\pi^2}{45h^2}(z-a)^2 + \frac{1999\pi^4}{300h^4}(z-a)^4 + O(z-a)^6 . \quad (5.2.15)$$

Thus, substituting (5.2.4), (5.2.13), (5.2.14), and (5.2.15) into (5.2.2) we find that the inner behaviour of the complex potential in the outer region should be

$$\Omega = \frac{2Uh}{\pi}\log(z-a) + \frac{Uh}{\pi}\log\frac{\pi^2}{4h^2} + \frac{Uh}{\pi}\frac{\pi^2}{12h^2}(z-a)^2 - \frac{Uh}{\pi}\frac{\pi^4}{1440h^4}(z-a)^4 + B_o + B_1\frac{4h^2}{\pi}(z-a)^{-2} - \frac{1}{3}B_1 + \frac{\pi^2 B_1}{60h^2}(z-a)^2 + \frac{B_1\pi^4}{240h^4}(z-a)^4 + \frac{B_2 16h^4}{\pi^4}(z-a)^{-4} - \frac{8B_2h^2}{3\pi^2}(z-a)^{-2} + \frac{176B_2}{45} - \frac{239\pi^2}{45h^2}B_2(z-a)^2 + \frac{1999\pi^4}{300h^4}B_2(z-a)^4 + O(z-a)^6. \quad (5.2.16)$$

Finally, from (5.2.8) we can readily obtain that

$$\log\zeta \to \log\frac{d_o}{b^2} + 2\log(z-a) + b^2 d_2(z-a)^{-2} + b^4\left(d_4 - \frac{d_2^2}{2}\right)(z-a)^{-4} + O(z-a)^{-6} . \quad (5.2.17)$$

If we substitute (5.2.8) and (5.2.17) into (5.2.1) we find that the outer behaviour of the complex potential in the inner region is of the form

$$\Omega = \frac{\dot{2}\dot{V}b}{\pi} \log (z - a) + \frac{\dot{V}b}{\pi} \log \frac{d_o}{b^2} + \frac{Vb^3 d_2}{\pi} (z - a)^{-2}$$
$$+ \frac{\dot{V}b^5}{\pi} \left(d_4 - \frac{d_2^2}{2}\right) (z - a)^{-4} + A_o + A_1 \frac{d_o}{b^2} (z - a)^2$$
$$+ A_1 d_o d_2 + b^2 A_1 d_o d_4 (z - a)^{-2} + A_2 \frac{d_o^2}{b^4} (z - a)^4$$
$$+ \frac{2A_2 d_2 d_o^2}{b^2} (z - a)^2 + 2A_2 d_4 d_o^2 + A_2 d_o^2 d_2^2$$
$$+ \frac{2A_2 d_o^2 d_2 d_4}{b^2} (z - a)^{-2} + \frac{A_2 d_4^2 d_o^2}{b^4} (z - a)^{-4} + O(z - a)^{-6}.$$

(5.2.18)

In the method of matched asymptotic expansions we use the fact that the outer behaviour of the complex potential for the inner region should match the inner behaviour of the complex potential for the outer region, i.e. the terms of (5.2.16) and (5.2.18) should match. Matching the coefficients of $\log (z - a)$, constants, $(z - a)^2$, $(z - a)^{-2}$, $(z - a)^4$ and $(z - a)^{-4}$ in these equations respectively, we obtain the obvious flux condition

$$Uh = Vb$$

i.e.
$$U = \frac{Vb}{h}, \qquad (5.2.19)$$

$$\frac{Uh}{\pi} \log \frac{\pi^2}{4h^2} + B_o - \frac{1}{3} B_1 + \frac{176 B_2}{45}$$
$$= \frac{Vb}{\pi} \log \frac{d_o}{b^2} + A_o + A_1 d_o d_2 + 2A_2 d_4 d_o^2 + A_2 d_o^2 d_2^2, \qquad (5.2.20)$$

$$\frac{Uh}{\pi} \frac{\pi^2}{12h^2} + \frac{\pi^2 B_1}{60h^2} - \frac{239\pi^2}{45h^2} B_2 = A_1 \frac{d_o}{b^2} + 2A_2 \frac{d_2 d_o^2}{b^2}, \qquad (5.2.21)$$

$$\frac{4h^2}{\pi^2} B_1 - \frac{8h^2}{3\pi^2} B_2 = \frac{Vb^3 d_2}{\pi} + A_1 b^2 d_o d_4 + 2A_2 b^2 d_o{}^2 d_2 d_4 \ , \quad (5.2.22)$$

and

$$\frac{16h^4}{\pi^4} B_2 = \frac{Vb^5}{\pi} (d_4 - d_2{}^2) + A_2 b^4 d_4{}^2 d_o{}^2 \ . \quad (5.2.24)$$

The last four equations can be regarded as a system of linear equations in A_1, A_2, B_1 and B_2, and have solution

$$A_1 = \frac{Uh}{\pi} \left[\frac{\pi^2 b^2}{12h^2 d_o} + \frac{\pi^4}{h^4} \frac{b^4 d_2}{180 d_o} \right] (1 + 0(\varepsilon^4)) \ , \quad (5.2.25)$$

$$A_2 = - \frac{b^4}{d_o{}^2} \frac{Uh}{\pi} \frac{\pi^4}{1440h^4} (1 + 0(\varepsilon^4)) \ , \quad (5.2.26)$$

$$B_1 = \frac{Uh}{\pi} \left[\frac{\pi^2 b^2}{4h^2} d_2 + \frac{\pi^4 b^4}{h^4} \left(\frac{1}{16} d_4 - \frac{1}{48} d_2{}^2 \right) \right] (1 + 0(\varepsilon^4)), \quad (5.2.27)$$

and

$$B_2 = \frac{Uh}{\pi} \frac{\pi^4 b^4}{16h^4} \left(d_4 - \frac{d_2{}^2}{2} \right) (1 + 0(\varepsilon^4)) \ . \quad (5.2.28)$$

Substitution of these solutions and (5.2.12) into (5.2.20) yields

$$B_o = \frac{Uh}{\pi} \left[\log \frac{4h^2 d_o}{b^2} + \frac{\pi^2 b^2}{12h^2} d_2 + \frac{\pi^4 b^4}{3h^4} \left(\frac{1}{16} d_4 - \frac{1}{48} d_2{}^2 \right) \right.$$
$$- \frac{176\pi^4 b^4}{720h^4} \left(d_4 - \frac{d_2{}^2}{2} \right) + \frac{\pi a}{b} + \frac{b^2 d_2 \pi^2}{12h^2}$$
$$\left. + \frac{\pi^4 b^4 d_2{}^2}{180h^4} - \frac{\pi^4 b^4 d_4}{720h^4} - \frac{\pi^4 b^4 d_2{}^2}{1440h^4} \right]. \quad (5.2.29)$$

This may be substituted into (5.2.9), giving

$$C = \frac{a}{\varepsilon} - a - \frac{2h}{\pi}\log\frac{\pi\varepsilon}{d_o^{\frac{1}{2}}} + \frac{d_2 h\pi}{6}\varepsilon^2 + \left(\frac{173 d_2^{\,2}\pi^4 h}{1440} - \frac{9 d_4 \pi^4 h}{40}\right)\varepsilon^4 + O(\varepsilon^6) , \qquad (5.2.30)$$

where $\varepsilon = \frac{b}{h}$. This is the general asymptotic formula for C, for shallow draft, when the outer behaviour of the inner transformation to the upper ζ-plane can take form (5.2.8).

It can be shown that the added mass coefficient λ_x and the constant C are related by

$$\frac{\lambda_x}{2\rho h^2} = \frac{1}{h}(C - a + a\varepsilon) . \qquad (5.2.31)$$

Thus the formula for the added mass coefficient, analogous to (5.2.30) is

$$\frac{\lambda_x}{2\rho h^2} = \frac{a}{\varepsilon h} - \frac{2}{\pi}\log\frac{\pi\varepsilon}{d_o^{\frac{1}{2}}} - \frac{2a}{h} + \frac{a\varepsilon}{h} + \frac{d_2\pi}{6}\varepsilon^2 + \left(\frac{173 d_2^{\,2}\pi^4}{1440} - \frac{9 d_4 \pi^4}{40}\right)\varepsilon^4 + O(\varepsilon^6) . \qquad (5.2.32)$$

5.3 RECTANGULAR CROSS-SECTIONS

The simplest particular cross-section satisfying the requirements of the arbitrary cross-section of the previous section is one which is purely rectangular. Conveniently this particular case also gives a very good check on the accuracy of (5.2.30), as the resulting formula will be found to compare exactly with that of Flagg and Newman [6].

In this case the outer region is clearly the same as that in the previous section. The inner region is shown in fig. 21, and it can be shown (e.g. by using a Schwarz-Christoffel transformation) that a general mapping between this region and an upper ζ-plane is given by

$$z - a - ib = \frac{eb}{\pi}\sqrt{\frac{4}{e^2} - \zeta} - \frac{2b}{\pi}\operatorname{arctanh}\frac{e}{2}\sqrt{\frac{4}{e^2} - \zeta}\,. \qquad (5.3.1)$$

It can be shown that as $\zeta \sim 0$, (5.3.1) reduces to

$$\zeta = e^{\frac{\pi}{b}(z-a)}\left[1 + O(e^x)\right]\,, \qquad (5.3.2)$$

where

$$x = \frac{z - a}{b}\,, \qquad (5.3.3)$$

this being identical to (5.2.6) and (5.2.7). As $|\zeta| \sim \infty$ it can be shown that (5.3.1) takes the form

$$\zeta \sim \frac{e^2\pi^2}{4^2b^2}(z - a)^2\left[1 + \frac{4b^2}{\pi^2}(z - a)^{-2} - \frac{16b^4}{3\pi^4}(z - a)^{-4} + O(z - a)^{-6}\right]\,, \qquad (5.3.4)$$

this being of the same form as (5.2.8), with

$$d_o = \left(\frac{e\pi}{4}\right)^2$$

$$d_2 = \frac{4}{\pi^2}$$

and

$$d_4 = \frac{16}{3\pi^4}\,. \qquad (5.3.5)$$

Substitution of (5.3.5) into (5.2.30) and (5.2.32) yields

$$C = \frac{a}{\varepsilon} + \frac{2h}{\pi} - a - \frac{2h}{\pi}\log 4\varepsilon + \frac{2h}{3\pi}\varepsilon^2 + \frac{281}{90\pi}\varepsilon^4 + O(\varepsilon^6), \quad (5.3.6)$$

and

$$\frac{\lambda_x}{2\rho h^2} = \frac{a}{\varepsilon h} + \frac{2}{\pi} - \frac{2}{\pi}\log 4\varepsilon - \frac{2a}{h} + \frac{a\varepsilon}{h} + \frac{2}{3\pi}\varepsilon^2 + \frac{281}{90\pi}\varepsilon^4 + O(\varepsilon^6)\ ^{1}. \quad (5.3.7)$$

Flagg and Newman [6] have derived an identical asymptotic formula to (5.3.7) except that their series is terminated with an estimate of $O(\varepsilon^3)$ after the ε^2 term.

5.4 POLYGONAL CROSS-SECTIONS

In this section we derive an asymptotic formula for C when the cross-section is polygonal, ignoring error terms, and maintaining only those of first order.

We suppose that the polygon has n vertices in the right-hand plane, as in fig. 22, with a flat bottom giving clearance b until the first vertex, and a vertical side at x = a after the n^{th} vertex.

Due to the vertical sides and small clearance we may assume that the outer region is the same as in the arbitrary case of the previous section, and as shown in that section, it is the inner mapping which contributes to a new formula for C. We can assume that the mapping between the z-plane and upper ζ-plane in this case is a Schwarz-Christoffel transformation of the form

---

[1] Flagg and Newman obtain a result double this value. This is because they consider a body of double area, and a channel of double width (a full body compared with the half body considered here.)

$$\frac{dz}{d\zeta} = \frac{\kappa \prod_{i=1}^{n}(\zeta - \zeta_i)^{\alpha_i}}{\zeta} \qquad (5.4.1)$$

where $\sum_{i=1}^{n} \alpha_i = \frac{1}{2}$, and ζ_i, i=1, ..., n are the points on the real axis in the ζ-plane mapped from z_i, i=1, ..., n. It is safe to assume that $0 > \zeta_1 > ..... > \zeta_n$.

As $\zeta \sim 0$, (5.4.1) becomes

$$\frac{dz}{d\zeta} \sim \kappa \prod_{i=1}^{n}(-\zeta_i)^{\alpha_i} \frac{1}{\zeta},$$

i.e.

$$z \sim \kappa \prod_{i=1}^{n}(-\zeta_i)^{\alpha_i} \ln \zeta + \text{const},$$

i.e.

$$\zeta \sim e^{\frac{1}{\kappa \prod_{i=1}^{n}(-\zeta_i)^{\alpha_i}}(z - \text{const.})} \qquad (5.4.2)$$

In order that the inner behaviour of this mapping maintains the character of (5.2.6), we set

$$\frac{1}{\kappa \prod_{i=1}^{n}(-\zeta_i)^{\alpha_i}} = \frac{\pi}{b}$$

i.e.

$$\kappa = \frac{b}{\prod_{i=1}^{n}(-\zeta_i)^{\alpha_i}}, \qquad (5.4.3)$$

and set const. = a.

Thus as $|\zeta| \sim \infty$, (5.4.1) becomes

$$\frac{dz}{d\zeta} \sim \frac{b}{\pi \prod_{i=1}^{n} (-\zeta_i)^{\alpha_i}} \zeta^{-\frac{1}{2}} ,$$

i.e.

$$z \sim \frac{2b}{\pi \prod_{i=1}^{n} (-\zeta_i)^{\alpha_i}} \zeta^{\frac{1}{2}} + a ,$$

i.e.

$$\zeta \sim \left(\frac{\pi \prod_{i=1}^{n} (-\zeta_i)^{\alpha_i}}{2}\right)^2 \left(\frac{z - a}{b}\right)^2 . \qquad (5.4.4)$$

This takes the form of (5.2.8), with

$$d_o = \left(\frac{\pi \prod_{i=1}^{n} (-\zeta_i)^{\alpha_i}}{2}\right)^2 . \qquad (5.4.5)$$

Thus, substituting (5.4.5) in (5.2.30) and ignoring terms of order ε^2 and higher we have an asymptotic formula for C for the polygonal cross-section of the form

$$C = \frac{a}{\varepsilon} - a - \frac{2h}{\pi} \log k\varepsilon , \qquad (5.4.6)$$

where

$$k = \frac{2}{\pi \prod_{i=1}^{n} (-\zeta_i)^{\alpha_i}} . \qquad (5.4.7)$$

Checks made on the accuracy of (5.4.6) have been limited to the case n = 2. The reason for this is that it is not entirely straightforward to calculate the values of ζ_i, given the vertices of the polygon. In Appendix A it is indicated how such values can

be obtained in this case, and an examination of the method shows that numerical errors can be expected in calculating them. With this, and the fact that (5.4.6) contains terms only of order one and greater, one could expect some discrepancies when comparing values obtained from (5.4.6) for particular polygonal cross-sections with values obtained from the numerical method of Chapter 4.

The method of Appendix A showed that in the case $a = \frac{1}{2}$, $b = \frac{1}{10}$ and $h = \frac{11}{10}$ the values $z_1 = 0.43394 - i$, $z_2 = 0.5 - 0.93394\,i$ mapped into the values $\zeta_1 = 0.2768$ and $\zeta_2 = 4.1520$, with a ratio $r = 15$. For this particular cross-section, the numerical program yielded the value $C = 6.158$, whereas (5.4.6) predicted a value 6.218. This appears to be an exceptionally close prediction, with error only of order 1%, but in fact the error is slightly larger than this, because the terms $\frac{a}{\epsilon} - a$ always appear in formulae for C, i.e. the error is always due to the log term. In the cross-section considered here the value of $\frac{a}{\epsilon} - a$ (the invariant part of the formula) is 5.0 which means that the log term was equal to 1.218 instead of a numerically predicted 1.158, an error of 5%. In view of the slight doubts expressed about the likely accuracy of C in the previous paragraph, this error is now quite realistic, but still small enough for (5.4.6) to be of good practical use.

5.5 A SPECIAL CURVED CROSS-SECTION

A further formula, that for a curved cross-section, can also be obtained by the method of the previous sections. In this case the cross-section corresponds to the streamline with infinite gradient at infinity in the problem of flow from a pipe into 2- D space (see Kober[10], p.117).

Reference to fig. 23 indicates that this cross-section still approximates the previous ones in the sense that there is basically a flat bottom with clearance b and approximately vertical walls 2a units apart. This is not as accurate as in the previous cases because of the curve in the shape. The mapping which transforms this shape on to an upper ζ-plane is given by

$$z = \frac{b}{\pi} \log \zeta + d\zeta^{\frac{1}{2}} + a \ , \qquad (5.5.1)$$

where d is a small parameter, of order b (shown in fig. 23) which uniquely specifies the curve.

For $\zeta \sim 0$ we obtain the asymptotic relation

$$\zeta \sim e^{\frac{\pi}{b}(z-a)} \ , \qquad (5.5.2)$$

which is of the same form as (5.2.6), whereas for $|\zeta| \sim \infty$, we obtain

$$\zeta \sim \frac{1}{d^2}(z - a)^2 = \left(\frac{b}{d}\right)^2 \left(\frac{z - a}{b}\right)^2 \ . \qquad (5.5.3)$$

This is of the same form as (5.2.8) with

$$d_o = \left(\frac{b}{d}\right)^2 \ .$$

In this particular case, if (5.5.3) is expanded it is found that although the error terms are of higher order than one, they are not of the same form as those in (5.2.8). In fact besides error terms of this type there are higher order terms which contain logarithms. This all suggests that the matching process as outlined in Section 5.2 cannot be applied in this case as there is nothing in the outer expansion to match these logarithmic terms. This is true, and is because what we have taken to be the outer region itself is not strictly correct, as this should contain a curved shape. However the matching process can be carried out as long as we only consider terms as far as those of order one, and after substitution of (5.5.4) into (5.2.30) and ignoring terms in (5.2.30) of order ε^2 and higher, we obtain

$$C = \frac{a}{\varepsilon} - a - \frac{2h}{\pi} \log \left(\pi \cdot \frac{d}{b} \cdot \varepsilon \right) , \qquad (5.5.5)$$

where we remember that $\frac{d}{b} = O(1)$.

Numerical checks on this formula show that it is the least accurate of those derived in this chapter, which is not surprising when we remember that the matching can only be done down to terms of order one. A sample calculation for $d = b = \frac{1}{18}$, $a = \frac{1}{2}$ and $h = \frac{5}{9}$ predicted $C = 4.9095$ compared with the numerical programme's estimate of $C = 5.2899$, a discrepancy of about 6%. If one were in this case to attempt to test the accuracy of the log term's contribution, by subtracting $\frac{a}{\varepsilon} - a$ from each value we would find a

considerable discrepancy, of the order of 50%. However this is not a fair test to make in this case because the error of (5.5.5) could be expected to be much higher, due to the inability to carry out the matching process. If we did make the matching process possible by considering an outer region with a suitably curved left-hand wall, we would find, in any case that there is an extra range of error terms, such as those of order $\varepsilon^2 \log \varepsilon$ which would increase expected discrepancies between numerically derived values, and those of (5.5.5).

5.6 PRACTICAL USE OF ASYMPTOTIC FORMULAE FOR C

One may now well ask: are asymptotic formulae as derived in Sections 5.2 - 5.5 of practical use in calculating C? If so for what types of cross-sections, and what order of magnitude would one expect of the error.

Clearly, when the cross-sections are purely rectangular, or even polygonal the formulae given are extremely accurate for practical purposes .

The significant feature about all asymptotic formulae derived here is that for cross-sections with basically vertical walls 2a units apart and basically flat bottoms giving a small clearance b in water of depth h, they are all dominated for small $\varepsilon = \frac{b}{h}$ by the term $\frac{a}{\varepsilon}$. One may then wonder whether for small ε, an evaluation of $\frac{a}{\varepsilon}$ gives a close assessment of the value of C for cross-sections

of this type. More precisely, one may wonder how small ε must be to give an assessment within a certain permissible bound. This is quite important when considering the ship motions problem of the following chapter, as it happens that most commercial ships have these types of cross-sections over most of their length, only varying from this close to the bow and the stern.

In the case of the pure rectangular cross-section, values of $\frac{a}{\varepsilon}$ are shown as circles in fig. 17. It will be seen that in these cases accuracy of closer than 5% is achieved for $\varepsilon < \frac{1}{4}$, when compared with the analytic results of Flagg and Newman. This suggests that the term $\frac{a}{\varepsilon}$ will be of extremely high practical utility. However, this good result is to a certain extent fortuitous. For instance, an analysis of the other terms of (5.3.6) shows that, to first order terms at least, we must expect the error to be of the order of $- a - \frac{2h}{\pi} \log \frac{4\varepsilon}{e}$. However it turns out that "a" always takes the opposite sign to $\frac{2h}{\pi} \log \frac{4\varepsilon}{e}$, and that in the rectangular cases considered, these almost cancel, causing the error to almost vanish. Both the term a and the logarithmic term, however, are clearly independent, and since each independently is significant, and capable of producing values equal to over 10% of $\frac{a}{\varepsilon}$ say for $\varepsilon = \frac{1}{10}$, we should expect this order of error to occur for some cross-sections where we do not have a and the logarithmic terms almost cancelling.

An example of this is the one which was given to demonstrate the formula (5.4.6) for the polygonal cross-section. In this case $\frac{a}{\varepsilon}$ was equal to 5.5 compared with the numerical value of C = 6.158, an error of the order of 10% for $\varepsilon = \frac{1}{11}$. In the case of the example for the curved section, however, we would have been more fortunate, as in this case $\frac{a}{\varepsilon}$ was equal to 5.0, compared with a numerical value of C = 5.28, an error near 5%.

Thus in deciding whether we can use asymptotic formulae such as (5.3.6) to estimate C in practice we must first of all determine the extent of error we are prepared to allow. If, in fact we decide that an error of 10% is tolerable, we are reasonably safe in simply using $\frac{a}{\varepsilon}$. However, if we are only prepared to allow an error of 5% we must clearly take into account at least all the first order terms. It appears then that (5.5.5) (for the curved shape) may not be satisfactory because of the larger error terms which still arise, due to the inability to carry the matching past the first order terms. It can also appear that (5.4.6) (for the polygonal shape) is not satisfactory from the point of view of practical utility, not because of the accuracy of the formula, which is quite satisfactory, but because extra work is required in its evaluation, in calculating the conformally mapped vertices, using the numerical method of Appendix A. Thus, although we can still conclude that (5.4.6) and (5.5.5) are very interesting from a theoretical viewpoint, they should not take the place of the numerical procedure in the practical calculations arising in the ship motions problems.

However, it is certainly suggested that (5.3.6) (for rectangular cross-sections), which is not only accurate, but easy to use, could be substituted in cases where the cross-section is sufficiently rectangular. Such cross-sections do occur along a significant proportion of the lengths of many commercial ships.

PART 3. THE SHIP HYDRODYNAMICS PROBLEM

CHAPTER 6

THE SWAY EXCITING FORCE ON A STATIONARY SHIP IN SHALLOW WATER DUE TO BEAM SEAS

6.1 FORMULATION OF THE PROBLEM

We use Cartesian co-ordinates, with the sea floor in the plane $z = -h$ and the equilibrium free surface in $z = 0$. The ship is a slender body situated at the free surface, the x-axis coinciding with its longitudinal axis. Dimensionless units are used such that the ship length is 2, with its ends being at the points $(\pm 1,0,0)$. Slenderness implies that every point of the hull lies within a small distance ε of the x-axis, where $\varepsilon \ll 1$. Shallowness of the water implies that $h = O(\varepsilon)$ is also small.

Assuming irrotational flow, at any point in the fluid the velocity is the gradient of a potential

$$\Phi(x,y,z;t) = \phi(x,y,z)e^{-i\sigma t} , \qquad (6.1.1)$$

where we have separated off an assumed sinusoidal time dependence with radian frequency σ. If the fluid is also assumed incompressible, then ϕ will satisfy Laplace's equation in three dimensions, i.e.

$$\nabla^2\phi = \left(\frac{\partial^2}{\partial x^2} + \frac{\partial^2}{\partial y^2} + \frac{\partial^2}{\partial z^2}\right)\phi = 0 . \qquad (6.1.2)$$

On the free surface at a great distance from the ship we suppose that there are plane waves of amplitude ζ_o and frequency σ,

incident from abeam. The velocity potential of these waves will be taken to be

$$\Phi_1 = \phi_1(x,y,z)e^{-i\sigma t} \quad , \tag{6.1.3}$$

where

$$\phi_1(x,y,z) = \left(-\frac{ig\zeta_o}{\sigma}\right) \frac{e^{iky} \cosh k(z + h)}{\cosh kh} \quad , \tag{6.1.4}$$

and

$$k^2 = \frac{\sigma^2}{gh} \quad , \tag{6.1.5}$$

which is valid as a shallow water approximation.

This potential certainly satisfies Laplace's equation, and we shall see that it also satisfies the linearized free surface boundary condition.

As a consequence of the presence of the ship, there will in addition to Φ_1 be a scattered wave of the same frequency, with potential

$$\Phi_2 = \phi_2(x,y,z)e^{-i\sigma t} \quad . \tag{6.1.6}$$

Thus $\phi = \phi_1 + \phi_2$, and ϕ_2 also satisfies Laplace's equation (6.1.2).

The boundary condition on the hull is simply

$$\frac{\partial \phi}{\partial n} = 0 \quad , \tag{6.1.7}$$

where $\frac{\partial}{\partial n}$ denotes differentiation normal to the surface of the hull. At infinity we shall require that the scattered potential ϕ_2 tends to zero suitably (i.e. in particular like an outgoing wave), while on the sea floor, assumed rigid, the boundary condition is

$$\frac{\partial \phi}{\partial z} = 0 \quad \text{on} \quad z = -h \quad . \tag{6.1.8}$$

The free surface condition is the usual linearized condition

$$\frac{\partial^2 \Phi}{\partial t^2} + g \frac{\partial \Phi}{\partial z} = 0 \quad \text{on} \quad z = 0 \ , \tag{6.1.9}$$

(see e.g. Wehausen and Laitone[22]). Recall that this condition arises from a small-motion assumption on the two exact conditions, namely constancy of pressure and lack of flow normal to the free surface. The corresponding linearized expression for the wave elevation

$$z = \zeta(x,y,t) \tag{6.1.10}$$

is

$$\zeta(x,y,t) = - \frac{1}{g} \frac{\partial}{\partial t} \Phi(x,y,0;t) \tag{6.1.11}$$

$$= \frac{i\sigma}{g} \phi(x,y,0) e^{-i\sigma t} \ . \tag{6.1.12}$$

It is easy to check that the plane wave defined by (6.1.3) and (6.1.4) satisfies (6.1.9) and corresponds to a wave elevation

$$\zeta_1(x,y,t) = \zeta_o \, e^{iky - i\sigma t} \ . \tag{6.1.13}$$

So long as we are dealing with pure sinusoidal time dependence $e^{-i\sigma t}$, we can write the free surface condition (6.1.9) entirely in terms of ϕ, i.e.

$$- \sigma^2 \phi + g \frac{\partial \phi}{\partial z} = 0 \ ,$$

or

$$\frac{\partial \phi}{\partial z} = hk^2 \phi \quad \text{on} \quad z = 0 \ . \tag{6.1.14}$$

The problem for the total potential ϕ is illustrated by Figure 24. In the following sections we outline how the scattered potential ϕ_2 may be found using the method of inner and outer expansions.

6.2 THE INNER EXPANSION

The inner region of flow is that near the ship, that is a region in which the co-ordinates have magnitudes

$$x = O(1),\ y,\ z = O(\varepsilon)\ . \tag{6.2.1}$$

The detailed development of inner approximations is similar to that given by Tuck [17]. As a first approximation in the inner region the total potential ϕ will satisfy the two-dimensional Laplace equation

$$\frac{\partial^2\phi}{\partial y^2} + \frac{\partial^2\phi}{\partial z^2} = 0 \tag{6.2.2}$$

in each cross-section x = constant, while the boundary condition on the hull will become

$$\frac{\partial\phi}{\partial N} = 0\ , \tag{6.2.3}$$

where $\frac{\partial}{\partial N}$ denotes a derivative normal to the cross-section curve at station x.

The boundary condition on the sea floor remains (6.1.8), i.e. $\frac{\partial\phi}{\partial z} = 0$, whereas the free surface condition (6.1.14) reduces also to

$$\frac{\partial\phi}{\partial z} = 0 \quad \text{on} \quad z = 0\ , \tag{6.2.4}$$

that is, the free surface appears rigid in the inner region.

Finally, we must provide a boundary condition at "infinity" in the inner region, which means at a relatively great distance $|y| \to \infty$ from the ship (but not so great as to take us out of the inner region). We cannot provide such a boundary condition yet,

since it must come from matching with the outer expansion. However, we can anticipate that the most general behaviour we can match will be to have a streaming flow as $|y| \to \infty$, equivalent to an underflow beneath the hull. Thus we state the velocity as $|y| \to \infty$ to be an as yet indeterminate quantity V, writing

$$\frac{\partial \phi}{\partial y} \to V \quad \text{as} \quad |y| \to \infty \ , \tag{6.2.5}$$

or on integrating separately for + ve and - ve y,

$$\phi \to V(y + C_{\pm}) \quad \text{as } y \to \pm \infty \ , \tag{6.2.6}$$

where C_+, C_- are constants of integration.

The above inner problem is clearly identical to the one formulated and solved in Chapter 4, and illustrated by Fig. 16. Thus for a given ship, we have the means to solve the above inner problem section by section, leading to an accurate evaluation of the function C(x) for the ship, x being the station along the length of the ship. Such a function C(x) is thus available for use in matching with the outer expansion.

6.3 THE OUTER EXPANSION

The outer region is that far to the side of the ship, that is, where the co-ordinates have the order of magnitude

$$x, y = O(1), \quad z = O(\varepsilon) \ . \tag{6.3.1}$$

In this region we assume that the potential $\phi(x,y,z)$ posseses a Taylor expansion of the form

$$\phi(x,y,z) = \phi^{o}(x,y) + (z + h)\phi^{1}(x,y)$$

$$+ \tfrac{1}{2}(z + h)^2\phi^{2}(x,y) + \ldots . \qquad (6.3.2)$$

centred on the sea floor $z = -h$ and valid in the whole fluid from $z = -h$ to $z = 0$. Tuck [19] shows that using this assumption, as well as the boundary condition (6.1.8) on the sea floor and the free surface condition (6.1.14) that

$$\nabla^2 \phi^{o}(x,y) + k^2\phi^{o}(x,y) = 0 , \qquad (6.3.3)$$

that is, the leading term in the outer expansion is a function $\phi^{o}(x,y)$ of x,y alone which satisfies the Helmholtz equation (6.3.3) in the (x,y) plane.

To obtain the boundary condition at infinity we observe that $\phi_2 \to 0$ implies that $\phi \to \phi_1$ at infinity. But if we make the outer approximations on ϕ_1 as given by (6.1.4), that is, expand in a Taylor series with respect to z, we obtain

$$\phi_1(x,y,z) \to \phi_1(x,y,0) = -\frac{ig\zeta_o}{\sigma_o} e^{iky} .$$

Thus the boundary condition for ϕ^{o} is

$$\phi^{o}(x,y) \to -\frac{ig\zeta_o}{\sigma} e^{iky} \quad \text{as} \quad r = \sqrt{x^2 + y^2} \to \infty . \qquad (6.3.4)$$

The outer problem has thus been reduced to an acoustic-type problem, since the same Helmholtz equation (6.3.3) describes two-dimensional acoustics. The boundary condition (6.3.4) at infinity is the same as that for an acoustic plane wave.

We still lack a boundary condition on the ship, which must come from matching with the inner expansion. First note that as $\varepsilon \to 0$ in the outer region the ship shrinks down to a "ribbon" of zero thickness, i.e. $y = 0_{\pm}$, $|x| < 1$. Clearly the boundary condition on this ribbon must be an assertion that as we approach it we get a behaviour ("inner expansion of outer expansion") identical to (6.2.6) ("outer expansion of inner expansion").

Thus the boundary condition for ϕ° on the ribbon is

$$\frac{\partial \phi^{\circ}}{\partial y} = V(x) \quad \text{on} \quad y = 0_{\pm} \ , \tag{6.3.5}$$

$$\phi^{\circ} = V(x)\, C_{\pm}(x) \quad \text{on} \quad y = 0_{\pm} \ . \tag{6.3.6}$$

The problem for ϕ° is illustrated by Fig. 25. It is convenient to again split ϕ° up into an incident and scattered term,

$$\phi^{\circ} = \phi_1^{\circ} + \phi_2^{\circ} \ , \tag{6.3.7}$$

where

$$\phi_1^{\circ} = - \frac{ig\zeta_o}{\sigma} e^{iky} \ , \tag{6.3.8}$$

and $\phi_2^{\circ} = \phi_2^{\circ}(x,y) = \phi_2(x,y,0)$ is the scattered outer potential.

In terms of the new unknown ϕ_2° the problem is to find a solution ϕ_2° of

$$\nabla^2 \phi_2^{\circ} + k^2 \phi_2^{\circ} = 0 \ , \tag{6.3.9}$$

subject to

$$\phi_2^{\circ} \to 0 \text{ like an outgoing wave as } r \to \infty \ , \tag{6.3.10}$$

and

$$\frac{\partial \phi_2^o}{\partial y}(x, 0_\pm) = -\frac{g\zeta_o k}{\sigma} + V(x) \ , \qquad (6.3.11)$$

$$\phi_2^o(x, 0_\pm) = \frac{ig\zeta_o}{\sigma} + V(x)\, C_\pm(x) \ . \qquad (6.3.12)$$

Notice that the derivative ϕ_{2y} does not jump across the ribbon,

$$\frac{\partial \phi_2^o}{\partial y}(x, 0_+) - \frac{\partial \phi_2^o}{\partial y}(x, 0_-) = 0 \ , \qquad (6.3.13)$$

but the potential itself does jump,

$$\begin{aligned} \phi_2^o(x, 0_+) - \phi_2^o(x, 0_-) &= V(x)(C_+(x) - C_-(x)) \\ &= 2V(x)C(x) \ . \end{aligned} \qquad (6.3.14)$$

6.4 CALCULATION OF SWAY EXCITING FORCE, ADDED MASS AND DAMPING COEFFICIENTS

It is now easy to show that the outer problem as defined in the previous section for ϕ_2^o is equivalent to that defined in Chapter 3 by (3.2.1), (3.2.2) and (3.2.3) for ϕ_2. We will then be able to use the method of Chapter 3 to solve this outer problem (in conjunction with the method of Chapter 4 to calculate C(x)) for a particular ship, and hence be able to calculate the sway exciting force, and added mass and damping coefficients, as in Tuck [19].

To show the equivalence between the problems of the previous section and that of Chapter 3, we first of all note that both have the Helmholtz equation ((3.2.1) and (6.3.9)) in common, as well as the condition of no jump in the normal derivative across the ribbon

((3.2.3) and (6.3.13)). In addition, we required in each case that the potential tend to zero like an outgoing wave as $r \to \infty$. It remains to show that the boundary condition on the ribbon in the problem of the previous chapter is of the same form as (3.2.2).

If we set $-\frac{g\zeta_o k}{\sigma} = 1$ in (6.3.11) and substitute (6.3.14) into this equation, we obtain

$$\frac{\partial \phi_2^o}{\partial y}(x, 0_\pm) = 1 + \frac{\phi_2^o(x, 0_+) - \phi_2^o(x, 0_-)}{2C(x)} . \qquad (6.4.1)$$

From the integral formulation of the Helmholtz equation (6.3.9) as in Chapter 3 for (3.2.1) we observe that $\phi_2^o(x,y)$ is antisymmetric in y. It then follows that (6.4.1) will take the same form as (3.2.2).

The procedure for calculating the sway exciting force and added mass and damping coefficients for a particular ship is now clear. First one inputs data concerning the ship's geometry into a computer program which calculates $C(x)$ using the method of Chapter 4. This is done separately for each individual cross-section, and one must choose a number of cross-sections which is large enough to give a smooth curve for $C(x)$, but small enough so as to use a minimum amount of computing time. It is found in practice that for a commercial ship, no more than 15 cross-sections need be used in order to get a reasonably smooth curve. Most tankers and freighters have a uniform cross-section along most of their length, and this cross-section need only be read in and the value of C computed once.

In general, for ships such as these, the graph of C(x) rises from zero at each end rather steeply, and levels out as a straight, horizontal line for most of the distance between the ends.

An example of this is Fig. 26, which shows the curves which were obtained for a Series 60, block 0.80 tanker (Todd[15]). The upper curve represents the case where the draft of the tanker takes up 0.9 of the available depth of water whereas the lower curve is for the same tanker with a draft/water depth ratio of 0.8.

Once the value of C(x) is known, it can be fed as input into the computer program which solves the outer problem using the method of Chapter 3. The recommended way of doing this is to feed in the discrete values of C as calculated in the method of Chapter 4, for a relatively small number of sections, and to include a linear interpolation procedure in the outer problem, to enable C to be calculated at the greater number values of x required there. Solution of the outer problem will lead to the function $\phi_2(x, 0_+) = \frac{1}{2}\Delta\phi_2(x)$ (using the notation of Tuck[19]) for the potential jump at point x on the ribbon.

We are then in a position to calculate

$$C_F(k,\beta) = -\frac{k \sin\beta}{2} \int_{-1}^{1} \Delta\phi_2(x)\, e^{ikx \cos\beta}\, dx \qquad (6.4.2)$$

which, from Tuck's[19] equation (82), is the non-dimensional sway exciting force coefficient due to incidence of waves of frequency k from an angle β. In the case of beam seas ($\beta = \frac{\pi}{2}$), Tuck shows that the sway exciting force becomes

$$C_F(k, \frac{\pi}{2}) = -\frac{k}{2} \int_{-1}^{1} \Delta\phi_2(x)dx \ , \qquad (6.4.3)$$

and that in this particular case the real part of $\frac{C_F}{k}$ is proportional to the sway added mass, and the imaginary part to the sway damping coefficient.

Values of $|C_F|$ for beam seas as well as the sway added mass and damping coefficients have been computed using the method of Chapter 3, and are plotted in Figures 27, 28 and 29 respectively. These are plotted against the frequency k for a Series 60, block 0.80 tanker with draft/water depth ratios of 1.0, 0.9 and 0.8.

The draft/water depth ratio of 1.0 is the case where the ship is touching the bottom, and this case corresponds to the Neumann diffraction problem of Chapter 2, as we are then considering the limiting case as $C \to \infty$. In this case the graph of $|C_F|$ is shown to have pronounced wobbles as functions of frequency. This is due to the interference between the waves diffracted around the two ends of the ship. This characteristic of the graph becomes reduced for the lower draft/water depth ratios, due to the fact that some of the wave energy can now pass under the ship, making the diffraction patterns weaker.

It is also noted that in the cases considered (all of which involve a significant blockage effect by the ship) the high frequency limit of C_F is 2.0. This limit corresponds physically to the case when the ship is many wavelengths long, and acts as a perfect

reflector, causing a pure standing wave to exist in its neighbourhood. It is also noted that the only component which contributes towards this limiting value is the damping, as the added mass tends to zero for high values of k. The limiting value is the same for all values of C(x), because as the wavelength gets shorter and shorter, the waves become less able to penetrate beneath the hull. Another feature of the graphs is that the forces tend to decrease as the draft/water depth ratio is decreased, this being when the ship becomes less of a barrier to the passage of wave energy.

Fig. 30 shows computations for $|C_F|$ in the case of $\beta = \frac{\pi}{4}$, i.e. a different angle of incidence. It is once again noticeable that the graph has distinct wobbles for the limiting case as $C \to \infty$ whereas these decrease for lower values of C, and the physical explanation is the same as for beam seas. As one would expect from physical considerations, the value of $|C_F|$ is always smaller than for the corresponding beam seas case. The only other difference in these cases is the high frequency limit which tends to zero in fact for all $\beta \neq \frac{\pi}{2}$, as can be verified by an inspection of (6.4.2). One should not attempt to make a physical explanation of this phenomenon, for two reasons. The first is that in the high frequency case the shallow water assumption breaks down. The other is that the matching process as carried out in this Chapter also breaks down, as it essentially requires that the wavelength of the incident wave is of the same order as the length of the ship.

The computations presented here should be compared with those given by Tuck[19] for a mathematically idealised ship with

$$C(x) = c_o \sqrt{1 - x^2} \quad . \qquad (6.4.4)$$

These computations are in fact not greatly different than those in Figs. 27, 28 and 29, and this leads us to two important conclusions. The first of these is that (6.4.4) is not an unreasonable approximation to the shape of the curves in Fig.26 (i.e. for suitable values of c_o). The second conclusion, and one which is very important from the point of view of practical application, is that as the value of $|C_F|$ appears to a large degree insensitive to the value of C(x) for small clearances it should not be necessary to use the numerical method of Chapter 4 to calculate C in these cases. For instance, it may be quite satisfactory to estimate C for these cross-sections by "$\frac{a}{\varepsilon}$", which was shown in Section 5.6 to have an accuracy of the order of 10%.

APPENDIX A

ANALYSIS OF CONFORMAL MAPPING BETWEEN TWO CORNERED POLYGONAL SHAPE AND UPPER HALF PLANE

In this Appendix we show a method for obtaining the values of ζ_1 and ζ_2 as referred to in Section 5.4. The mapping between the two cornered polygon in the z-plane and the upper ζ-plane was given as

$$\frac{dz}{d\zeta} = \frac{b}{\pi} \frac{(\zeta - \zeta_1)^{\alpha} (\zeta - \zeta_2)^{\frac{1}{2}-\alpha}}{(-\zeta_1)^{\alpha} (-\zeta_2)^{\frac{1}{2}-\alpha}} \frac{1}{\zeta} = F(\zeta) \text{ say,}$$

$$= \frac{b}{\pi} \frac{1}{\zeta} + E \ ,$$

where

$$E = \frac{\zeta F(\zeta) - \frac{b}{\pi}}{\zeta} \sim 0 \quad \text{as} \quad \zeta \sim 0 \ . \tag{A.1}$$

Thus, since the constant of integration is a,

$$z = \frac{b}{\pi} \log \zeta + a + \int_0^{\zeta} \frac{\zeta F(\zeta) - \frac{b}{\pi}}{\zeta} d\zeta$$

$$= \frac{b}{\pi} \log \zeta + a + \frac{b}{\pi} \int_0^{\zeta} \frac{dt}{t} \left[\frac{(t - \zeta_1)^{\alpha} (t - \zeta_2)^{\frac{1}{2}-\alpha}}{(-\zeta_1)^{\alpha} (-\zeta_2)^{\frac{1}{2}-\alpha}} - 1 \right] . \tag{A.2}$$

If we let $\zeta = -\zeta_1\zeta'$ such that $\zeta = \zeta_1 \Rightarrow \zeta' = -1$ and $\zeta = \zeta_2 \Rightarrow \zeta' = -1$ and $\zeta = \zeta_2 \Rightarrow \zeta' = -r$, where $r = \zeta_2/\zeta_1$, and let $t = -\zeta_1 t'$, we have

$$z = \frac{b}{\pi} \log (-\zeta_1\zeta') + a + \frac{b}{\pi} \int_0^{\zeta'} \frac{dt'}{t'} \left[(1 + t')^{\alpha} \left(1 + \frac{t'}{r}\right)^{\frac{1}{2}-\alpha} - 1 \right] . \tag{A.3}$$

Furthermore, if we substitute $\tau = -t$, we have

$$z = \frac{b}{\pi} \log (-\zeta_1\zeta') + a + \frac{b}{\pi} (-1)^{\alpha} F(\alpha,r,\zeta') - \frac{b}{\pi} \int_0^{-\zeta'} \frac{d\tau}{\tau} ,$$

where

$$F(\alpha,r,\zeta') = \int_0^{-\zeta'} \frac{d\tau}{\tau} (-1+\tau)^{\alpha} (-\frac{\tau}{r} + 1)^{\frac{1}{2}-\alpha}. \qquad (A.4)$$

Evaluating (A.4) at $\zeta = \zeta_1$ and $\zeta = \zeta_2$ gives the equations

$$z_1 = \frac{b}{\pi} \log \zeta_1 + a + \frac{b}{\pi} (-1)^{\alpha} F(\alpha,r,1) - \frac{b}{\pi} \int_0^{1} \frac{d\tau}{\tau} , \qquad (A.5)$$

and

$$z_2 = \frac{b}{\pi} \log r\zeta_1 + a + \frac{b}{\pi} (-1)^{\alpha} F(\alpha,r,r) - \frac{b}{\pi} \int_0^{r} \frac{d\tau}{\tau} \qquad (A.6)$$

respectively.

Subtracting (A.5) from (A.6) leads to the equation

$$\frac{|z_2 - z_1|}{b} = \frac{1}{\pi} (F(\alpha,r,r) - F(\alpha,r,1)) . \qquad (A.7)$$

This will give a value of $r(= \zeta_2/\zeta_1)$, given the values of z_1 and z_2 (and hence α), and then ζ_1 can be obtained from (A.5). Thus ζ_1 and ζ_2 can be determined as functions of z_1 and z_2 . The function $F(\alpha,r,\zeta',)$ defined by (A.4) and required at $\zeta' = r$ and $\zeta' = 1$ in (A.7) can be evaluated by standard numerical quadratures. For the results given in Section 5.4, the trapezoidal rule was used.

REFERENCES

1. ABRAMOWITZ, M., and STEGUN, I. A., "Handbook of Mathematical Functions", Dover, 1965.

2. BECK, R. F., and TUCK, E. O., "Heave and Pitch of Ships in Shallow Water", Fourth Australian Conference on Hydraulics and Fluid Mechanics, Melbourne, Australia, 1971.

3. BORN, M., and WOLF, E., "Principles of Optics", 2nd Edition, Pergamon Press, 1964.

4. CARRIER, G. F., "Integral Equation Boundary Layer Problems", 50 Jahre Greuzschichtforschung, (Gortler, H., and Tollimeir, W., eds.), Friedrich Vieweg, Braunschweig, 1955.

5. COPLEY, L. G., "Fundamental Results Concerning Integral Representations in Acoustic Radiation", Journal of the Acoustical Society of America, pp. 28-32, Vol. 44, 1968.

6. FLAGG, C. N., and NEWMAN, J. N., "Sway Added-Mass Coefficients for Rectangular Profiles in Shallow Water", submitted to Journal of Ship Research, 1971.

7. FRANK, W., "Oscillation of Cylinders in or below the Free Surface of Deep Fluids", N.S.R.D.C. Report No. 2375, Washington, D.C., 1967.

8. GUREVICH, M.I., "Added Mass of a Lattice Consisting of Rectangles" (in Russian), Prokl. Mat. i. Mech., pp. 95-100, Vol. 4, No. 2, 1940.

9. HÖNL, H., MAUE, A. W., and WESTPHAL, K., "Theorie der Beugung", Handbuch der Physik, editor S. Flugge, pp. 218-573, Vol. 25, Springer-Verlag, Berlin, 1961.

10. KOBER, H., "Dictionary of Conformal Representations", Dover, 1957.

11. LAMB, H., "Hydrodynamics", (6th edn.), C.U.P. and Dover, 1932.

12. MORSE, P. M., and INGARD, K. U., "Theoretical Acoustics", McGraw-Hill, 1968.

13. MORSE, P. M. and RUBENSTEIN, P. J., "The Diffraction of Waves by Ribbons and by Slits", Physical Review, pp. 895-898, Vol. 54, 1938.

14. MUSKHELISHVILI, N. E., "Singular Integral Equations", Noordhoff, Groningen, 1953.

15. TODD, F. H., "Series 60, Methodical Experiments with Models of Single-Screw Merchant Ships", N.S.R.D.C. Report No. 1712, Washington, D.C., 1963.

16. TRICOMI, F. G., "Integral Equations", Interscience, New York, 1957.

17. TUCK, E. O., "Shallow Water Flows Past Slender Bodies", Journal of Fluid Mechanics, pp. 81-95, Vol. 26, 1966.

18. TUCK, E. O., "Calculation of Unsteady Flows due to Small Motions of Cylinders in a Viscous Fluid", Journal of Engineering Mathematics, pp. 29-44, Vol. 3, No. 1, 1969.

19. TUCK, E. O., "Ship Motions in Shallow Water", Journal of Ship Research, pp. 317-328, Vol. 14, No. 4, 1970.

20. TUCK, E. O., and TAYLOR, P. J., "Shallow Water Problems in Ship Hydrodynamics", 8th Symposium on Naval Hydrodynamics, Pasadena, 1970.

21. VAN DYKE, M., "Perturbation Methods in Fluid Mechanics", Academic Press, New York, 1964.

22. WEHAUSEN, J. V., and LAITONE, E. V., "Surface Waves", Handbuch der Physik, editor S. Flugge, pp. 446-778, Vol. 9, Springer-Verlag, Berlin, 1960.

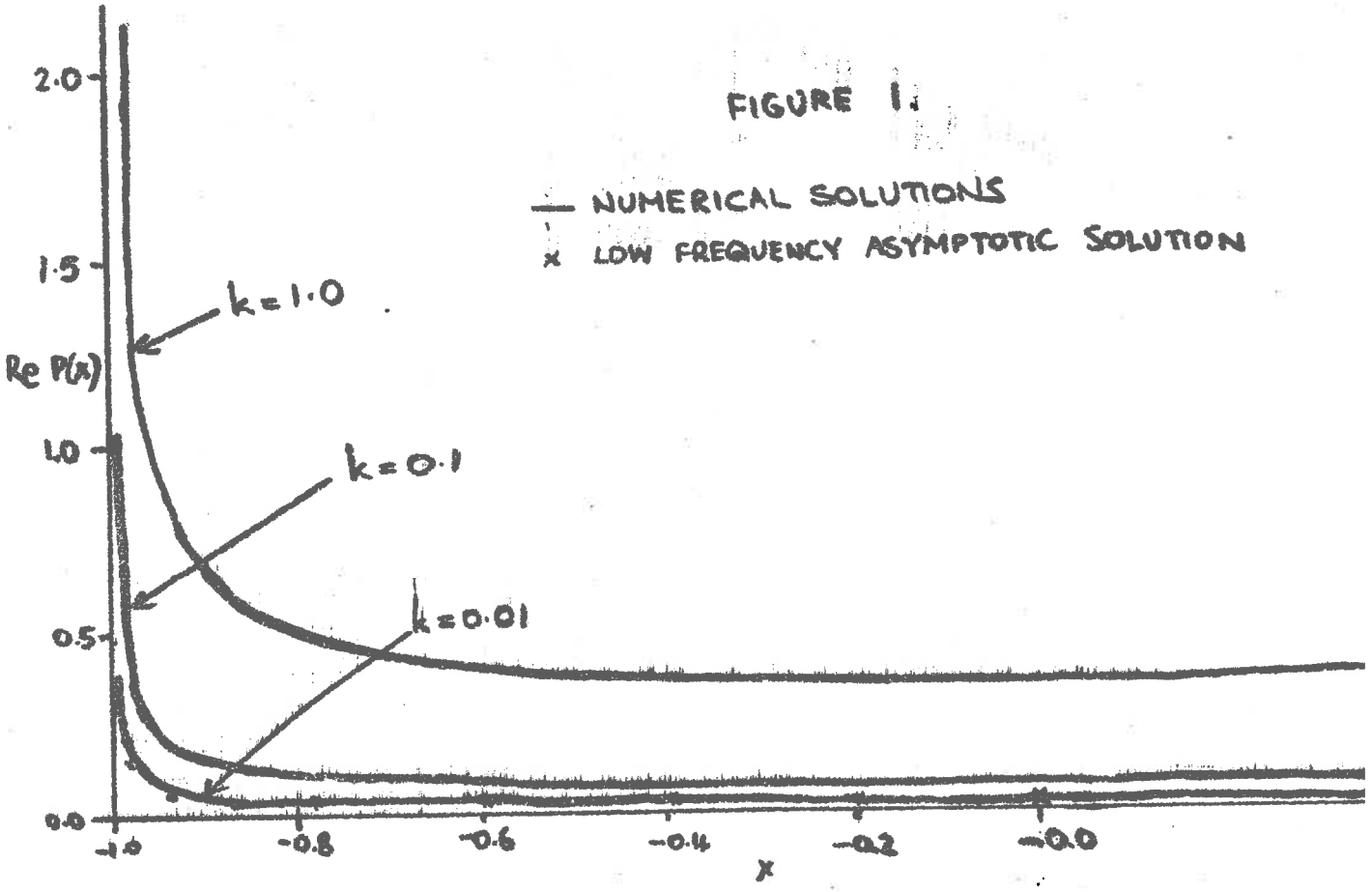

FIGURE 1.

— NUMERICAL SOLUTIONS
x LOW FREQUENCY ASYMPTOTIC SOLUTION

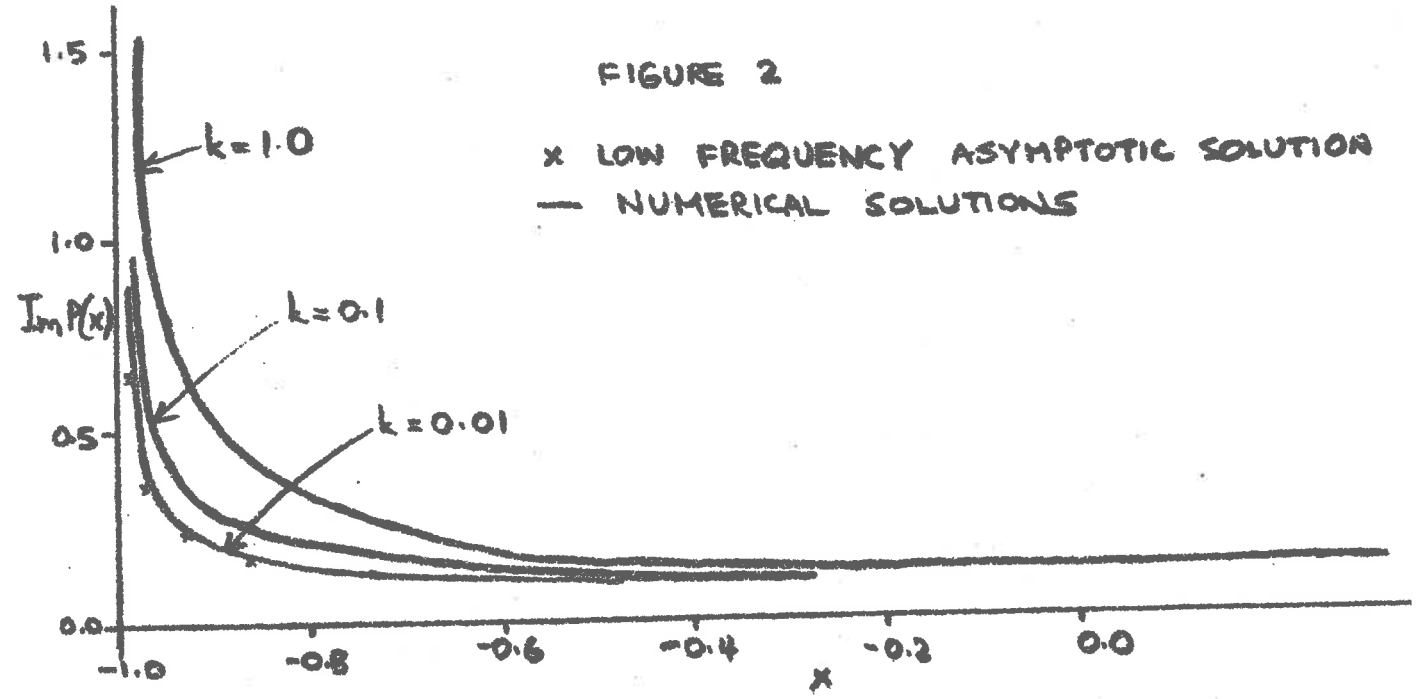

FIGURE 2

x LOW FREQUENCY ASYMPTOTIC SOLUTION
— NUMERICAL SOLUTIONS

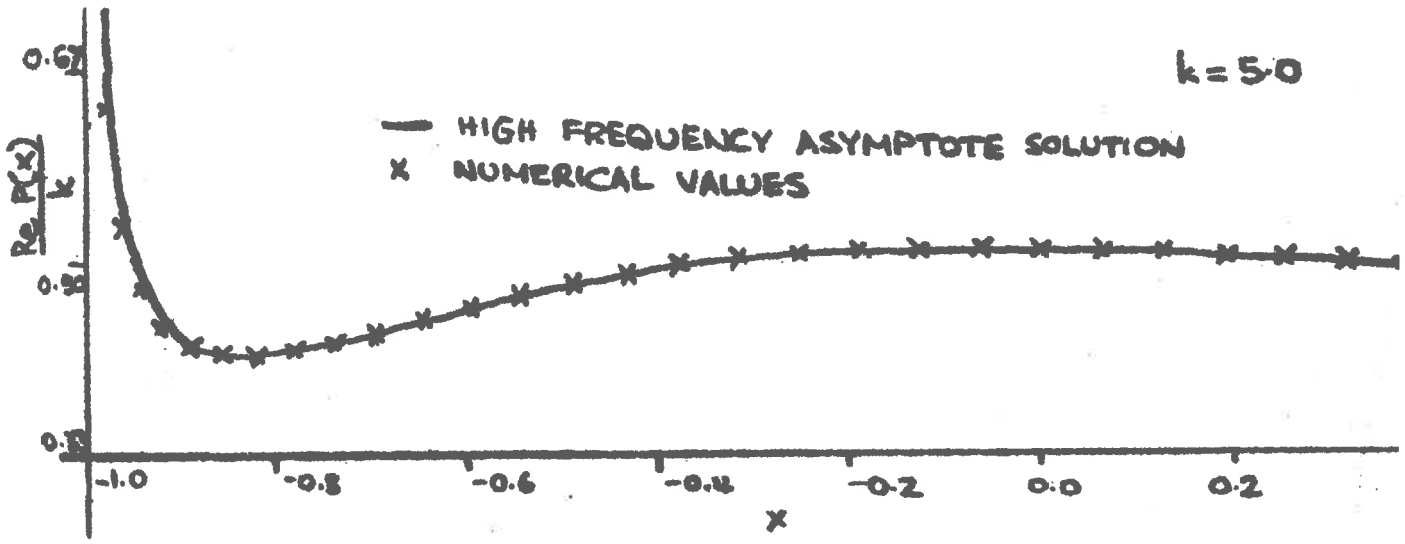

FIGURE 3.

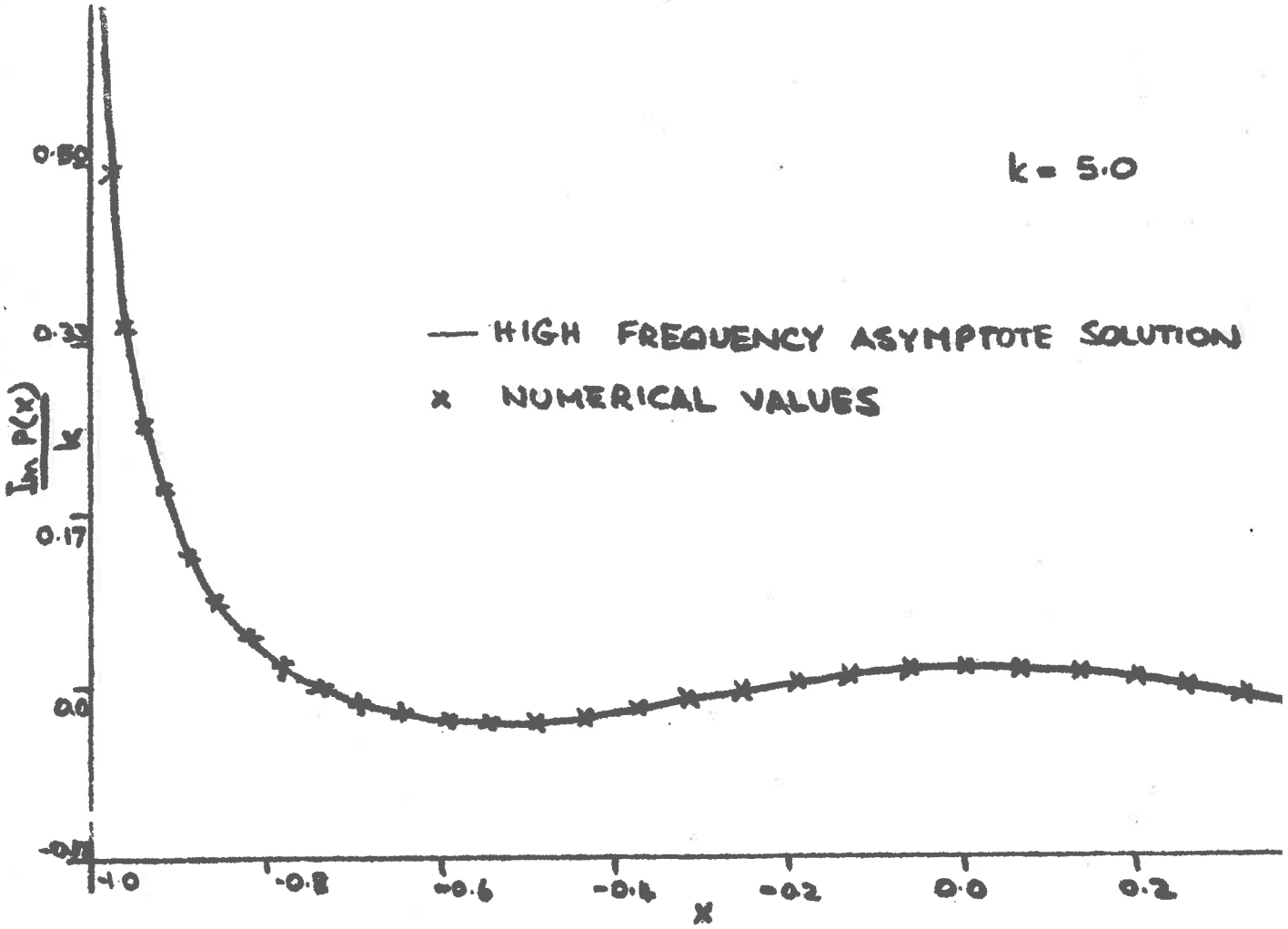

FIGURE 4.

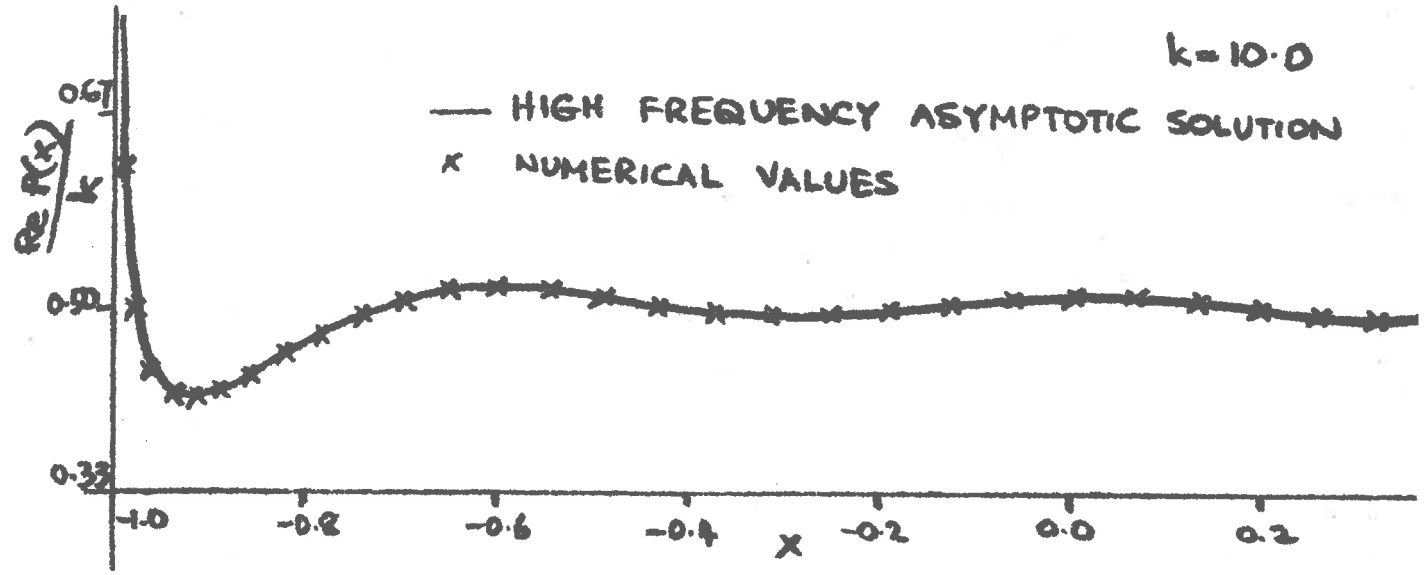

FIGURE 5.

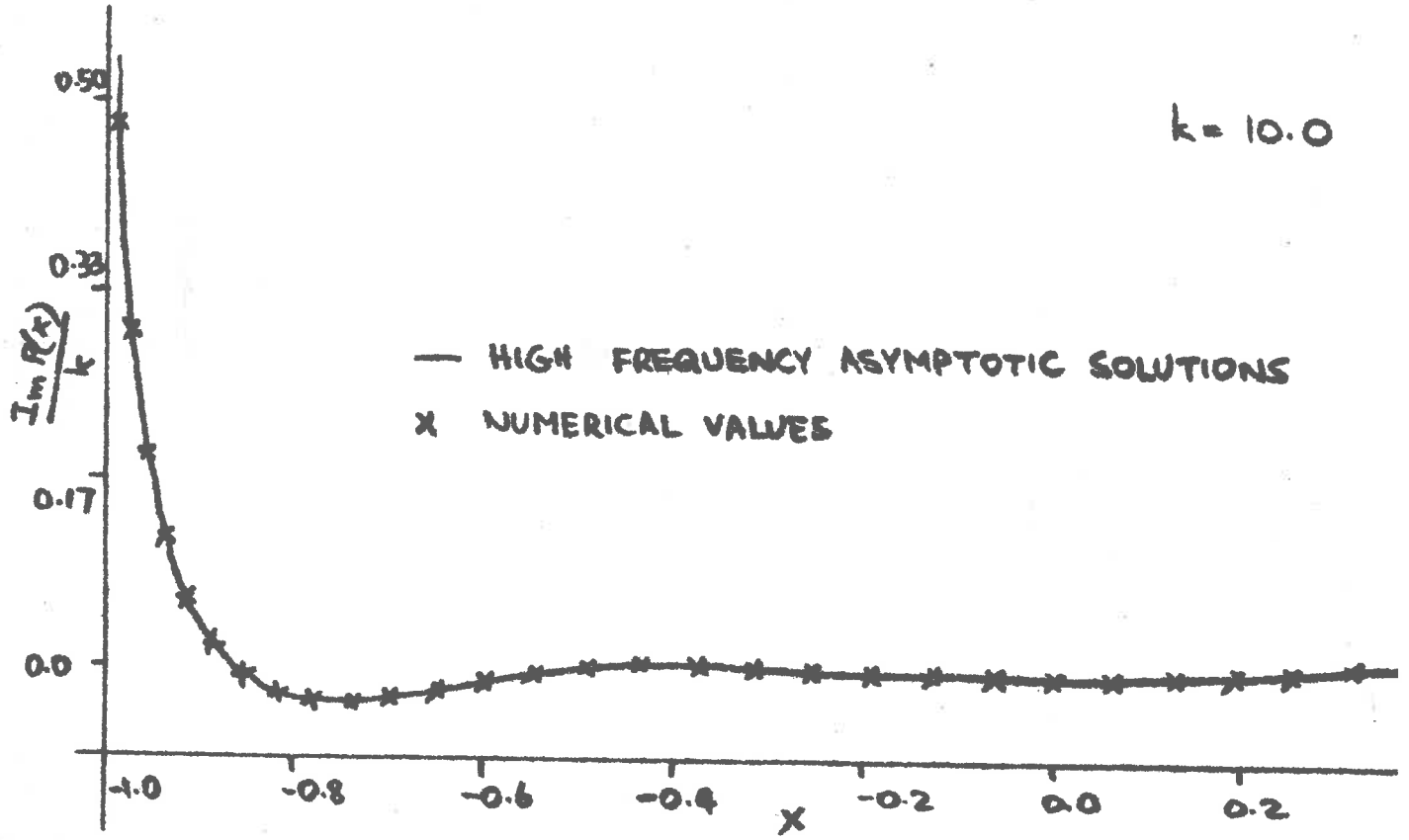

FIGURE 6.

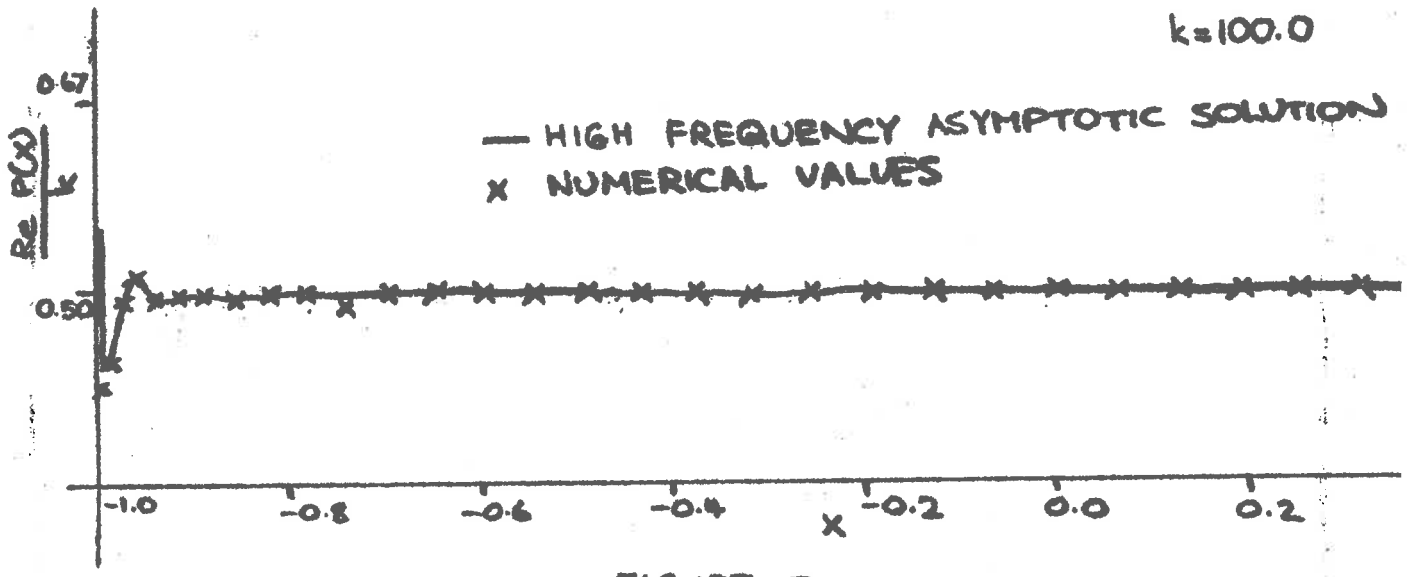

FIGURE 7.

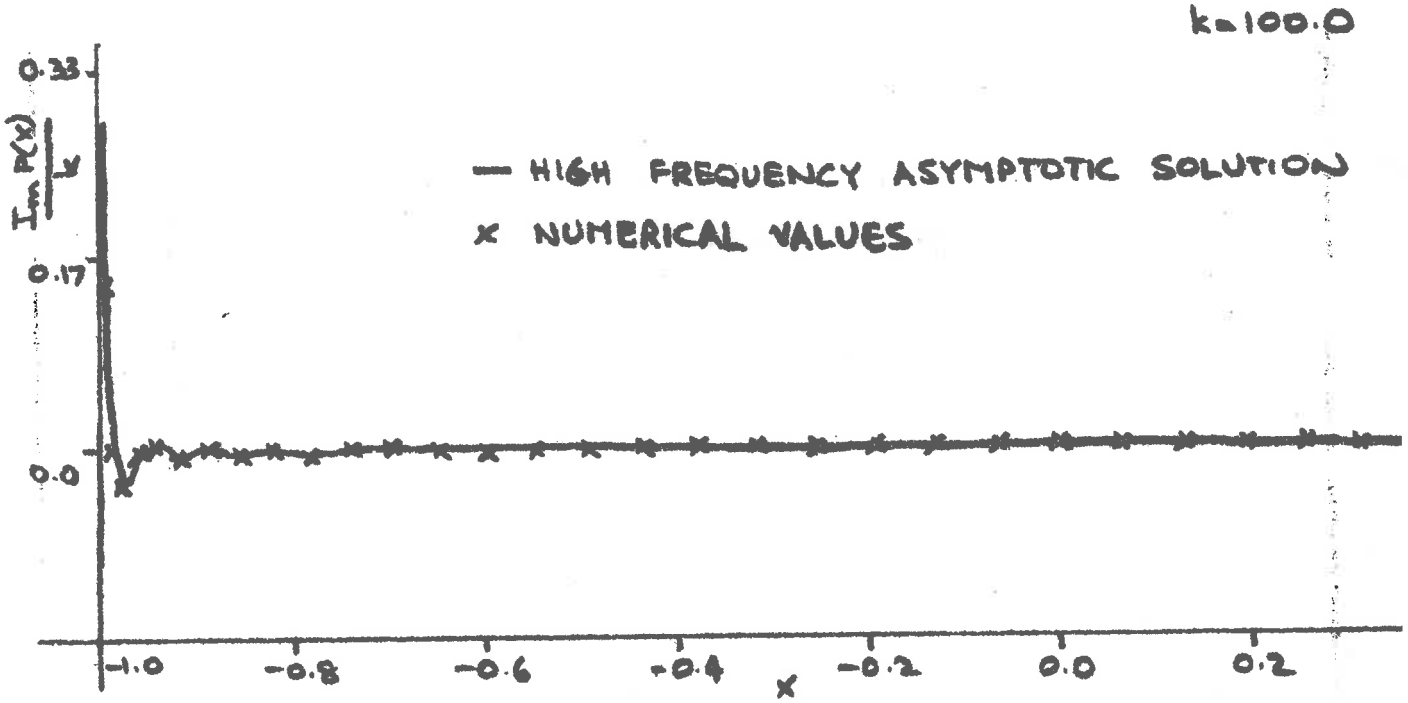

FIGURE 8.

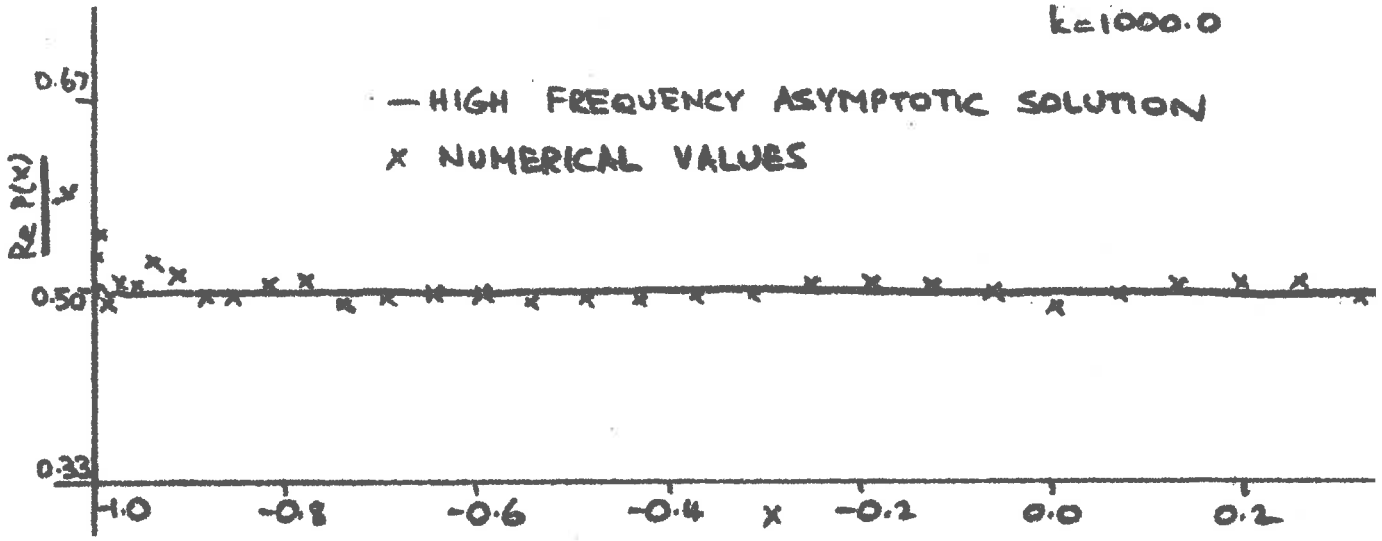

FIGURE 9.

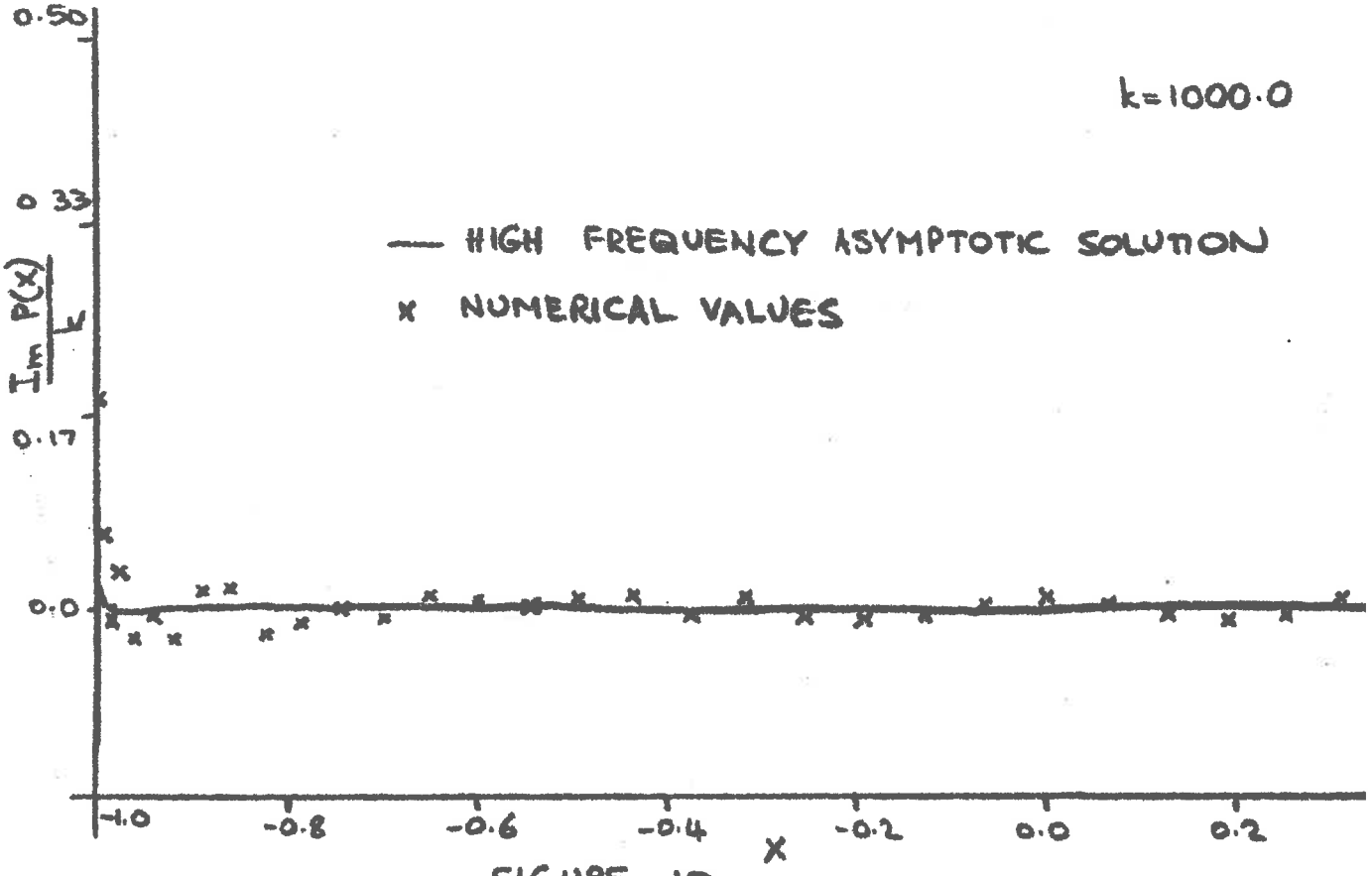

FIGURE 10.

FIGURE 11.
FARFIELD INTENSITY DIAGRAMS.

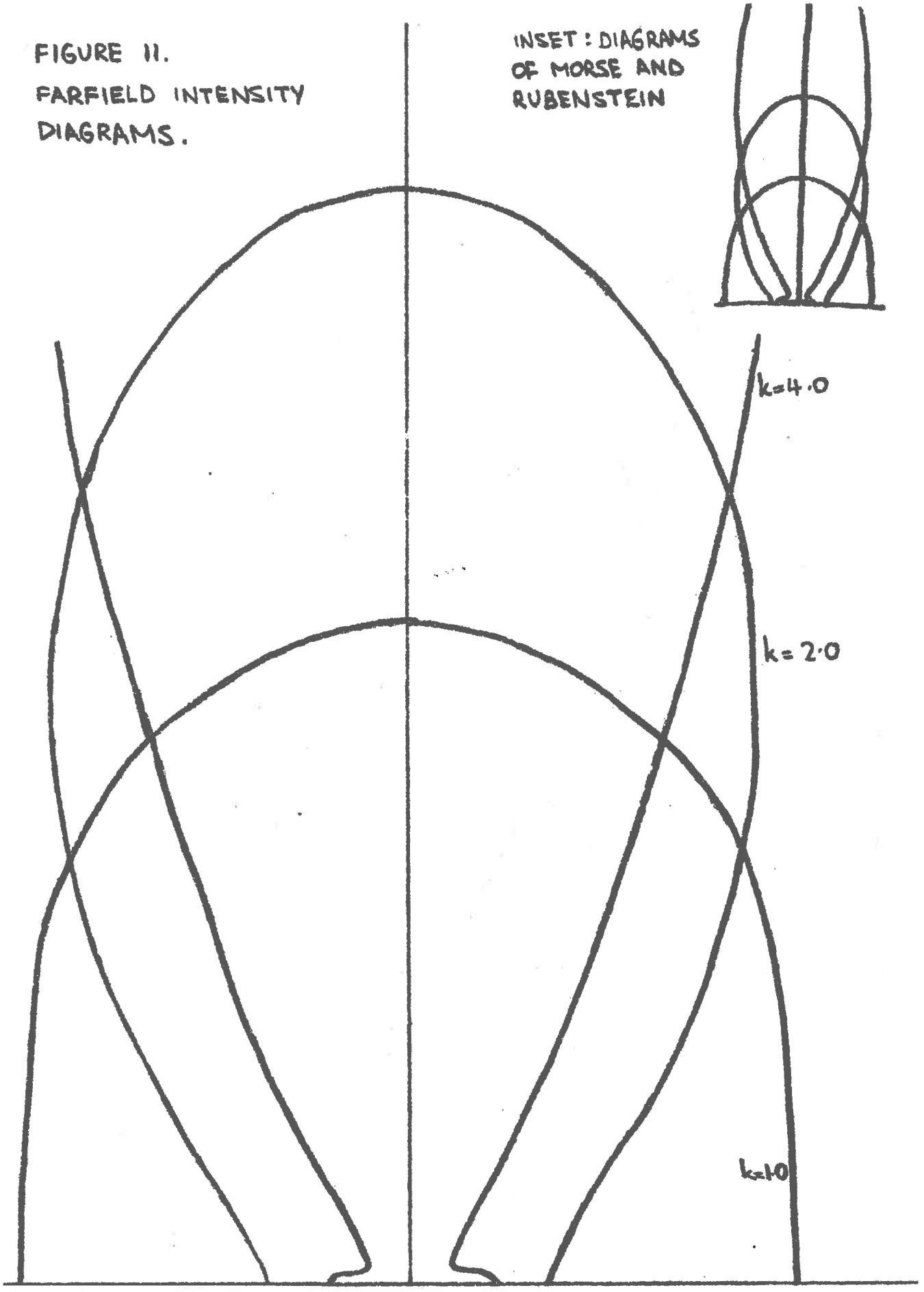

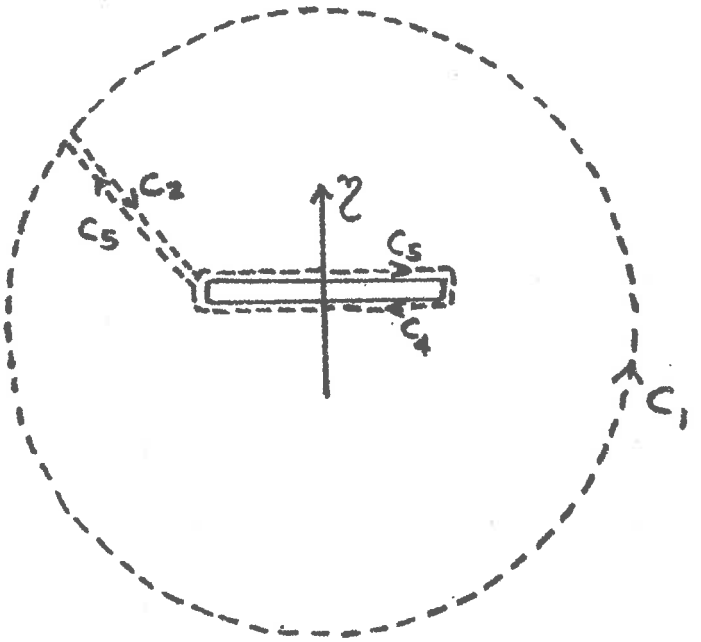

Figure 12. The Contour C of Integration used in Green's Theorem for the Helmholtz Equation.

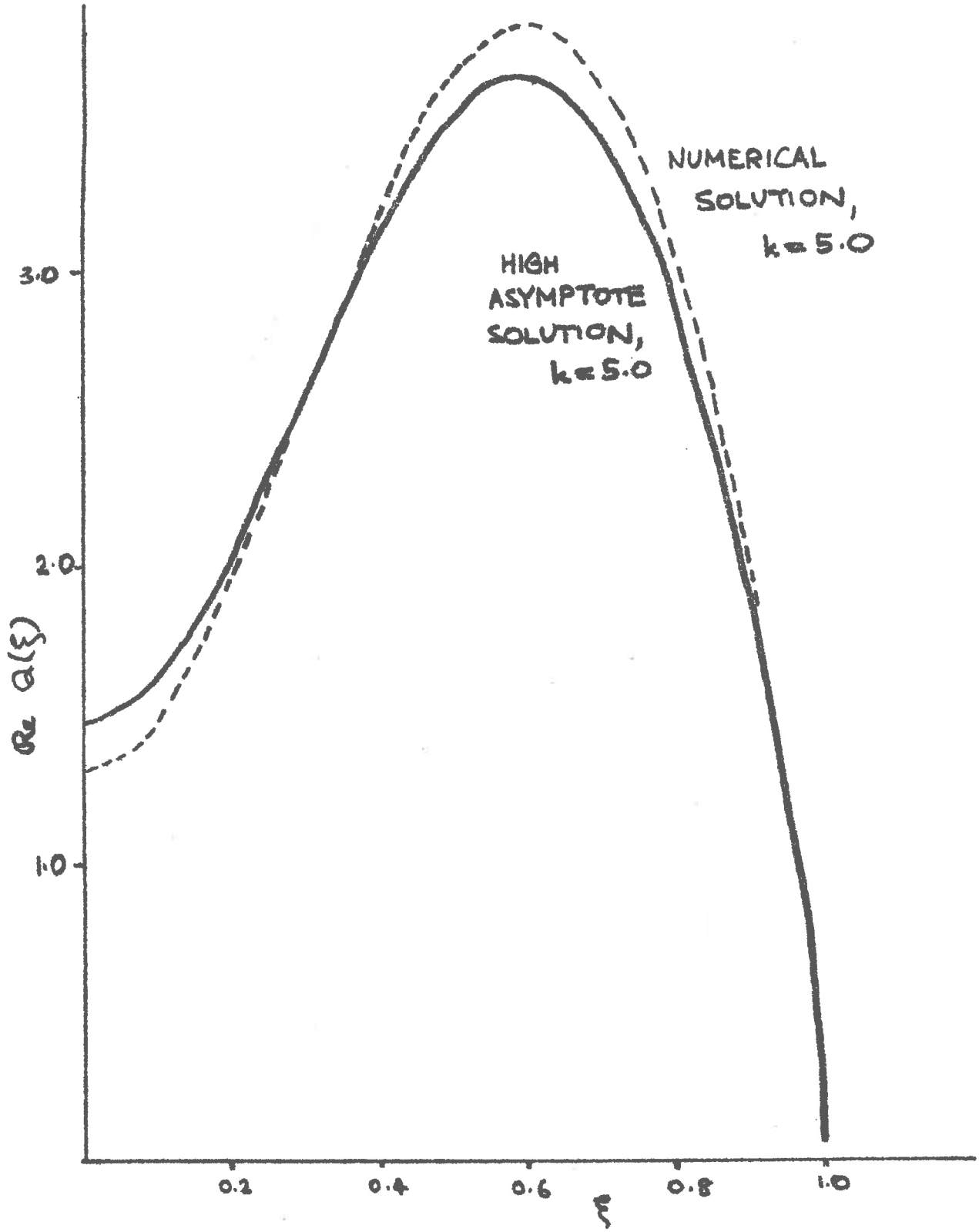
NUMERICAL SOLUTION, k=5.0
HIGH ASYMPTOTE SOLUTION, k=5.0
3.0
2.0
1.0
Re a(ξ)
0.2
0.4
0.6
0.8
1.0
ξ

Figure 13.

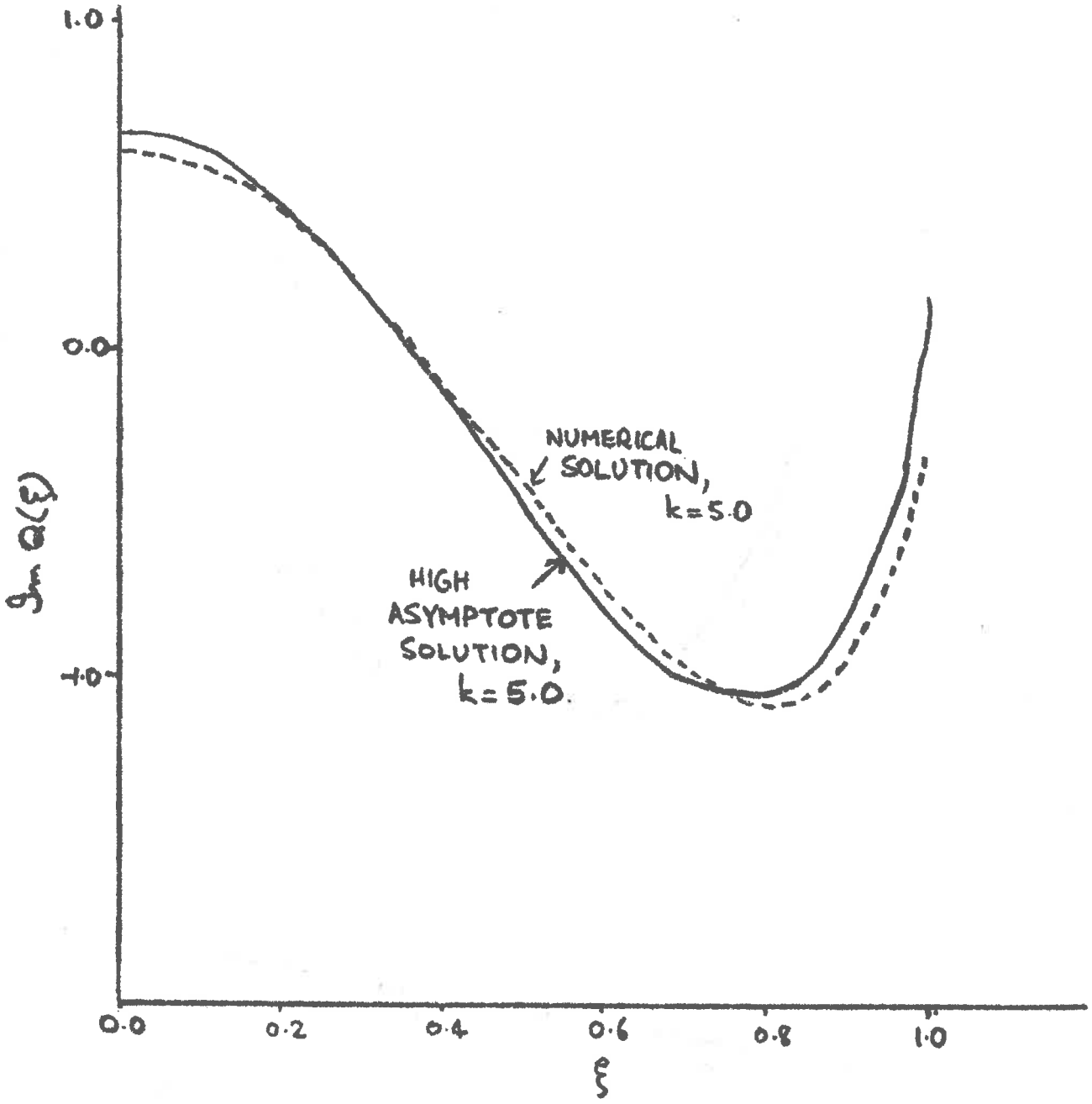
1.0
0.0
-1.0
Im Q(ξ)
NUMERICAL SOLUTION, k=5.0
HIGH ASYMPTOTE SOLUTION, k=5.0
0.0
0.2
0.4
0.6
0.8
1.0
ξ

Figure 14.

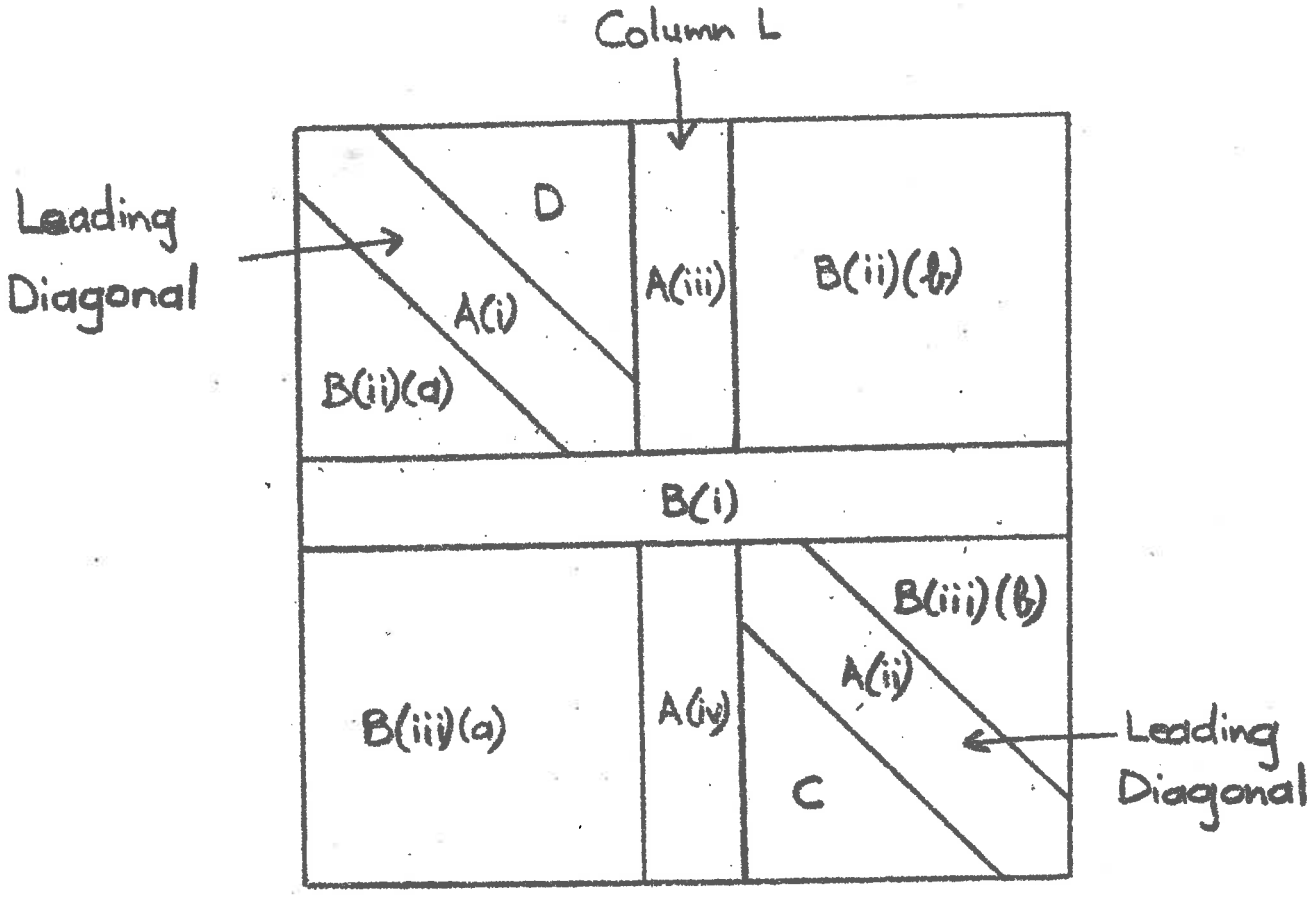

Figure 15. Structure of D_{kj}, $L = \frac{N+1}{2}$, where N is odd.

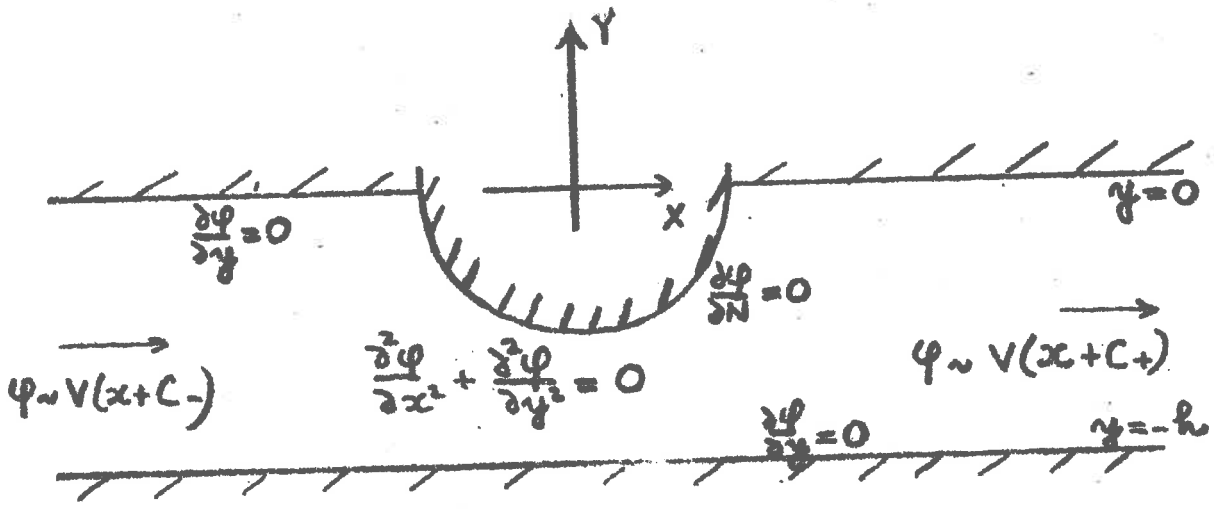

FIGURE 16. THE BOUNDARY VALUE PROBLEM.

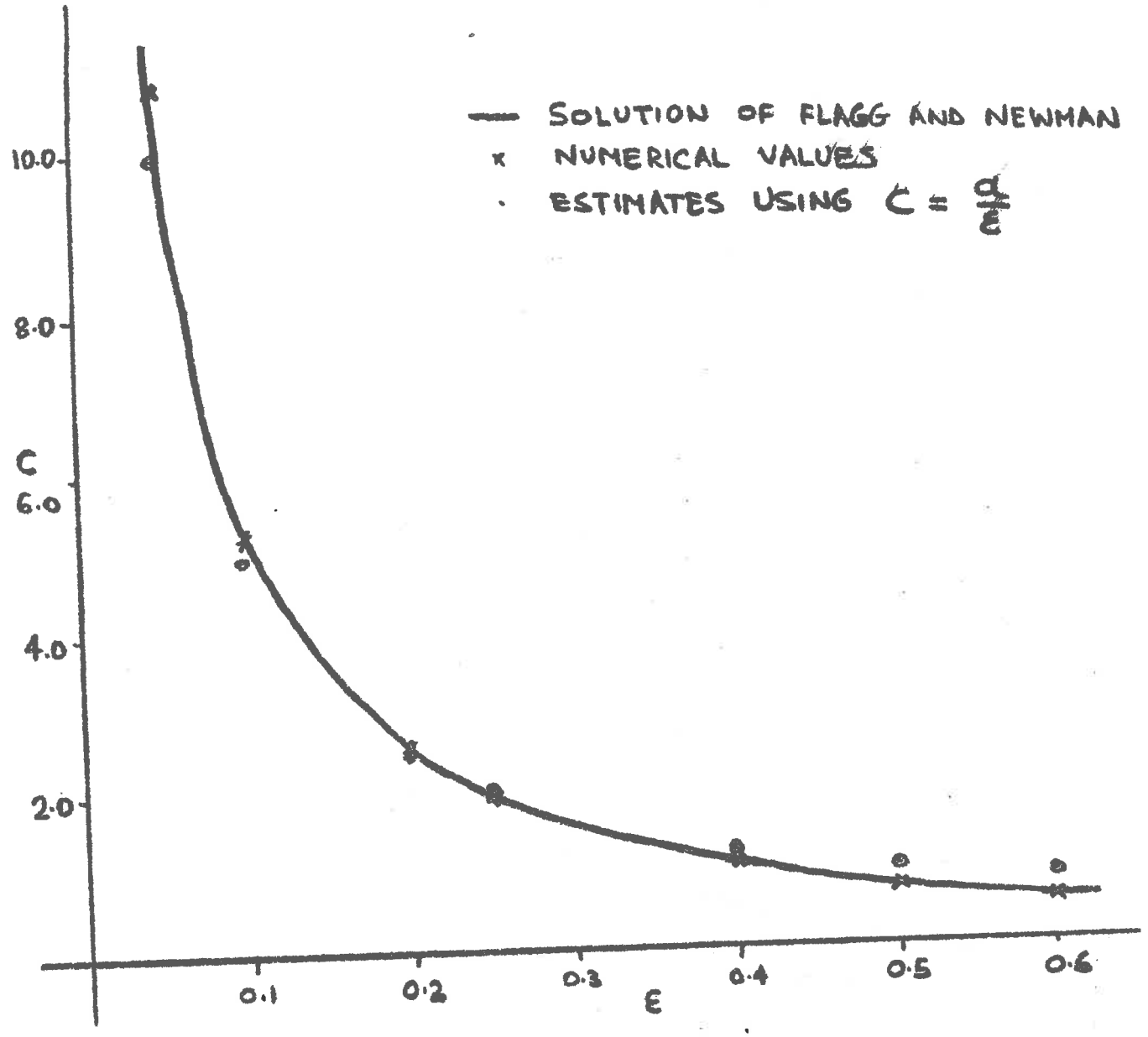
SOLUTION OF FLAGG AND NEWMAN
NUMERICAL VALUES
ESTIMATES USING C = q/ε
10.0
8.0
C
6.0
4.0
2.0
0.1
0.2
0.3
0.4
0.5
0.6
ε

FIGURE 17

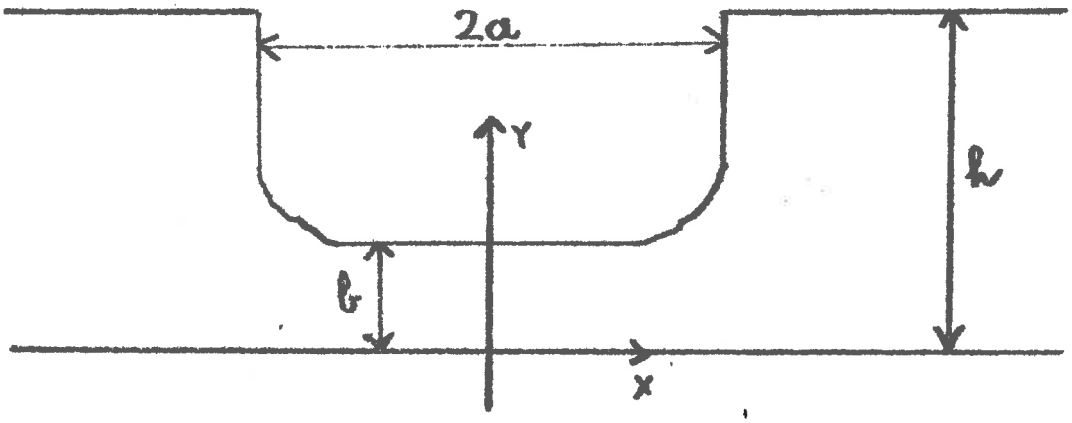

FIGURE 18.
AN ARBITRARY CROSS-SECTION

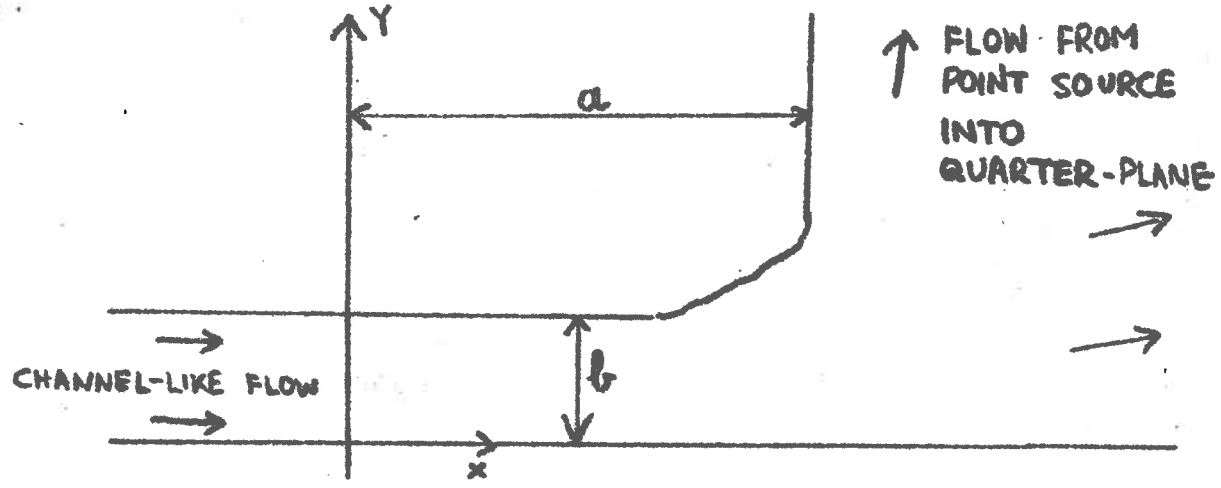

FIGURE 19.
THE INNER REGION FOR
AN ARBITRARY CROSS-SECTION.

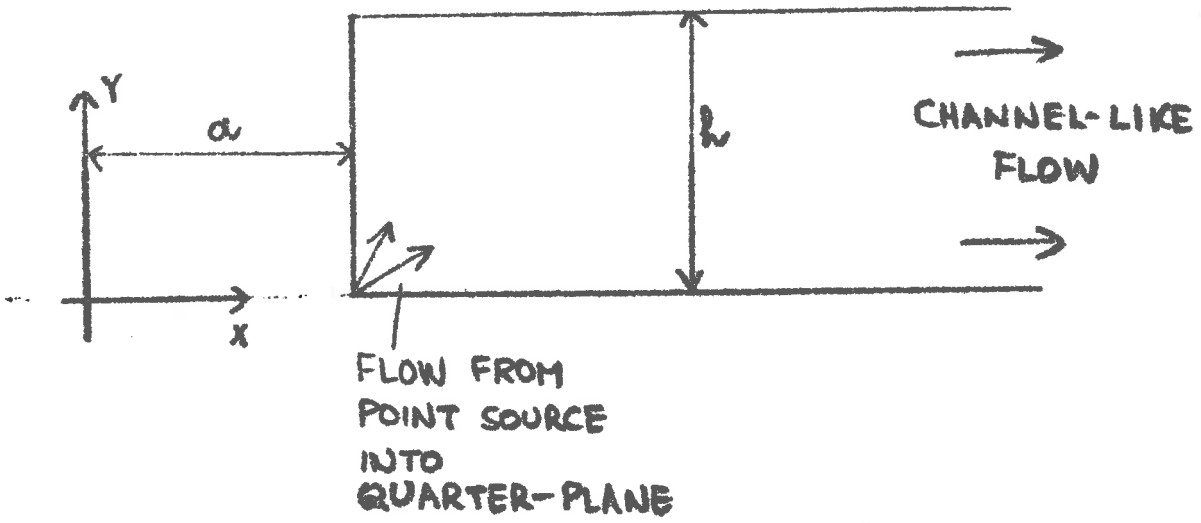

FIGURE 20. THE OUTER REGION.

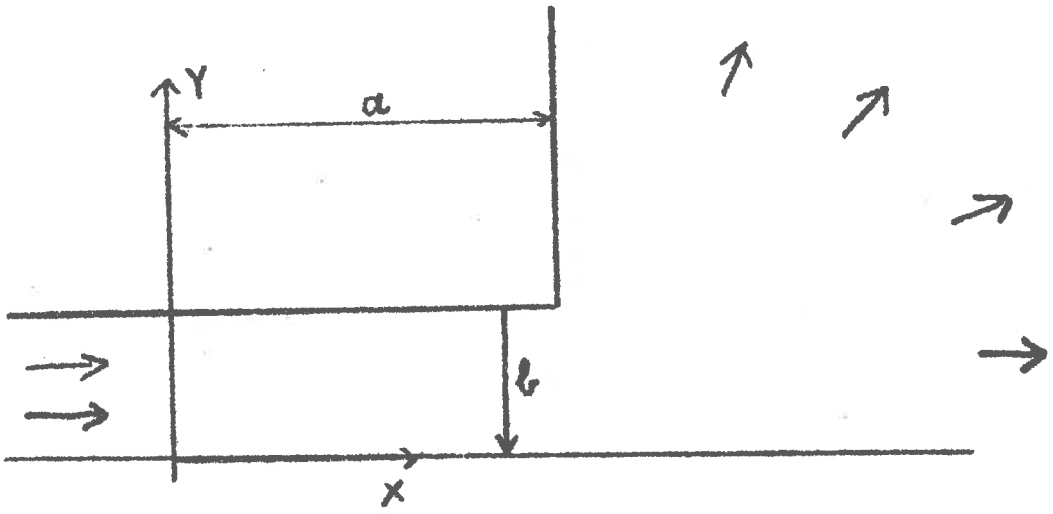

FIGURE 21. THE INNER REGION
FOR THE RECTANGULAR CROSS-SECTION.

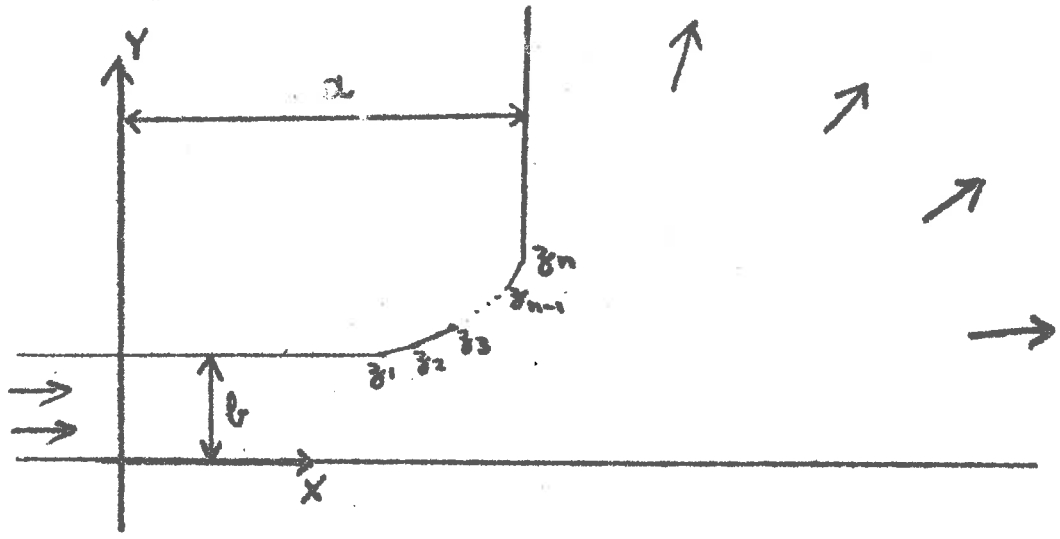

FIGURE 22. POLYGONAL CROSS-SECTION WITH n VERTICES.

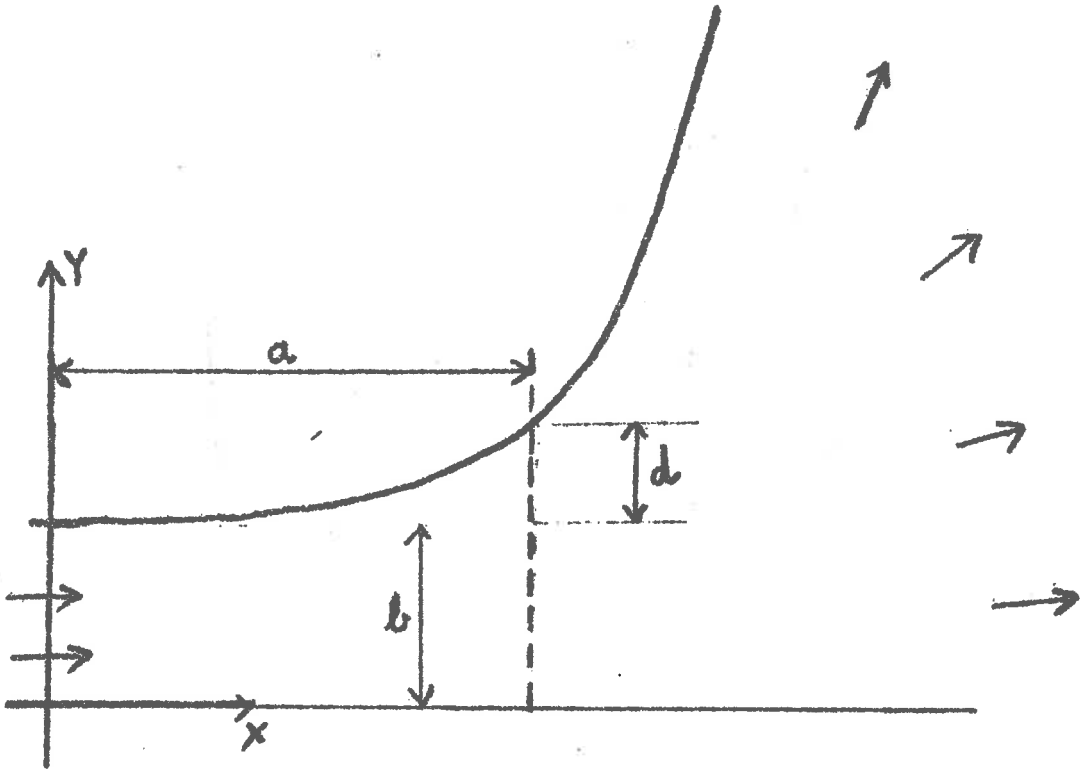

FIGURE 23. THE SPECIAL CURVED CROSS-SECTION.

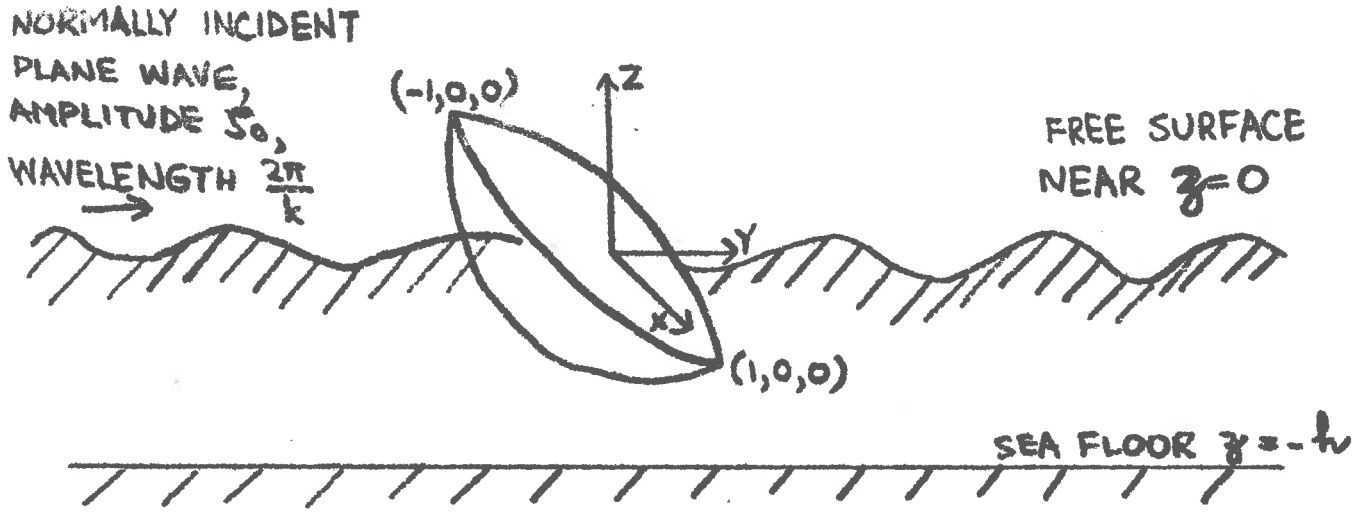

FIGURE 24. THE THREE DIMENSIONAL SCHEME SHOWING THE CO-ORDINATE SYSTEM.

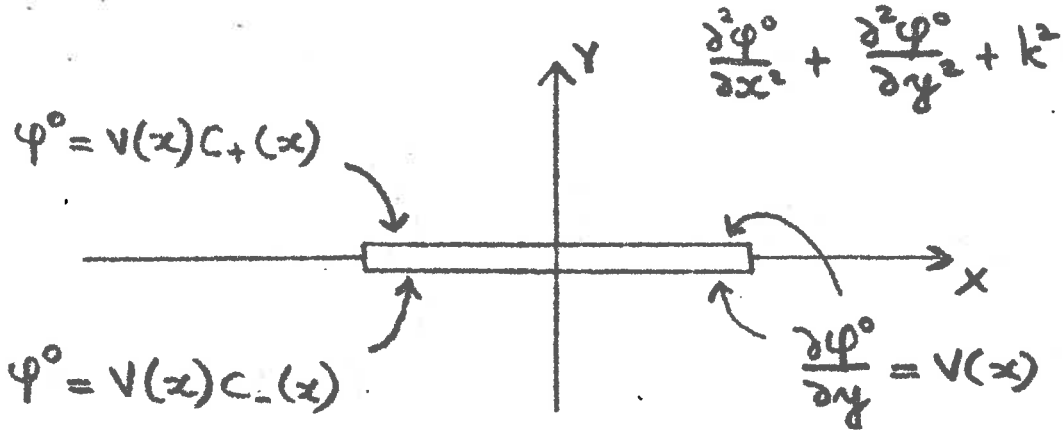

FIGURE 25. THE OUTER FLOW REGION.

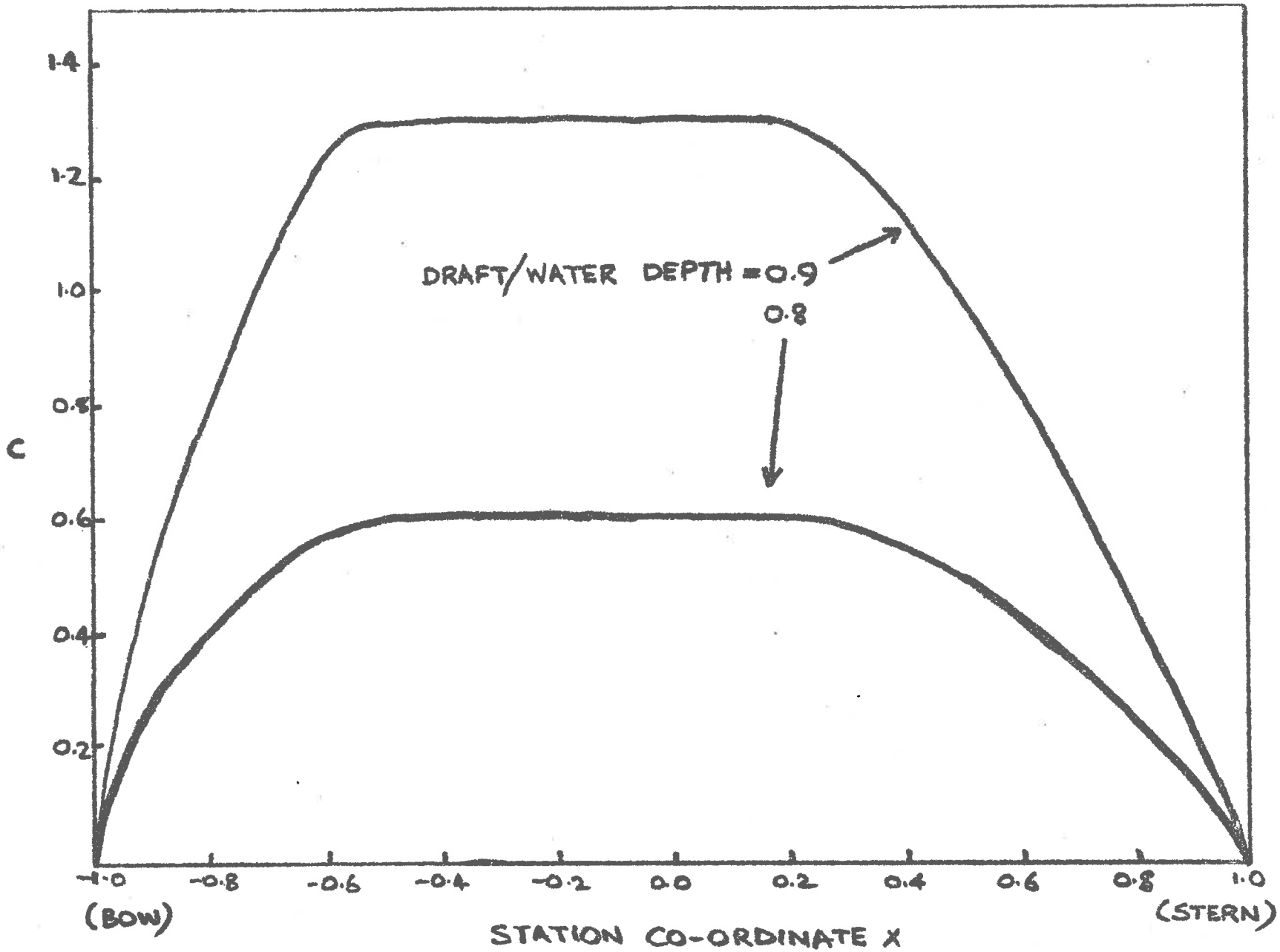
1·4
1·2
1·0
0·8
0·6
0·4
0·2
C
DRAFT/WATER DEPTH = 0.9
0·8
-1·0
-0·8
-0·6
-0·4
-0·2
0·0
0·2
0·4
0·6
0·8
1·0
(BOW)
(STERN)
STATION CO-ORDINATE X

FIGURE 26.

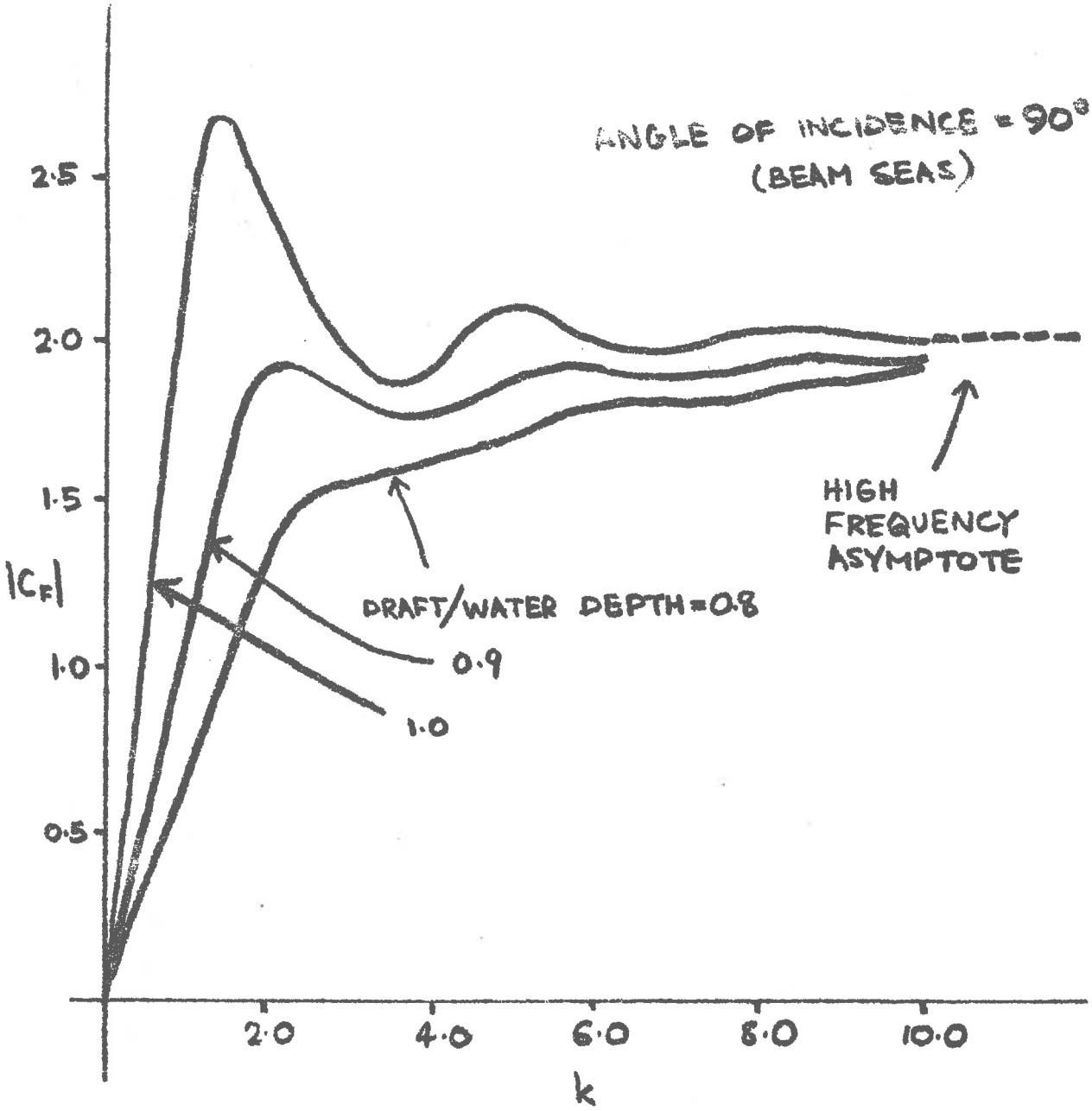

FIGURE 27.
SWAY EXCITING FORCE MAGNITUDE

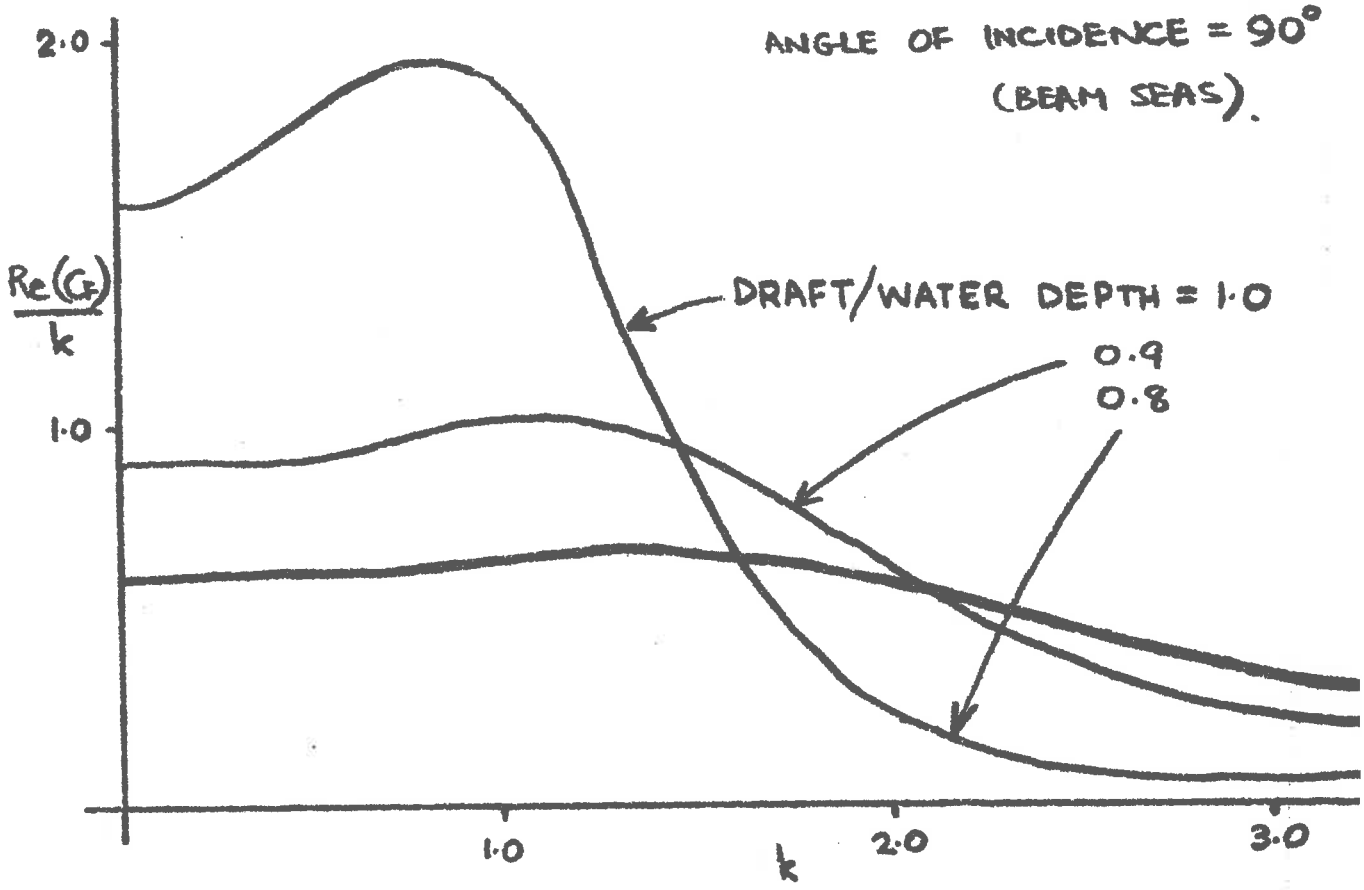

FIGURE 28. SWAY ADDED MASS

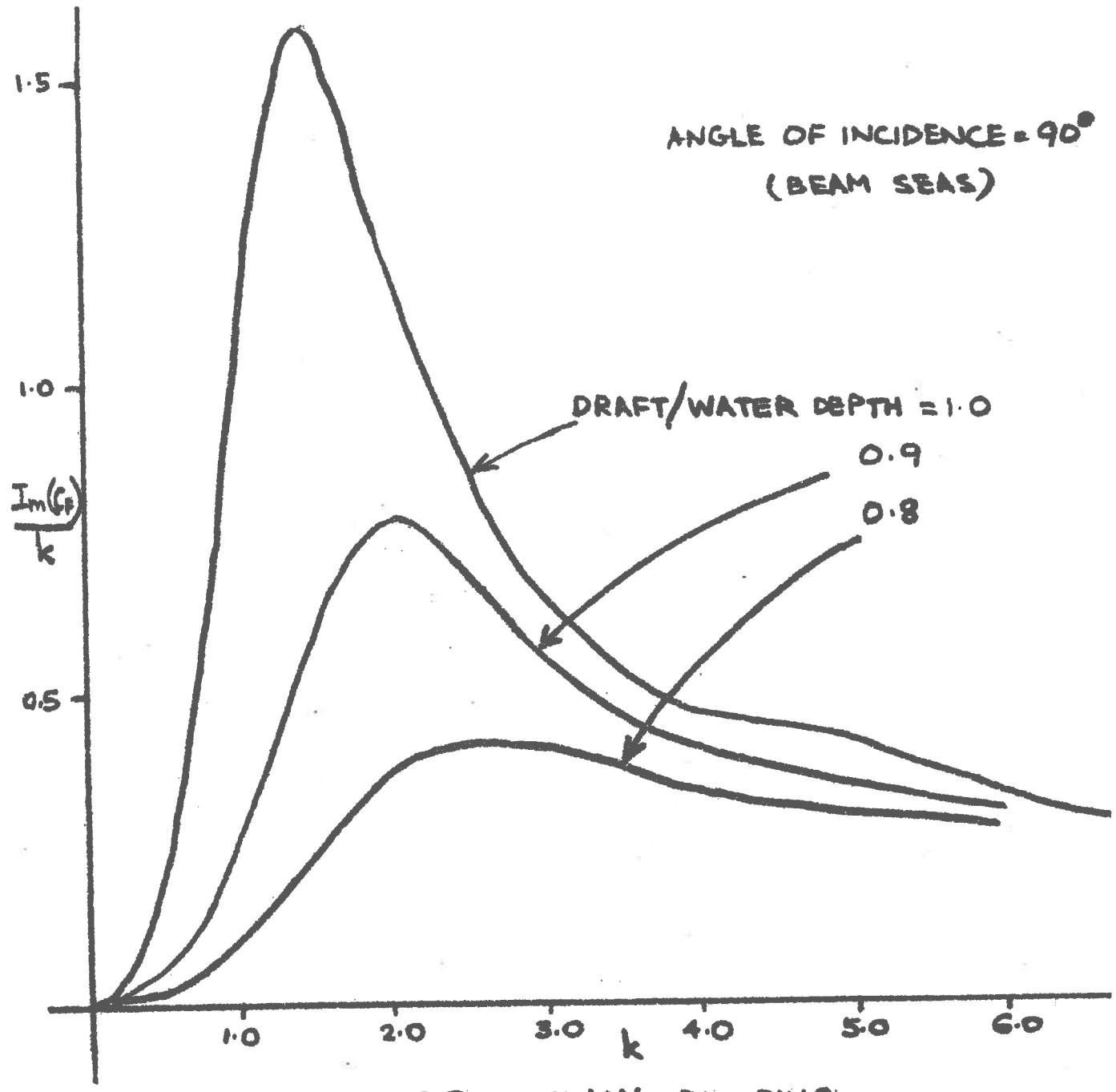

FIGURE 29. SWAY DAMPING.

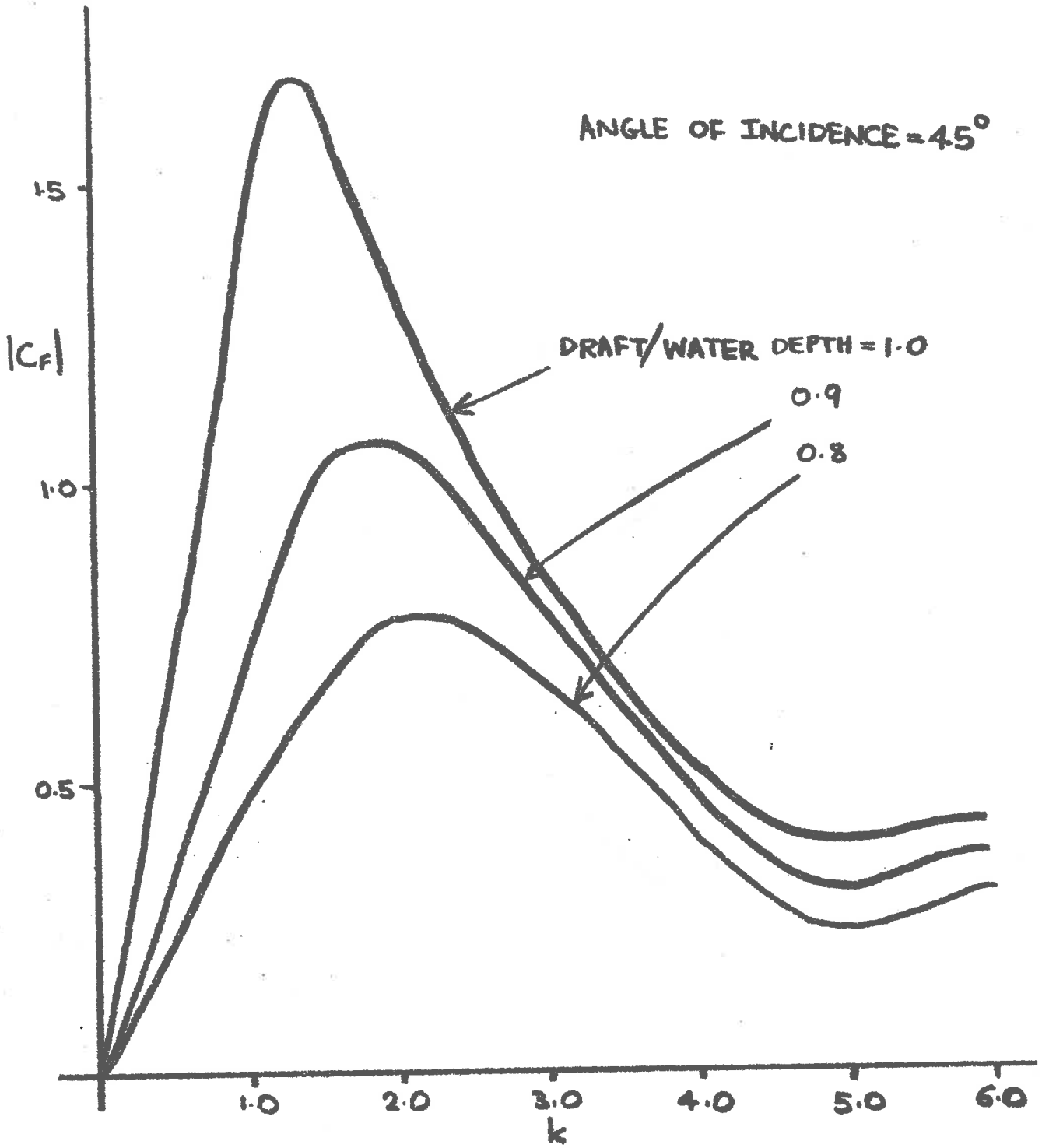

FIGURE 30.
SWAY EXCITING FORCE MAGNITUDE